POLYMERIC NANO/ MICROPARTICLES FOR MANAGEMENT OF PULMONARY DISEASES

by

JYOTHI UNNIKRISHNA MENON

Presented to the Faculty of the Graduate School of

The University of Texas at Arlington in Partial Fulfillment

of the Requirements

for the Degree of

DOCTOR OF PHILOSOPHY

THE UNIVERSITY OF TEXAS AT ARLINGTON

May 2014

Acknowledgements

It is with great pleasure that I present to you my completed PhD dissertation in the following pages. This journey would not have reached its fruitful culmination without the support and encouragement of a number of people. I would like to take this opportunity to convey my deepest appreciation and gratitude to all of them.

First and foremost, I would like to express my gratitude to Dr. Kytai T. Nguyen – my mentor and advisor, for giving me the opportunity to gain invaluable research experience in her laboratory. Her patience, wisdom and commitment have been a constant source of inspiration and motivation and have helped mold me into a well-rounded scientist. Her faith in my abilities has helped me grow both as a person and as an independent researcher. I am also extremely grateful to Dr. Connie Hsia and Dr. Debabrata Saha, who have provided indispensable advice and assistance for the completion of my Aims 1 and 2, respectively. Their valuable insights and guidance have been a positive influence throughout my doctoral study. I am also indebted to Dr. Liping Tang, Dr. Yi Hong and Dr. Baohong Yuan for taking time out of their busy schedules to review my work and provide invaluable advice for its improvement. I would also like to take this opportunity to acknowledge Dr. Jer-Tsong Hsieh at the University of Texas Southwestern Medical Center at Dallas (UTSW) for his help with animal studies.

In addition, I would like to thank members of the Nanomedicine and Drug Delivery Lab at UTA for maintaining a healthy and motivating research environment. In particular, I would like to thank my mentees Amruta Pise and Aneetta Kuriakose for their dedication and involvement in the research. I am also grateful to Dr. Priya Ravikumar and Dr. Zhang Zhang for their help with animal studies as well as Dr. Masaya Takahashi and Dr. Shanrong Zhang for their help with the MRI studies at UTSW. I would also like to appreciate other students, technicians and post-doctoral candidates of our collaborators

for their assistance in the completion of *in vivo* studies. My special thanks are also due to Dr. Aniket Wadajkar, Dr. Ashwin Nair, Michael Palmer and Pranusha Ravula for their friendship, advice, and encouragement over the course of my PhD study at UTA.

Most importantly, I would like to thank my family for being the incredible support system that they are. I am deeply grateful to my elder brother Mr. Sandeep Menon for being the perfect role model and for always being there for me. I am forever indebted to my parents Mr. U. Unnikrishna Menon and Mrs. Baby U. Menon for their unconditional love and support in all my endeavors. Without their encouragement and blessings, this dissertation would not have been possible. To them, I dedicate this thesis.

Lastly, I am grateful to God for giving me the strength, perseverance and intellect to come this far and pray that I will continue to be blessed thus in all my future endeavors.

March 26, 2014

Abstract

POLYMERIC NANO/MICROPARTICLES FOR MANAGEMENT OF PULMONARY DISEASES

Jyothi Unnikrishna Menon, PhD

The University of Texas at Arlington, 2014

Supervising Professor: Kytai T. Nguyen

Drug delivery via pulmonary route has emerged as an attractive area of study in the past two decades. This method of administration has multiple advantages for both systemic and local drug delivery due to the availability of a large surface area for drug absorption and higher solute permeability in the lung. Most importantly, inhalational drug delivery provides direct accessibility to the lung via a noninvasive route of administration. Recent literature has shown a surge in the use of nano/micro particles for a wide range of pulmonary applications ranging from targeted and controlled drug delivery to drug screening and tissue regeneration. In this research, polymeric nano and micro particles were first screened and characterized for diagnosis and treatment of pulmonary ailments such as restrictive lung diseases and lung cancer. Initially, various natural and synthetic polymer-based nanoparticles (NPs) were screened for delivery of protein and deoxyribonucleic acid (DNA) to the lung. Poly lactic-co-glycolic acid (PLGA) NPs showed the highest stability, controlled drug release and cytocompatibility. Although natural polymer-based NPs showed the highest cellular uptake *in vitro*, results from *in vivo* studies indicated more sustained and uniform tissue distribution on nebulization of PLGA NPs. Our major contribution to the field of drug delivery is that *in vitro* NP properties need not necessarily reflect their behavior *in vivo*. It is therefore necessary to validate *in vitro*

findings of NPs encapsulating biological agents with *in vivo* results in order to choose the most favorable nanocarrier for the desired application.

The PLGA NPs thus chosen were incorporated with superparamagnetic iron oxide (SPIO) and coated with a poly N-isopropylacrylamide – carboxymethyl chitosan (PNIPAAm-CMC) shell to form novel temperature- and pH-sensitive multi-layered NPs to provide better controlled drug delivery options for lung cancer treatment. Additionally, these core-shell particles were conjugated with folic acid for targeted lung cancer therapy. The particles produced good negative contrast using MRI *in vivo*. The NU7441 (radiosensitizer)- and gemcitabine hydrochloride (chemotherapeutic drug)- loaded NPs also significantly slowed down tumor growth when administered in combination with radiation *in vivo*. These observations indicate that our novel core-shell NPs could potentially be used as a drug carrier to provide efficient chemo-therapy and/or combined chemo- and radiation-therapy to treat lung cancers.

Finally, PLGA was used to synthesize stable, degradable and porous microparticles using porogens such as sodium bicarbonate, gelatin and poly-N-isopropylacrylamide (PNIPAAm) particles, to form 3D lung cancer models for screening of chemotherapeutic drugs *in vitro*. An innovative aspect of this research is the use of PNIPAAm NPs to generate uniform pores on the PLGA microparticles. Comparison between particles prepared using different porogens to form an *in vitro* tissue model is also novel. Our preliminary *in vitro* results indicate that the responses of 2D cancer cell monolayer and our 3D lung tumor model vary significantly when exposed to chemotherapeutic drugs of the same concentration. These results suggest the potential of our porous microparticles for screening of therapeutic agents in an *in vitro* setting, while mimicking *in vivo* conditions more closely than a conventional 2D model.

Table of Contents

List of Illustrations

List of Tables

Declaration of Academic Achievement

The research presented in this dissertation was conceived, performed, analyzed, written and submitted for publication primarily by the author of this dissertation with the following exceptions:

- All *in vivo* work in Chapter 2 including nebulization of NPs into the animals, histology, biomaging, Prussia blue staining and TEM (Sections 2.2.7, 2.2.11, 2.3.3, 2,3,6) were conducted by Dr. Priya Ravikumar, Dipendra Gyawali and Roshni Iyer from Dr. Connie Hsia's laboratory at UTSW. MRI in Chapter 2 was conducted in Dr. Masaya Takahashi's laboratory at UTSW (Figure 2.13).
- LCST measurements (Figure 3.5B) were done by Dr. Mingyuan Wei in Dr. Baohong Yuan's laboratory in UTA.
- MRI in Chapter 3 was performed by Dr. Shanrong Zhang in Dr. Masaya Takahashi's laboratory at UTSW (Figures 3.4B, 3.15 A-D) and the data obtained was analyzed by the author of this dissertation.
- Intratumoral injections and histology for studies in Figure 3.15 were done by Elizabeth Hernandez and Leah Gandee respectively from Dr. J.T. Hsieh's laboratory at UTSW. Intratumoral injections and tumor irradiation for studies in Figure 3.16 were performed by Dr. Zhang Zhang and Dr. Debabrata Saha at UTSW.

Chapter 1

Introduction

1.1. Respiratory Physiology and Common Ailments

Interest in respiratory physiology has been prevalent since the time of Plato several thousand years ago [2]; however, significant steps were taken towards understanding lung anatomy during the time of Leonardo da Vinci over 500 years back when he famously conducted his experiments on human cadavers. Although an improved understanding of lung physiology was acquired about 200 years ago, our current knowledge on pulmonary exchange of gases was established as late as during World War II [3]. The second half of the 20th century saw increased interest in the area of pulmonary drug delivery and nanotherapeutics [4]. Today, inhalational drug delivery has become an attractive route for localized delivery of therapeutic agents to the lung as well as systemic drug delivery to treat diseases like diabetes mellitus. The following sections will briefly outline the two pulmonary ailments that form the focus of this thesis, pulmonary drug delivery and its design considerations, as well as the long term goal and specific aims of this research.

1.1.1. Pulmonary Physiology

The human respiratory tract begins with the nose and mouth and continues to the larynx, trachea, bronchi and bronchioles which eventually lead to the alveoli. The human trachea (25 mm in diameter) [5] is separated from the alveoli by 23 generations of dichotomous branching [5]. At the 23rd generation of branching, the alveolar ducts end in the alveolar sacs lined with alveoli, 300 million of which are present in an average human lung [6].

The respiratory tract is lined with cells specializing in specific functions. The elongated, columnar ciliated and goblet cells found in the trachea and bronchial surfaces are primarily involved in secreting mucus, which lines the upper respiratory tract and preventing entry of foreign materials [6]. The ciliated cells assist in fluid and electrolyte movement down the respiratory tract [7]. Triangular basal cells found in the trachea and bronchi are responsible for cellular regeneration. Further, non-ciliated and secretory Clara cells in the bronchiole carry out surfactant protein secretion [7]. Type I and Type II cells are found mainly in the alveolar region. In this thesis, we are chiefly interested in the flat and thin Type I cells which form 95 % of alveolar epithelial cells in the lung [8]. Type II cells on the other hand can expel characteristic lamellar structures which contain surfactant proteins [6]. Coordination between these different cells is necessary for carrying out respiration and other necessary lung functions.

In addition to its main function of carrying out gas exchange, the respiratory system also plays a major role in metabolism, pulmonary circulation, and filtration of impurities and harmful substances entering the body during breathing [9]. Airborne NPs are taken in during inhalation and are expected to overcome clearance mechanisms in the lung in order to reach the site of interest and release the encapsulated therapeutic agents. The mucus layers and ciliated cells lining the trachea can remove foreign objects and drug particles taken in during inhalation. Alveolar macrophages form the primary clearance mechanism in the alveoli. There are about 5 to 7 macrophages per alveoli, and they function to remove microorganisms, insoluble particles and drugs in the region. Drugs and particles not taken up by the macrophages either stay indeterminately in the alveoli or are conveyed to other parts of the body via pulmonary circulation [10].

1.1.2. Common Pulmonary Ailments

Pulmonary ailments such as lung cancer, pulmonary arterial hypertension (PAH), chronic obstructive pulmonary disease (COPD), restrictive diseases, genetic lung diseases, and infectious diseases like tuberculosis are a global burden that affects thousands of people worldwide [9]. The two key lung ailments that form the focus of this thesis, i.e. Restrictive Lung Diseases (RLDs) and lung cancer have been briefly described below.

1.1.2.1. Restrictive Lung Diseases

Restrictive lung disease (RLD) is a condition where lungs are 'restricted' from expanding fully due to the development of scarring or inflammation. There are two categories for this disease, namely intrinsic and extrinsic RLDs. Intrinsic diseases usually affect the pulmonary interstitium and other parts of the lung parenchyma while extrinsic RLDs generally result in decreased gas exchange in the lung due to damage to chest wall, pleura and respiratory muscles [11]. In response to RLD, there will be an increase in exertion of mechanical stresses on the remaining functioning lung units, which involves potent stimuli for gene transcription, protein expression, cellular growth and remodeling of alveolar septa. This phenomenon is collectively known as compensatory lung growth (CLG) [12]. Pneumonectomy is a model that mimics the consequences of lung destruction and can be used to study CLG. Although CLG can significantly improve structure and function of the lungs, the compensation is incomplete in adult lungs, where the function of both lungs is not fully restored. In order to overcome this limitation, exogenous growth promoters can be provided to encourage balanced alveolar remodeling. The screening and characterization of different polymeric nanocarriers to

eventually deliver growth factors to the lung to promote uniform alveolar remodeling will be the focus of Chapter 2.

1.1.2.2. Lung Cancer

Lung cancer is the most deadly form of cancer accounting for nearly 1.6 million newly diagnosed cancer cases around the world annually [13]. According to the National Cancer Institute, this disease is expected to responsible for about 224,210 new cases of cancer diagnoses and 159,260 deaths in the US in 2014 [14]. An estimated 26% of female cancer-related deaths and 28% of male cancer-related deaths was expected to occur due to lung cancer in 2013 [15]. Due to the asymptomatic nature of lung cancer during its early stages, more than 56% of the diagnoses take place at a later stage of this ailment [16]. The 5-year survival rate of lung cancer patients is less than 15% partly due to the advanced disease stage at the time of diagnosis [17]. Conventionally, lung cancer has been treated using surgery, chemotherapy and radiation therapy. Surgical resection is feasible only when the tumor is localized [18]. Chemo- and radiation therapy administered alone or in combination have only shown temporary remission [16]. Additionally, due to the non-specific nature of these treatments, undesirable systemic side effects and toxicity may occur as they act on and inhibit normal cells in the body [19, 20]. Therefore it is crucial that a comparatively precise, targeted treatment regimen be put in place to overcome the limitations of conventional lung cancer therapy following diagnosis. Chapters 3 and 4 of this dissertation focuses on the development of nano/micro particles which can be used for targeted drug delivery for lung cancer therapy as well as to form tumor models for screening lung cancer drugs *in vitro*.

1.2. Nanomedicine in Pulmonary Drug Delivery

1.2.1. Type of NPs

Drug delivery by inhalation is attractive due to its numerous advantages such as non-invasive method of administration, local action of therapeutic agent , availability of large alveolar surface area and reduced systemic side effects due to site-specific delivery of encapsulated payload [21]. Based on the application and desired release kinetics of the therapeutic agent, different types of NPs such as liposomes, micelles, dendrimers and polymeric NPs can be synthesized for pulmonary delivery, as shown in Figure 1.

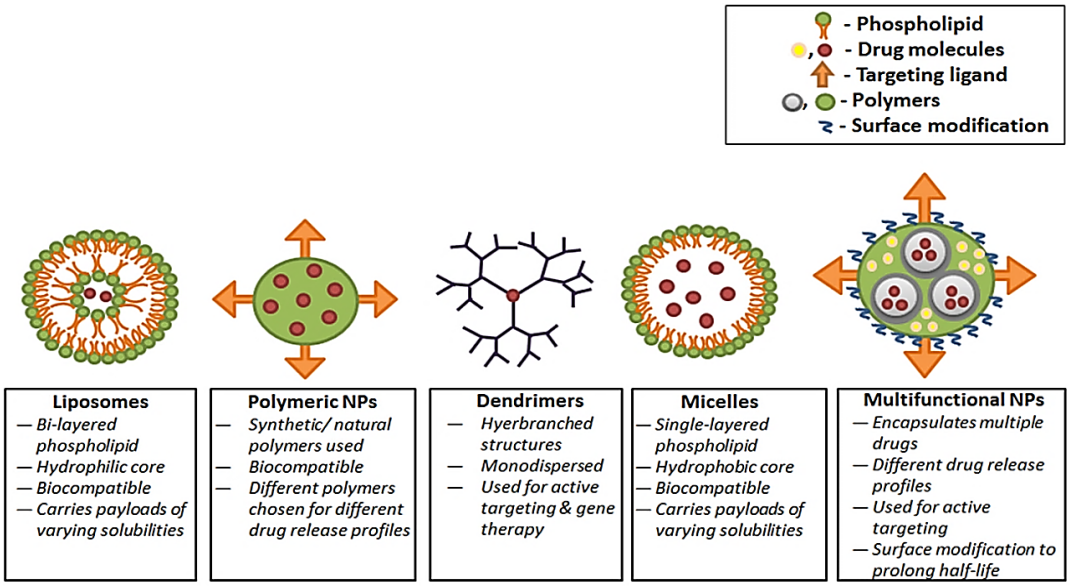

Figure 1.1 Types of NPs employed today for pulmonary drug delivery and their corresponding attributes [1]

The size range of NPs can be determined based on several factors. For example, intravenous injection of microparticles greater than 5 μm has been shown to cause pulmonary embolism leading to fatal outcomes. On the other hand, particles in the 0.5-3 μm size range tend to be taken up by macrophages and cleared from the body, thereby reducing their effectiveness as drug delivery systems. Nanoparticles in the 50 to

200 nm size range can theoretically escape macrophage clearance and show greater alveolar deposition following pulmonary delivery [22].

1.2.1.1. Liposomes

Liposomes are bi-layered phospholipid-based nanocarriers used to entrap hydrophilic agents on their surface and core, and hydrophobic/lipophilic payloads in between. Liposomes are attractive carriers for pulmonary drug delivery as they have similar composition as lung surfactants, which are made of about 85% phospholipid [23]. One of the first liposomal carriers to reach the market for pulmonary delivery is Bovactant or Alveofact, which was prepared from artificial lung surfactants [24]. Recently, Chen et al. [25] synthesized salbutamol sulfate (SBS) encapsulating liposomes (~57 nm) for asthma treatment via inhalation. *In vivo* studies on Sprague Dawley rats showed that the liposomes were distributed homogenously in the lung and showed bronchodilating effects following aerosolization. Further, administration into guinea pig asthma models showed anti-asthmatic effect of the liposomes up to 18 h following administration while free SBS administered *in vivo* were effective only up to 6 h. Despite their many advantages, liposomes in suspension are limited by inadequate drug encapsulation efficiency, expensive method of production [26] as well as stability and leakage issues that tend to arise during aerosolization and nebulization. Therefore research is now focused on the development of liposomal dry powders [27].

1.2.1.2. Micelles

Micelles are colloidal systems consisting of a hydrophilic shell and hydrophobic core which can be used to entrap drugs of varying solubility. The hydrophilic surface of micelles can evade the reticuloendothelial system (RES) and prevents fast elimination

from the lung following administration [28]. Sahib et al. [29] used polyethylene glycol–phosphatidylethanolamine conjugate-based stable micelles for pulmonary delivery of beclomethasone dipropionate (BDP) to treat asthma or chronic obstructive pulmonary diseases (COPDs). *In vivo* studies following nebulization into asthmatic rat models showed greater pharmacodynamic activity than delivery of solubilized BDP powder alone. Micelles can also be prepared using phospholipids native to the lung, as demonstrated by Gill et al. [30]. These micelles (5 nm) consisted of a PEG-phospholipid hydrophilic surface (PEG5000) and distearoylphosphatidylethanolamine (DSPE) hydrophobic core. These biocompatible micelles enhanced paclitaxel retention in the lung compared to free paclitaxel. Although some micelles such as NK012 polymeric micelle encapsulating SN-38 [31] have reached clinical trials lung cancer treatment, these formulations tend to be limited by their instability and degradation issues [32]. Therefore alternative nano-sized vehicles are being investigated for better drug delivery.

1.2.1.3. Dendrimers

The term ‘dendrimer’ is derived from the Greek words ‘dendron’ meaning tree and ‘meros’ meaning part [33]. Dendrimers are monodispersed and hyperbranched structures consisting of a core moiety of an atom or group of atoms attached to branches of repeating units. These repeating units are concentrically arranged and possess functional groups that allow ligand conjugation for cell-specific targeting [34]. Polyamidoamine (PAMAM) is most commonly used in dendrimer formation due to the presence of both carboxylic acid and amine functional groups on their surface for bioconjugation. For example generation 4 (G4) branched PAMAM dendrimers synthesized by Liu et al. [35] was bound to non-small-cell lung carcinoma (NSCLC) - targeting peptide for specifically targeting lung cancer cells following pulmonary delivery.

These dendrimers showed time- and dose- dependent cellular uptake *in vitro* and also showed good uptake by lung cancer cells *in vivo*. Kukowska-Latallo et al. [36] also prepared PAMAM dendrimers complexed with pCF1CAT plasmid DNA for gene therapy in the lung. CAT expression was observed mostly in the alveolar epithelium following intravenous administration while high expression was seen in the epithelia of respiratory bronchioles after endobronchial administration. Despite their many attractive qualities, dendrimers are limited by their uncontrolled and burst drug release as well as low encapsulation efficiency [37]. Therefore there is an urgent need for improved nanocarriers that can carry out sustained and controlled drug release following pulmonary delivery.

1.2.1.4. Polymeric Micro/Nano particles

Polymeric micro/ nano particles are being extensively investigated today for pulmonary drug delivery applications. The properties of both natural and synthetic polymers can be tuned based on their intended application. A wide selection of natural polymers such as gelatin, chitosan, alginate and cellulose are available for nanoparticle formulation. Poly lactic acid (PLA), poly lactic-co-glycolic acid (PLGA), polyanhydrides and poly- ε- caprolactone are some of the synthetic polymers in use today [27, 38]. Chitosan NPs have been synthesized by Mehrotra et al [39] to deliver Lomustine for inhibiting lung cancer cell growth. On the other hand, highly porous PLGA microparticles developed by Kim et al. [40] have demonstrated good aerosolization efficacy and sustained doxorubicin release for lung cancer therapy.

NPs have also been developed by combining natural and synthetic materials so that the final product demonstrates the characteristics of both polymers. For example, El-Sherbiny et al. [41] prepared microgels by graft copolymerization of poly (ethylene glycol)

(PEG) with chitosan and Pluronic®-F108. The mucoadhesiveness of chitosan coupled with the hydrophilicity and biocompatibility imparted by PEG aids in sustained drug delivery and enhanced circulation time. Within 240 h of exposure to lysozymes, the microparticles had degraded up to 41% of their weight and displayed tri-phasic drug release involving an initial burst release followed by sustained release and eventually rapid release due to particle degradation. *In vitro* studies also showed significantly delayed uptake of these particles by macrophages due to stealth characteristics imparted by PEG. Zou et al. [42]synthesized bioadhesive NPs using a combination of PLGA and bioadhesive Carbopol to enhance DNA binding for gene therapy to treat lung cancer. The NPs (~126 nm) were biocompatible and maintained stability of bound DNA while protecting it from degradation. Research thus far has gradually paved the way for the development of multi-functional NPs for targeting the cells of interest and disease diagnosis, as well as encapsulation and release of different drugs at varying rates for accurate and targeted therapy.

1.2.2. Targeting Mechanisms

Conventional therapies for treatment of lung disorders such as lung cancer are limited by systemic toxicity of the therapeutic agents [10]. Targeted delivery of the drug is advantageous as it helps increase the drug concentration at the disease site thereby limiting toxicity to other organs in the body. Therefore, targeted drug delivery has been receiving considerable attention in recent years [43]. Current literature has also revealed an emerging trend in the development of nanocarriers for targeted delivery in order to achieve more efficient therapy. Two methods of targeting have been used for drug delivery: passive and active targeting.

1.2.2.1. Passive Targeting

Passive targeting can take place by two methods. The first involves drug diffusion through mucus layer and epithelial cell layer to reach lung tissue [44]. The second method of passive targeting takes advantage of the leaky vasculature seen in tumors and uses the enhanced permeability and retention (EPR) effect to accumulate the drug in the tumor regions [45]. Passive targeting in lungs was studied by Yu et al. [46] has been used via thermally crosslinked iron oxide NPs containing doxorubicin, for lung cancer therapy and imaging. In vivo studies on orthotopic lung cancer mouse model showed preferential accumulation of NPs in the tumor region by EPR effect. The process of passive targeting can be time-consuming and could result in drug accumulation in other healthy tissues resulting in adverse side effects [45]. Further, repeated dosages of the nanoparticle formulation would be applied in order to achieve the desired effect by passive targeting. This causes patient inconvenience and may harm normal airway tissues from mouth to alveoli at the cellular level [40]. Therefore active targeting is being explored as an alternative method for better nanoparticle delivery to the disease site.

1.2.2.2. Active Targeting

Active targeting can be done either by bioconjugation of targeting molecules for receptor-mediated targeting or by guiding the nanoparticle to the site of interest using an external force/stimulus [45]. Vascular endothelial growth factor receptors (VEGFR), platelet-derived growth factor receptors (PDGFR), EGFR and folate receptors [10, 47, 48] are some common receptors known to be overexpressed by lung cancer cells. Conjugation of their corresponding ligands onto the nanoparticle surface helps in delivery of the nanoparticle specifically to these disease cells. An example was demonstrated by Zhou et al.[49] who had developed folate-decorated biodegradable pluronic F127-b-

poly(ε-caprolactone) copolymeric micelles for active targeting of lung cancer. These micelles were specifically taken up by the A549 lung cancer cells compared to normal fibroblasts. Another attractive method of targeting is the use of an external magnet to aid SPIO-encapsulated NPs to the disease site. Goodwin et al. [50] synthesized a gamma-emitting isotope Technetium 99 (^{99m}Tc) conjugated composite particle of Fe and C. These magnetic particles could be magnetically targeted and retained in the lung of swine model as compared to groups not exposed to magnetic targeting. A combination of magnetic and receptor-mediated targeting is attractive for accurate and site-specific delivery of the therapeutic vehicle [51]. This was demonstrated by Yoo et al. [52] who had developed folate-PEG-superparamagnetic iron oxide NPs for lung cancer targeting. Significantly higher accumulation of these NPs was observed in lung cancer mouse model compared to the NPs not conjugated with folate.

1.2.2.3. Cellular Uptake Mechanisms

Following arrival at the targeted site, the NPs can be internalized by the cells via different endocytic pathways. This includes clathrin- and caveolae-mediated endocytosis as well as phagocytosis and pinocytosis [53]. Caveolae-mediated endocytosis is the most common pathway for cellular uptake of NPs. This is because caveolin is abundantly expressed in many cells including lung tissues [53, 54]. Clathrin-mediated endocytosis is also well-characterized as it is commonly seen in all mammalian cells. Alveolar macrophages in the respiratory tract usually take up NPs by phagocytosis [53, 55-57]. This method of internalization is important for the delivery of nano/microparticles specifically to the alveolar macrophages to treat tuberculosis or other inflammatory and infectious diseases [58]. The different uptake mechanisms employed by cells in the lung for taking up NPs have been summarized in Figure 1.2.

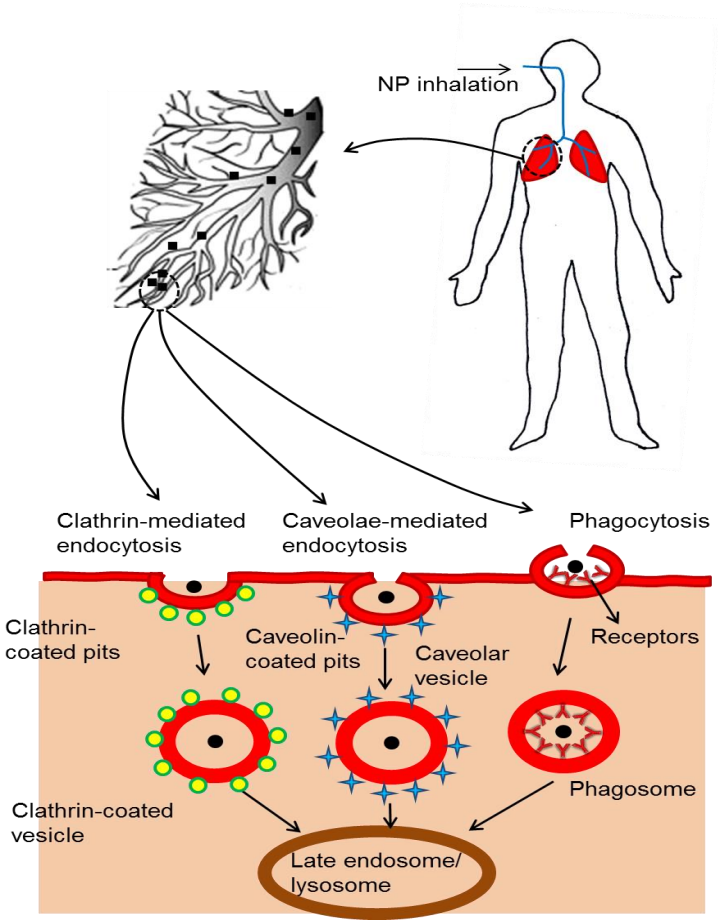

Figure 1.2 Representation of uptake of NPs by lung cells of interest following inhalation. Uptake can occur via clathrin-mediated endocytosis, caveolae-mediated endocytosis or phagocytosis

1.2.3. Methods of Pulmonary Administration

During administration, it is critical that the particles maintain optimum size as this can determine the region of their deposition following administration. Different methods of pulmonary administration of drugs/NPs can be used based on the region of the lung being targeted, as described below.

1.2.3.1. Nebulization

Nebulization is the oldest and most frequently used method of nanoparticle administration to the lung. This technique maintains a relatively small size of particles with minimal aggregation and can thus be aimed at the distal regions of the lung. For example, majority of the celecoxib- containing lipid nanocarriers prepared by Patlolla et al. [59] could be delivered to the alveolar region of mice lung by nebulization while larger particles (~ 10 µm) were delivered to the central airways and oropharynx [60]. During nebulization, the particles are generally suspended in a 0.9% (w/v) NaCl solution and are broken down into aerosol droplets (4-6 µm) by a jet or ultrasonic nebulizer using compressed air or ultrasonic power [61, 62].

Studies done by Dailey et al. [63] showed that although aerosol size of the particles are not affected by nebulization, their mass median aerodynamic diameter (MMAD) tends to vary based on the types of nebulizers used. MMAD represents the point at which this aerodynamic diameter of the particles administered crosses the 50^{th} mass percentile [64]. For example, the Pari LC star nebulizer gave a narrow size distribution and smaller lose rate of NP mass than other tested Omron nebulizers [63]. Particles sometimes tend to aggregate in the nebulized fluid due to various factors including high shear forces within the nebulizer and interaction between the hydrophobic NP surfaces. This aggregation can be minimized by varying different parameters such as viscosity and surfactant concentration and by addition of hydrophilic polymers [62]. Recently, vibrating-mesh nebulizers have been gaining prominence as they reduce particle aggregation, maintain consistent temperature and reduce residual volume, thus addressing the issues commonly seen in nebulizers today [62].

1.2.3.2. Metered Dose Inhalation (MDI)

Metered dose inhaler is used to deliver fixed NP amounts using set pulses through a dosage valve. Particles delivered by this method generally have an MMAD between 2-4 µm [60]. For example, thymopentin NPs prepared by Tan et al. [65] and delivered via pressurized MDI (pMDI) were stable over time and the aerosol droplets had a cut-off diameter of less than 6.4 µm. Selvam et al. [66] developed swellable PEG/chitosan microgels containing PLGA NPs for delivery via pMDI. These hydrogel microparticles (1- 2 µm) could reach the deep lungs following administration and evaded alveolar macrophage uptake by swelling to larger sizes. Some of the disadvantages of this mode of administration are particle deposition in the oropharyngeal region due to high speed administration, and inconsistent dose delivery when the device is not shaken properly [60]. Therefore, there is a need for either improving this device or developing alternative devices to perform the same function more efficiently.

1.2.3.3. Dry Powder Inhalation (DPI)

Dry powder inhalers were developed to overcome limitations of pMDI by administering nanoparticle powders to the patient's lung based on their ability to inhale. The turbulent airflow generated by inhalation forms nanoparticle-containing aerosols (MMAD of 1-2 µm) [60]. The relatively low cost, ease of administration, high drug bioavailability and patient convenience makes this method an attractive route for drug delivery [67]. For example, Sinha et al. [68] had developed porous PLGA particles (2.47 µm) loaded with voriconazole for treatment of fungal infection in the lung following DPI. *In vivo* studies showed uniform distribution of the particles within the bronchial and alveolar epithelium as well as capillaries. However, DPIs are also limited by their dependency on the patient's inspiratory flow rate and subsequent inconsistency in

dosage and limited availability worldwide [69]. In addition, dry powders tend to remain suspended in air and hence do not get deposited in the tissue. Therefore alternative methods of pulmonary delivery of NPs need to be investigated. The aerodynamic properties of NPs can also be improved by spray-drying, spray freeze-drying or electrostatic flocculation [70].

1.2.3.4. Intratracheal Administration

Delivery of NPs directly to the trachea would be a more specific and accurate mode of drug delivery. This method of delivery is generally done by creating an incision on the trachea and fitting a cannula for particle administration [71]. Ungaro et al. [72] developed antibiotic-loaded PLGA-chitosan and PLGA-alginate NPs in the size range of ~200-600 nm, spray dried with lactose and delivered intra-tracheally to male Wistar rats. The alginate-PLGA NPs reached the deep lung following administration while chitosan-PLGA NPs were found in the upper respiratory airways indicating that polymer properties affected the deposition pattern of the particles. The PEG5000-DSPE micelles mentioned earlier showed greater accumulation and release of paclitaxel in the lungs following intratracheal administration (almost 45-fold compared to intravenous administration) demonstrating the effectiveness of this method of administration in treatment of lung diseases [30]. However, reduced patient comfort and compliance are possible disadvantages to this administration method.

1.3. Medical Applications of Pulmonary Nanomedicine

1.3.1. Nanodiagnostic/Imaging Applications

MRI is an attractive modality for imaging NPs containing contrast agents due to its high spatial and temporal resolution as well as good soft tissue contrast [73]. SPIO is an MRI contrast agent frequently used in drug delivery due to their slow renal clearance rate and high relaxation values [74]. As a result, NPs incorporating SPIO can be imaged using MRI for diagnostic applications, as well as for non-invasive visualization of their biodistribution following administration. For example, Guthi et al. [73] developed a multifunctional micelle (MFM) system loaded with SPIO and Doxorubicin and conjugated with a lung cancer targeting peptide (LCP) for lung cancer imaging and therapy. *In vitro* MRI study showed high T_2 relaxivity in H2009 cells incubated with these micelles, indicating that these micelles can be detected using ultrasensitive MR. SPIO can further be subjected to an alternating magnetic field to induce hyperthermia for heat generation in the region resulting in tumor ablation [18]. Other imaging agents such as manganese for MRI [75] and gold NPs for computed tomography (CT) imaging [76] have also been used as diagnostic tools in pulmonary drug delivery.

1.3.2. Therapeutic Applications

NPs are widely researched for delivering the encapsulated therapeutic agent in a sustained and controlled manner. Conventional treatment methods are limited in that the drug can cause systemic side effects to other organs in the body upon administration [77]. Pulmonary drug delivery has the advantage of ensuring delivery of encapsulated therapeutic agents directly to the target organ, i.e., the lung. Further due to the sustained release of the drug over time, repeated dosages need not be given thus reducing patient discomfort and drug toxicity. For instance, the porous PLGA NPs containing the anti-

fungal drug voriconazole developed by Sinha et al.[68] could be detected in the lungs for up to 7 days following administration in mice. Similarly, Lomustine-encapsulated chitosan NPs synthesized by Mehrotra et al.[39] for lung cancer treatment showed bi-phasic drug release and demonstrated greater inhibition of L132 human lung cancer cell line in vitro than delivery of Lomustine alone.

1.3.3. In Vitro Models for Drug Screening

An *in vitro* 3D tissue model is expected to mimic cell growth, proliferation and function as seen in cells in an *in vivo* environment. These 3D models would thus be a more accurate representation of cell behaviors than conventionally used 2D cell monolayers. Research has recently started to focus on the development of 3D tissue models using large polymeric microparticles which would provide a biocompatible surface for cell attachment and growth. Porous microparticles would have the added advantage of allowing nutrient diffusion and greater surface area for cell attachment and growth. This method of cell culture would greatly benefit research on tumor drug delivery as these 3D tissue/tumor models can be used for *in vitro* screening of various drugs to relatively accurately determine their therapeutic efficacy before administering them during pre-clinical and clinical trials. This cost effective method would also help thoroughly evaluate the efficacy of drug delivery systems *in vitro* to ensure that they will have the desired effect when used *in vivo* [78].

1.4. Design Considerations and Optimization of Nano/ Microparticles

Based on the components and diameter of the NP system as well as the clearance mechanisms involved, varied half-lives are seen following pulmonary

administration. Ferric oxide NPs delivered by intratracheal instillation was removed from the lung at a rate of 3.06 µg per day and showed a plasma half-life of 23 days [79]. On the other hand, biocompatible hydrophobically modified glycol chitosan (HGC) NPs developed by Choi et al. [80] are stable in vivo and showed a lung half-life of ~6 days following intratracheal administration in mice. 20 nm polystyrene beads administered by airway exposure to rats showed a lung half-life of 18 days compared to 44 and 35 days for 100 nm and 1000 nm particles respectively, indicating that particle size does play a role in determining half-life [81].

Besides, half-life, drug release profile is another criterion to be considered while designing NP systems. Different polymers are expected to show different drug release rates. For instance, Hitzman et al. [82] synthesized 5- Fluorouracil (5-FU)-loaded liposomes for adjuvant therapy for lung cancer. A burst drug release of 100% was seen from the liposomes within 12 hours. On the other hand, polymeric (PLGA, poly-lactic acid (PLA) or poly (lactide-co-caprolactone) (PLCL)) microspheres encapsulating 5-FU prepared by the same group showed a bi-phasic drug release in which there was an initial burst release of 40-60% of the drug within 4 hours followed by a sustained release of 70-90% of the drug within about 24 hours. Docetaxel-loaded HGC NPs prepared by Hwang et al. [83] for lung cancer therapy also showed a burst release of 35% of loaded drug within 6 hours followed by sustained release over a period of 2 weeks. The inherent pH-sensitivity of chitosan is also beneficial for drug release in the acidic tumor microenvironment for lung cancer treatment. These results indicate that the choice of materials and environmental stimulus plays a major role in determining the release kinetics of NPs.

In addition to release kinetics, the clearance mechanism involved in nanoparticle removal should also be considered. As mentioned earlier, mucociliary clearance and

phagocytosis by alveolar macrophages can occur during particle clearance. Literature has shown that NPs, which tend to adhere to the mucosal surface avoid rapid mucociliary clearance as well as minimize recognition and subsequent clearance by macrophages [61]. Large particles and drug deposited from the 0 to 16th generation of the respiratory airways are cleared by mucociliary clearance (MCC) mechanism. The ciliary lining transports mucus containing particles or drugs down to the larynx/pharynx and subsequently to the GI tract for elimination from the body [61]. Alveolar macrophages help in eliminating unwanted molecules from the alveoli, where cilia are not present. Phagocytosis by macrophages occurs within 6 to 12 hours of deposition of large particles in the alveoli and then they are broken down by enzymatic degradation [61]. Particle clearance can also occur by dissolution (if the polymer is soluble), exhalation, coughing and also via systemic circulation [61, 84]

1.5. Overview of Research Project

This research has been designed to extensively investigate several polymer-based nano and micro carriers for various pulmonary drug delivery and *in vitro* drug screening applications. The long-term goal and specific aims of this project have been described in detail below:

1.5.1. Goals/Objectives

The long-term goal of this project is to develop biocompatible polymeric nano/microparticles for diagnosis and treatment of chronic lung diseases as well as for drug screening to provide effective cancer therapy. A vast array of published works in recent times has attempted to deliver therapeutic agents to the lung for treatment of diseases ranging from asthma and lung cancer to diabetes. However, there have been

no studies to our knowledge that have screened and characterized several commonly used natural and synthetic polymer-based NPs in terms of their efficacy as drug carriers for pulmonary drug delivery. The most promising polymeric nanocarrier chosen from the screening process can be surface modified/functionalized for various pulmonary applications. Incorporation of contrast agents such as SPIO can aid in imaging and determination of nanoparticle biodistribution following delivery using MRI. Conjugation of targeting ligands on the nanoparticle surface can further help in accurate targeting of the diseased cells that overexpresses the corresponding receptor. Finally, the chosen biocompatible polymer is used to develop porous microparticles that can facilitate cell adhesion and proliferation on their surface in order to develop *in vitro* lung cancer models for screening of various commonly used lung cancer drugs. Therefore the final objective of this research is to design and screen various polymeric NPs for pulmonary delivery and chose the most promising nanoparticle for further studies involving drug screening, diagnosis and treatment of lung diseases.

1.5.2. Specific Aims

As a first step towards achieving my long-term goal of developing polymeric nano/micro carriers for effective diagnosis and treatment of pulmonary diseases, the following three specific aims were proposed and performed:

To screen and characterize various natural and synthetic polymer-based NPs for pulmonary protein and DNA delivery via nebulization. Commonly used biocompatible natural and synthetic polymers were extensively compared and characterized in order to determine the most favorable polymeric NP formulation for further studies.

To develop multi-functional core-shell NPs for targeted lung cancer therapy. The polymer chosen based on above studies - (poly lactic-co-glycolic acid, PLGA) was used

to develop multifunctional core-shell particles conjugated with folic acid for active targeting and treatment of lung cancer.

To synthesize and screen porous microparticles as *in vitro* 3D tumor models for lung cancer drug screening. Porous PLGA microparticles were formulated and characterized for use as 3D culture systems. The effectiveness of large porous PLGA microspheres as *in vitro* lung tumor models for drug screening applications was also investigated

1.5.3. Innovative Aspects

There are several innovative aspects to this research. Firstly, this work has extensively compared multiple natural and synthetic polymer based NPs in terms of their biocompatibility and drug release capabilities following nebulization. The results would aid future research in pulmonary drug delivery in terms of choosing the most suitable polymer for controlled and efficient delivery of therapeutic agents to the lung. Further, the cellular uptake results obtained *in vitro* have been corroborated with results *in vivo*. The most promising polymer chosen was further modified to develop a novel core-shell NP system for targeted and stimuli-responsive pulmonary drug delivery to diagnose, target, and treat advanced stages of lung cancer. Finally, the biocompatible and biodegradable polymer chosen was used to develop porous microparticles which were extensively characterized in order to develop *in vitro* 3D lung tumor models. Three different porogens were used to prepare particles with varying pore sizes. There have been no previous studies where particles prepared using varying porogens have been compared in terms of their potential as *in vitro* 3D tissue/tumor models. These tumor models are expected to be more effective than 2D cell monolayers in determining the efficacy of lung cancer drugs for i*n vivo* administration. This is due to the ability of the 3D tumor models to mimic

in vivo tumor environments comparatively more accurately through extracellular matrix production and maintenance of cell functions.

1.5.4. Successful Outcome

The successful completion of this research will be helpful in the design and development of nanoparticle formulations that can achieve good treatment efficacy following pulmonary delivery. Since diagnosis of lung cancer generally takes place at an advanced stage of the disease, it is important that an effective and rigorous treatment regimen be provided so that the tumor can be quickly and effectively removed from the body. The novel multi-functional NPs presented in this research can be potentially used to diagnose, treat and track the progress of lung tumor following administration while causing minimal discomfort to the patient. Due to the ability of these particles to provide simultaneous diagnosis and sustained drug release over time, the patient will not have to be given repeated drug dosages. Further, systemic side effects of the lung cancer drugs would be reduced due to the site specific and targeted drug delivery. Further, *in vitro* 3D tumor models can help choose the most effective lung cancer drug so that immediate and effective treatment can be provided to the patient following diagnosis. This research is also an important step towards the development of personalized medicine where the patient's own cells can be used to form *in vitro* tissue or tumor models. These models would aid in tailoring the medication more accurately according to the condition of the patient thus providing effective therapy.

Chapter 2

Screening of Polymeric NPs for Protein and DNA Delivery to the Lung by Inhalation

2.1. Introduction

Drug delivery using polymeric NPs is an attractive area of study since the polymers can be co-polymerized, surface-modified or bioconjugated to incorporate desired properties such as hydrophilicity, cell-specific targeting and optimum drug release kinetics. Commonly used nanocarriers for pulmonary drug delivery are made from natural polymers such as gelatin, chitosan and alginate as well as synthetic polymers like poloxamer, PLGA and Poly-(ethylene glycol) (PEG) [85]. Gelatin is a biocompatible and biodegradable natural polymer that can covalently bind to the active compound [86] ensuring greater loading efficiency. Chitosan is a mucoadhesive polysaccharide and permeation enhancer that facilitates prolonged NP retention in the lung following administration [85]. Alginate is another highly biocompatible natural polymer with a hydrophilic matrix useful for protein loading [87]. PLGA is a well-established FDA-approved biocompatible and biodegradable synthetic polymer that demonstrates a bi-phasic drug release over a period of few weeks or months based on the ratio of its constituent monomers [88]. The functional groups on PLGA can also be used for surface modification for incorporation of desired properties of other monomers [3]. Literature has shown that PLGA nano/micro particles are biocompatible and do not cause lung tissue damage after administration [72]. For instance, *in vitro* studies by Tahara et al. [89]confirmed that PLGA NPs in the presence and absence of chitosan coating were cytocompatible with A549 lung epithelial cells up to a high concentration of 5 mg/ml. Also, recent *in vitro* studies on PLGA NPs containing poly vinyl alcohol (PVA) surfactant revealed minimal inflammatory reaction and good cytocompatibility at <1 mg/ml

concentration with A549 cells [90]. Further, histological examination of lung tissue sections following *in vivo* intratracheal instillation of PLGA NPs have shown that these particles do not cause lung tissue damage [91]. Poly-(ethylene glycol) (PEG)-based NPs are well-known for their hydrophilicity, good aerodynamic characteristics and good retention time within the lung following administration [41, 92].

The small size of NPs can make direct delivery to and deposition in the deep lung difficult as they tend to remain suspended in air. Therefore, the mode of pulmonary delivery also plays a crucial role in facilitating NP deposition and distribution in distal lung tissue. As mentioned earlier, an MDI or DPI could result in significant oropharyngeal NP deposition and variation in dosage when the device is not shaken correctly [93]. A nebulizer, on the other hand, can maintain relatively constant size of aerosol droplets in the range that easily allow the suspended NPs to reach the distal lung. For example, Patolla et al. [94] developed celecoxib-loaded lipid nanocarriers (~217 nm size) which could be deposited in the alveolar region of murine lungs following nebulization. A recent study also demonstrated that an Aeroneb™ nebulizer could generate aerosol droplets containing 5(6)-carboxyfluorescein-loaded NPs (195 nm) with aerodynamic properties suitable for alveolar deposition [95].

Recent years have seen an increase in publications on nanoparticle delivery to the lung; however, there have been no studies to our knowledge that corroborated the *in vitro* cellular uptake and retention of NPs with their behavior *in vivo*. Also the optimum NP formulation for prolonged core compound delivery and release as well as relatively longer retention in the lung is unknown. Previously published works have compared the properties of select polymeric (e.g. PLGA, chitosan, gelatin) nano/micro particles for pulmonary delivery of compounds ranging from antibiotics (e.g. tobramycin) to therapeutic drugs (e.g. rifampicin) [96, 97]. However, there have been no comprehensive

studies to our knowledge that attempted to characterize and screen a broad range of commonly used natural and synthetic polymer-based NPs in terms of their potential as carriers of DNA and protein to deep lung tissue by nebulization. Such a study is vital so as to maximize therapeutic efficacy of these NPs following delivery to various lung cells for treatment of pulmonary ailments. Therefore, the goal of this project was to compare various nanoparticle formulations prepared using natural and synthetic polymers and encapsulating protein/dye/cDNA models (bovine serum albumin [BSA], indocyanine green [ICG], rhodamine conjugated to recombinant human erythropoietin [EPO] or plasmid cDNA encoding yellow fluorescent protein [eYFP] or green fluorescent protein, [GFP]) in terms of their physical and chemical properties, *in vitro* cytocompatibilty and cellular uptake by human alveolar Type1 cells, and *in vivo* action following nebulization into rats. This was done to determine the most promising nanocarrier for successful and effective delivery of therapeutic agents to the lung.

2.2. Experimental Section

2.2.1. Materials Used

All chemicals, if not specified, were purchased from Sigma-Aldrich (St. Louis, MO). PLGA (inherent viscosity—0.4 dL/g, copolymer ratio 50:50) was purchased from Lakeshore Biomaterials (Birmingham, AL), chitosan from Polyscience Inc. (Warrington, PA) and NH2-PEG-COOH from Laysan Bio Inc. (Arab, AL). Iron oxide NPs were purchased from Meliorum technologies (Rochester, NY). Primary human alveolar Type 1 cells, Prigrow III media and collagen-coated T25 flasks were obtained from Applied Biological Materials Inc. (Richmond, BC, Canada). Fetal bovine serum (FBS), penicillin-streptomycin, and trypsin-Ethylenediaminetetraacetic acid (EDTA) were procured from Atlanta Biologicals (Lawrenceville, GA).

2.2.2. Synthesis of Natural Polymer-Based NPs

A two-step desolvation method described by Shutava et al. [98] was employed for the synthesis of gelatin NPs. First 1.25 g of Type A gelatin was dissolved in deionized (DI) water and 25 ml of acetone was rapidly added to it. A gel-like precipitate was obtained, which was re-dissolved in water. Then 75 ml of acetone was added dropwise at 40°C to obtain a milky-white solution. 0.2ml of glutaraldehyde crosslinker was then added and the solution was stirred overnight to allow acetone evaporation. The following day, the nanoparticle suspension was dialyzed and lyophilized to obtain gelatin NPs.

Chitosan NPs were prepared by a simple ionic gelation method involving sodium tripolyphosphate (TPP) [99]. Briefly, 10mg of chitosan was added into 5 ml of 1% (w/v) acetic acid and the final pH of the solution was adjusted to 5.5. Following dropwise addition of 2 ml of 1 mg/ml TPP, the solution was stirred for 1 h to allow nanoparticle formation. Dialysis and lyophilization was then carried out to obtain the final chitosan NPs.

Alginate NPs were prepared by cation-induced controlled gelification by modifying the procedure described by Rajaonarivony et al. [100]. Firstly, 9.5 ml of sodium alginate solution (0.06% w/v) was prepared and 0.5ml of 18 mM of calcium chloride was added dropwise to it. 2 ml of chitosan solution (0.05% w/v) was then added and the resultant solution was stirred overnight. Centrifugation at 19,000 rpm for 30 mins followed by lyophilization was done the following day in order to obtain the NPs.

2.2.3 Fabrication of Synthetic Polymer-based NPs

PLGA NPs were prepared by a standard emulsion-solvent evaporation method. For this procedure, 90 mg of PLGA was first dispersed in 3 ml chloroform to form the

organic phase. This was then added dropwise to poly vinyl alcohol (PVA) solution (5% w/v) and sonicated at 50 W for 3 mins. This particle suspension was then stirred overnight at room temperature to allow solvent evaporation. NPs were recovered by ultracentrifugation at 25,000 rpm for 30 mins at 10°C. For BSA loaded NPs, 30 mg of BSA solution was mixed in 300µl of DI water and then emulsified in the PLGA-chloroform solution. Similarly for cDNA loaded NPs, 9 mg of the cDNA was dispersed in DI water and used for emulsification with PLGA solution.

For the preparation of PLGA-chitosan (PLGA-CS) NPs, carboxymethyl chitosan (CMC) was mixed with polyvinyl alcohol (PVA) surfactant solution. The NP preparation procedure is similar to that of PLGA NPs described above, except for the addition of 0.5% (w/v) CMC in 4.5% (w/v) PVA solution.

In order to copolymerize PLGA and PEG, N-hydroxysuccinimide (NHS) group was first introduced onto PLGA using EDC-NHS chemistry, Briefly, 5 g of PLGA was taken in DCM and 1-ethyl-3-(3-dimethylaminopropyl)-carbodiimide (EDC) and N-hydroxysuccinide (NHS) was added to it. Following shaking for 2 h, the PLGA-NHS was collected by washing with ethyl acetate and methanol. 1 g of PLGA-NHS was then dissolved in 4 ml of chloroform and then 250mg of COOH-PEG-NH_2 and 28 mg N,N-diisopropylethylamine was added and stirred for 12 hours. The copolymer was precipitated with cold methanol and washed three times to remove unreacted PEG. This polymer was dried under vacuum and used for NP preparation by the emulsion procedure described above [101]. Bovine serum albumin (BSA) was used as protein model while YFP or GFP-encoded plasmid cDNA was used as cDNA model for encapsulation within all six NPs. All NPs were lyophilized and stored in powder form at -20^{o}C when not in use and were freshly reconstituted in DI water/media/saline/Gamble's solution for our experiments.

2.2.4 Characterization of NPs

The NP size, charge and polydispersity were determined using ZetaPALS dynamic light scattering (DLS) detector (Brookhaven Instruments, Holtsville, NY). Briefly, 20 µl of 1mg/ml NP suspension was added to a transparent cuvette containing 3 ml DI water and placed in the instrument. The NP properties were detected by scattering of laser light due to Brownian motion of the NPs in solution. Transmission electron microscopy (TEM, FEI Tecnai G2 Spirit BioTWIN, Hillsboro, OR) was used to study the morphology of the particles. Briefly, a drop of particle suspension (1 mg/ml) was placed on a Formvar-coated 200-mesh copper grid (Electron Microscopy Sciences, Hartfield, PA) at room temperature and air-dried. The sample was then inserted into the TEM instrument for visualization.

2.2.5. Physical-Chemical Characterization

The *in vitro* stability of the NPs was determined by dispersing them in 4 different solutions, namely DI water, saline (0.9% sodium chloride solution), fetal bovine serum (FBS) or simulated lung fluid (Gamble's solution, prepared as described by Marques et al. [102]). The NP suspensions were then incubated at 37^{o}C and particle sizes measured using DLS at predetermined timepoints up to 5 days. In addition, drug release studies were conducted on the NP formulations. The amount of un-entrapped reagent collected in the supernatant after centrifugation was quantified to determine the drug loading efficiency of the NPs. The protein/cDNA encapsulation efficiency can be calculated as the percentage of protein/cDNA used initially during nanoparticle formulation (Equation 1).

$$Loading\ efficiency\ (\%) = \frac{Protein/cDNA\ used - Protein/cDNA\ in\ supernatant}{Protein/\ cDNA\ used} \quad (1)$$

For *in vitro* release studies, BSA was used as the protein model for encapsulation within the NPs. Briefly, 1 ml of nanoparticle suspension (1 mg/ml) was added to dialysis bags with molecular weight cut-off of 100 kDa (Spectrum Laboratories Inc., Rancho Dominguez, CA) and dialyzed against DI water at 37°C for 21 days. At each time points, 1 ml of dialysate was collected from the samples and replaced with 1 ml of fresh DI water. Pierce BCA protein assays (Fisher Scientific, Hampton, NH) was used according to the manufacturer's instructions in order to quantify the amount of protein released.

2.2.6. In Vitro Cell Studies

Human alveolar Type 1 epithelial cells (AT1) were seeded in 96–well tissue culture plates at a density of 16,000 cells/cm^2 and incubated at 37^oC and 5% CO_2 overnight for cell attachment. The following day, media in each well was aspirated and replaced with increasing concentration (0, 100, 200, 300, 500, 1000, 2000 µg/ml) of NP suspensions in media for 24 hours. The wells were then washed twice with 1X Phosphate buffered saline (PBS) and incubated with MTS reagent (CellTiter 96®AQueous One Solution Cell Proliferation Assay, Promega, Madison, WI) in media. Absorbance readings were taken at a wavelength of 490 nm using a UV–Vis spectrometer (Infinite M200 plate reader, Tecan, Durham, NC), to determine cell viability. In order to confirm the MTS assay results, a Picogreen dsDNA assay was also performed to determine the DNA content per sample. For this assay, the cells were first lysed using 1% Triton X-100 and then the assay was conducted on the cell lysates per manufacturer's instructions.

For cellular uptake, AT1 cells were seeded in tissue culture plates and incubated as described above. Then the cells were incubated with increasing concentrations (0,

100, 200, 300, 500 µg/ml) of ICG-loaded NPs suspended in media for 2 h. Following incubation, the cells were washed 3 times with PBS and lysed using 1% Triton X-100. Fluorescence intensity measurement of each sample was carried out using a spectrophotometer at excitation of 780 nm and emission of 810 nm to determine the amount of ICG-loaded particles taken up by the cells. These measurements were analyzed against nanoparticle standards. The particle uptake was then normalized with the total DNA content per sample using Picogreen dsDNA assays (Invitrogen, Grand Island, NY) at excitation of 480 nm and emission of 520 nm. The cell lysate sample is usually quantified for the total cell protein or DNA, which presents the cell number per sample, using protein or DNA assays. However, EPO- and cDNA-loaded NPs will interfere with the readings for both these assays. Therefore, we used ICG-loaded particles for this study since the fluorescence readings will not interfere with our quantification of the total cell protein/DNA in the cell lysate samples.

Finally, a cell activation study was conducted to determine whether NP uptake causes oxidative stress in the cells *in vitro*. Briefly, human AT1 cells were seeded in tissue culture plates and incubated overnight as described earlier. The following day, cells were exposed to two different concentrations of each NPs (250 µg/ml and 1000 µg/ml) and incubated for a further 24 hours. Cells exposed to 10 µg/ml lipopolysaccharide (LPS) were considered as a positive control while cells exposed to media only served as the negative control. To detect the Intracellular Reactive Oxygen Species (ROS) production on NP exposure, cells were then washed thrice with PBS and incubated with 5µM of 2', 7'-dichlorodihydrofluorescein diacetate (H_2DCFDA) solution in PBS for 30 mins. The cells were then again washed with PBS and fluorescence was measured at λ_{ex} of 485 nm and λ_{ex} of 530 nm using a spectrophotometer.

2.2.7. In Vivo Studies

2.2.7.1. Acknowledgements

All *in vivo* work for this project including nebulization of NPs into the animals, histology and biomaging were conducted by Dr. Priya Ravikumar, Dipendra Gyawali and Roshni Iyer from Dr. Connie Hsia's laboratory at UTSW.

2.2.7.2 *In Vivo* Delivery of Protein- or cDNA- Loaded Gelatin and PLGA NPs

All animal procedures were conducted at UTSW following approval from the Institutional Animal Care and Use Committee (IACUC) at UTSW. First Sprague-Dawley rats (300-400 grams body weight) were given intraperitoneal injection of ketamine (50 mg/kg) and xylazine (5 mg/kg) for anesthesia. An otoscope was used to visualize the larynx and then a guide wire was used to insert a 14 gauge cannula into the trachea. Heart rate and transcutaneous oxygen saturation was monitored throughout the experiment. Based on the characterization results, PLGA and gelatin NPs were chosen for *in vivo* studies. 4.5 mg of NPs encapsulating a) yellow fluorescent protein (pEYFP-N1, kindly provided by Dr. Makoto Kuro-o, Dept. of Pathology, UTSW) encoded plasmid DNA or b) recombinant human EPO (Cell Sciences, Canton, MA, 100 IU/kg body weight) was dispersed well in 0.5 ml of sterile 0.9% saline, and aerosolized through the cannula for 3 min using a pediatric mesh nebulizer (Aeroneb™, 4-6µm droplets). Only one nanoparticle formulation was given per animal. NPs encapsulating empty vectors were aerosolized into the control group by the same method. The rats were observed until complete recovery from anesthesia following NP administration.

At predetermined timepoints (3, 5 and 7 days post-treatment), rats were sacrificed by giving an intraperitoneal injection of Euthasol™ overdose (pentobarbital 86

mg/kg and phenytoin 11 mg/kg) which stops the heart. Tracheal instillation of 4% paraformaldehyde at 25 cm H_2O of airway pressure was done to inflate the lungs and then remove them intact. The lobes were then fixed and serially sliced at 3 mm intervals. The slices were then imaged by a biofluorescence imager (CRI Maestro 2, Cambridge Research & Instrumentation Inc, Waltham, MA). The tissue was fixed by embedding in paraffin, and the histological sections (4 µm thickness) were visualized using a confocal microscope. Similarly in order to study the biodistribution of NPs, the kidney and liver was also removed and serially sliced followed by imaging using biofluorescence imager and confocal microscopy.

2.2.8. Development of PLGA-SPIO NPs

Based on the results obtained in the above studies, PLGA NPs was found to be most promising as nanocarriers for delivery of active compounds (protein and DNA) to the lung by nebulization. In order to validate pulmonary delivery of PLGA NPs and release of its encapsulated agents at the intended site, SPIO-encapsulated PLGA NPs (PLGA-SPIO NPs) were developed. A similar procedure as that of PLGA nanoparticle preparation was followed. 20 mg of SPIO and 90 mg of PLGA was added to 2 ml chloroform and sonicated for 8 mins at 20 W. This mixture was then added dropwise to PVA solution (5% w/v) and sonicated at 50W for 10 mins. Following overnight stirring for chloroform evaporation, the NP solution was centrifuged at 1000 rpm for 2 min to remove unloaded SPIO aggregates, which forms the pellet. The supernatant containing the prepared PLGA-SPIO NPs was then centrifugation at 25,000 rpm, 20 mins followed by lyophilization to get the NPs.

2.2.9. Characterization of PLGA-SPIO NPs

In addition to particle characterization by DLS and TEM, Fourier transform infrared (FTIR) spectroscopy was also performed to ensure that SPIO has indeed been incorporated within our PLGA particles. Iron content within these particles was further assessed using a standard iron assay as described previously [103]. Briefly, a 48 well plate was taken and 100 µl of PLGA-SPIO NPs (1 mg/ml) was added to the wells. Then 100 µl of 50% v/v hydrochloric acid (HCl) was added and the plates were incubated overnight at 37^{o}C. The following day, 1mg/ml of ammonium per sulfate (APS) solution was added to the wells. The wellplate was incubated at 37^{o}C for 15 mins following which 0.1 M potassium thiocyanate (PTC) solution was added. The wellplate was incubated at 37^{o}C for 15 mins more following which absorbance readings were taken at 478 nm using a spectrometer. A superconducting quantum interference device (SQUID; Quantum Design) magnetometer was used to study the magnetic properties of the particles prepared, as detailed by Wadajkar *et al*. [104]. Briefly, the nanoparticle powder was embedded in epoxy resin beads and exposed to varying magnetic fields at room temperature to obtain the hysteresis loop. This was then compared to the hysteresis loop of bare SPIO obtained by the same method.

In addition to characterization of magnetic properties, the particles were also studied for their stability in various solutions such as DI water, 10% FBS, 0.9% saline and Gamble's solution as mentioned earlier. Release studies were also conducted as explained above using BSA- and Texas Red Albumin (TR-A)-loaded PLGA SPIO NPs. TR-A release was measured based on fluorescence readings at λ_{ex} 596 nm and λ_{em} 615 nm.

2.2.10. In Vitro Studies on PLGA-SPIO NPs

The cytocompatibility of PLGA-SPIO NPs was tested on both human AT1 cells as well as human dermal fibroblasts (HDFs). The influence of nanoparticle dose and incubation time on cellular uptake was also determined. Dose-dependent cellular uptake was done as explained in section 2.2.6. To study time-dependent uptake, the cells were incubated with NPs at a fixed concentration of 100 µg/ml for varying durations (1, 2, 4 and 6 hrs). Following particle incubation, the cells for both uptake studies were extensively washed to remove free NPs and lysed using 1X- Triton solution. The amount of NPs taken up by the cells was measured using iron assays. The amount of total cell protein per well was measured by Pierce BCA assay and used to normalize the iron uptake results.

A study was also conducted to determine activity of compounds released from PLGA NPs. Briefly, PLGA NPs encapsulating recombinant human erythropoietin (EPO, Cell Sciences, Canton, MA) (2mg/ml) was incubated in incomplete RPMI media at 37ºC for 5 days. At the end of the study, the samples were centrifuged and the supernatant was collected. This supernatant containing released EPO was tested for its ability to maintain the viability of Ba/F3 cells known to stably overexpress EPO receptor and require EPO for survival (courtesy of Dr. Lily Huang, Dept. of Cell Biology, UT Southwestern Medical Center). The groups used for this study include a) RPMI only, b) EPO (100 IU/ml) in RPMI, c) EPO (100 IU/ml) with empty PLGA NPs (2 mg/ml) in RPMI, and d) RPMI containing EPO released from PLGA NPs. Briefly, Ba/F3 cells grown in WEHI (Walter and Eliza Hall Institute)-conditioned medium at a density of $5x10^5$ cells per well were washed and switched to RPMI medium. These cells were incubated for 72 h at 37ºC following addition of 90 µl of supernatants obtained earlier after the 5 day

incubation. Cell viability was determined by MTT assays following manufacturer's instructions.

2.2.11. In Vivo Studies on PLGA-SPIO NPs

2.2.11.1. Acknowledgements

All the *in vivo* work including nebulization, histology, Prussian blue staining, TEM and bioimaging for this part of the project was conducted by Dr. Priya Ravikumar from Dr. Connie Hsia's laboratory at UTSW. MRI was performed at Dr. Masaya Takahashi's laboratory at UTSW.

2.2.11.2 *In Vivo* Delivery of PLGA-SPIO NPs Encapsulating Various Payloads

Animal procedures were conducted at UTSW with the approval of the Institutional Animal Care and Use Committee (IACUC) at UTSW. PLGA-SPIO NPs were synthesized as described above, loaded with different fluorescent probes: near-infrared dye (NIR-797), rhodamine conjugated bovine serum albumin (BSA-rhodamine), Green Fluorescent Protein (GFP) (Santa Cruz Biotechnology Inc., Santa Cruz, CA), or plasmid DNA vector encoding yellow fluorescent protein (pEYFP-N1). These particles were administered to Sprague Dawley rats as explained previously. One hour following inhalational delivery of PLGA-SPIO NPs, the anesthetized animals underwent MRI (3T whole-body human scanner Achieva^{TM}, Philips Medical Systems, Best, Netherlands) with a small animal solenoid radio- frequency (RF) coil (63 mm in diameter and 100 mm in length; Philips Research Europe, Hamburg) using a three-dimensional ultrashort echo time (UTE, echo time <500 μs) sequence with projection acquisition of free induction decay. This sequence enabled us to compare endogenous signal intensity (SI) of the lung

parenchyma [105] with SI of our experimental group as well as the control group which was given saline only.

At 3, 5 and 7 days post-treatment, rats were killed by an intraperitoneal injection of Euthasol™ overdose and lung slices imaged by a biofluorescence imager while histological sections were examined under a fluorescent microscope. Further, Prussian Blue staining was done to visualize iron particles uptake by lung cells, using light microscopy and TEM.

2.3. Results and Discussions

2.3.1. Characterization of Natural and Synthetic Polymer-Based NPs

In this study, six common NP preparations made of natural and synthetic polymers were screened to determine the most promising formulations for pulmonary delivery and uptake by distal lung cells. Our characterization results indicate that most NPs except PLGA-PEG and alginate NPs maintained a hydrodynamic diameter under 300 nm (Table 2.1). The larger size of alginate NPs (556±56 nm) agrees with results of Yang et al.[106] who prepared alginate NPs based on the ionic gelation method, with sizes in the 536 nm to 1.8 µm range for gene therapy. However, as mentioned earlier, NPs in the 50 to 200 nm size range have demonstrated greater alveolar deposition [22]. Thus, most of our NP formulations except alginate and PLGA-PEG were in the desirable size range as nanocarriers for pulmonary delivery. The smaller polydispersity values of PLGA and PLGA-CS NPs (0.14 and 0.07, respectively) indicate that they are relatively uniformly dispersed. Chitosan and alginate NPs on the other hand demonstrated larger polydispersity values (0.28 and 0.29, respectively), indicating more variation in their particle size distribution. The positive zeta potential value of chitosan NPs indicates

presence of cationic NH_2 groups on the surface of the particle while high negative zeta potential values of the other NP formulations are indicative of good stability.

Table 2.1 Size, charge and polydispersity characterization of NP formulations

Polymer	Particle Diameter (nm)	Polydispersity	Zeta Potential (mV)
Gelatin	187 ± 83	0.22 ± 0.01	-18.2 ± 2.6
Chitosan	253 ± 110	0.28 ± 0.02	4.8 ± 1.1
Alginate	556 ± 56	0.29 ± 0.01	-28.7 ± 0.9
PLGA	160 ± 63	0.14 ± 0.02	-20.2 ± 1.2
PLGA - CS	191 ± 60	0.07 ± 0.01	-17.2 ± 1.3
PLGA - PEG	335 ± 131	0.22 ± 0.03	-25.4 ± 1.0

Transmission Electron Microscopy (TEM) images were taken to observe the morphology and distribution of all nanoparticle formulations. It was seen that all particles are relatively spherical in morphology and are uniformly dispersed (Figure 2.1). In addition, the particle sizes in the images are in accordance with the size ranges observed

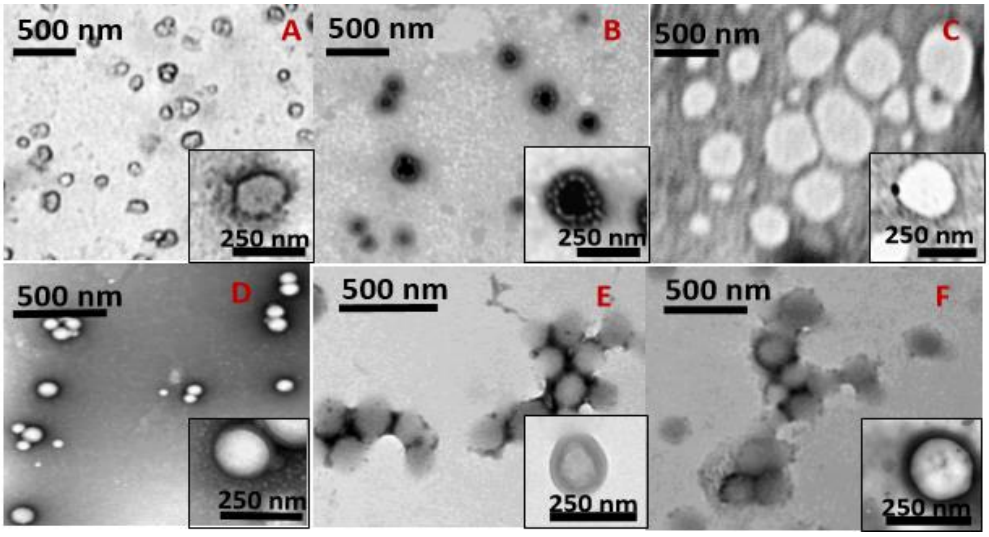

Figure 2.1 TEM images of NPs prepared using (A) gelatin, (B) chitosan, (C) alginate, (D) PLGA, (E) PLGA-CS and (F) PLGA-PEG. The insets represent the morphology of a single nanoparticle from each formulation

using the dynamic light scattering (DLS) instrument.

Stability studies of NPs suspended in DI water, 10% fetal bovine serum, 0.9% saline and simulated lung fluid were also conducted. PLGA NPs were relatively stable in all 4 solutions over 5 days with no significant aggregation or particle size change, which is in agreement with previous studies [88, 107]. Gelatin NPs were also stable in all solutions agrees with previous studies on these particles prepared by the layer-by-layer method, that demonstrated stability up to 4 weeks after preparation [108]. The observed aggregation of our chitosan NPs in media and serum concur with the results by Gan et al. [109], where chitosan particle aggregation was observed at different pH conditions and

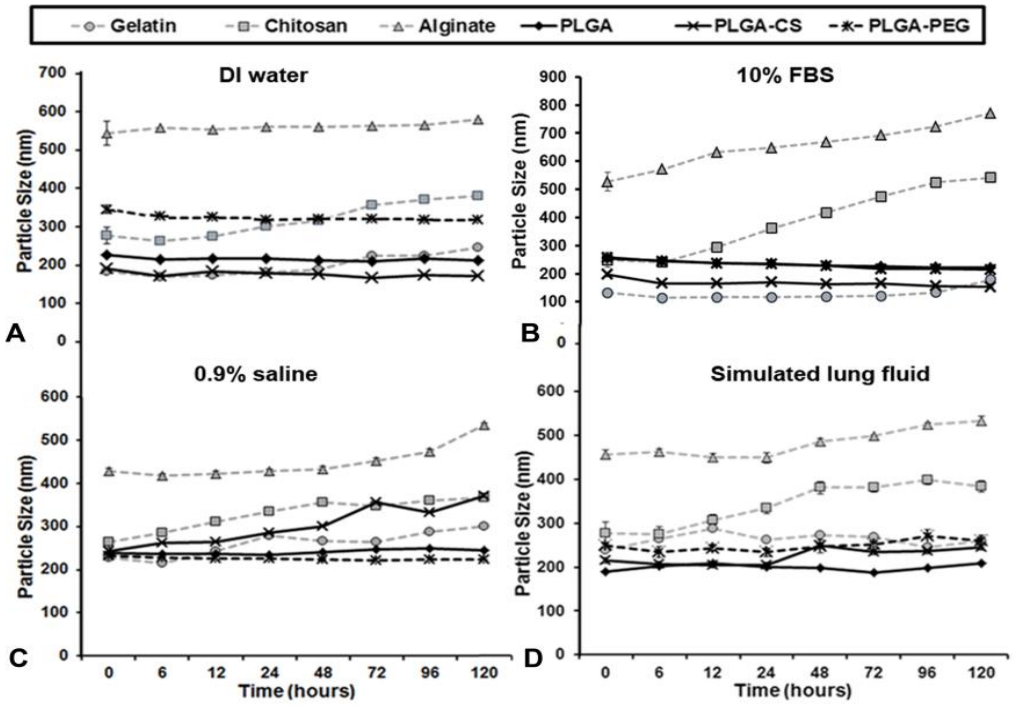

Figure 2.2 Stability of all NPs tested by measuring particle size in (A) DI water, (B) 10% FBS (C) saline solution and (D) simulated lung fluid at 37^{o}C. The PLGA-based and gelatin NPs remained stable for up to 5 days while alginate NPs tended to show aggregation by the 4th day. Chitosan NPs showed fluctuations in size indicating comparatively less stability (n=4)

particle concentrations due to thermodynamic instability of the system. Alginate NPs also showed significant aggregation in serum, saline and simulated lung fluid as demonstrated by previous studies where alginate-chitosan NPs tended to break apart at a pH of 7.0 due to their instability at physiological pH [110]. PLGA-CS NPs remained relatively stable in DI water, serum and simulated lung fluid although some aggregation was observed in saline solution possibly due to chitosan's thermodynamic instability with pH changes (Figure 2.2).

Further, drug release studies indicate that >80% of incorporated BSA was released from all particles in a biphasic manner within 3 weeks. Among natural polymer-based NPs, gelatin demonstrated a burst release of about 32% of the drug in 2 days while chitosan and alginate NPs showed burst release of 43% and 27% of the drug, respectively, within the same time period. The high burst release (about 43%) from chitosan NPs within 2 days was similar to the ~40% BSA release within 48 h observed by Gan et al. [109] using NPs prepared with medium molecular weight chitosan, which was also used by us in our preparation (Figure 2.3A).

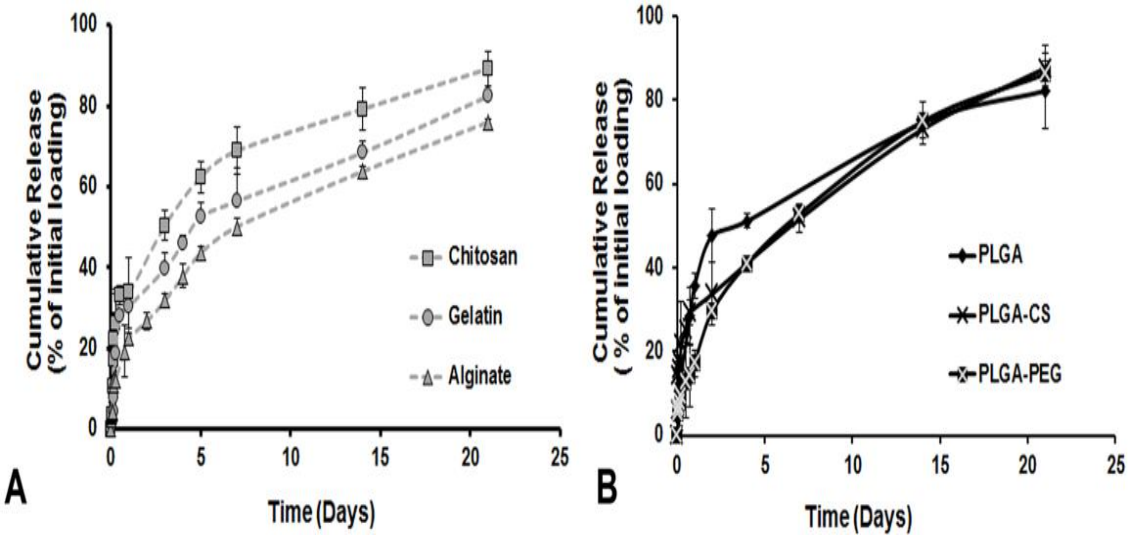

Figure 2.3 Bi-phasic drug release profile of all NPs indicating a burst release for the first 2 days followed by sustained release over 3 weeks. Gelatin, Chitosan and PLGA NPs showed an initial burst release of more than 40% loaded drug within 4 days (n=4)

The highest burst release among all NPs was observed for PLGA NPs (about 48%) within 2 days followed by a characteristic sustained release up to 21 days (Figure 2.3B), which was similar to the drug release profile seen in the literature [88, 111]. Although we observed higher burst release from PLGA than from PLGA-PEG NPs (about 30%) , Li et al. [112] detected higher initial BSA release from the latter. This may have occurred due to the different PEG compounds used in their experiments and the availability of different functional groups on the NPs that may interact different with different encapsulated compounds. On the other hand, Parveen et al. [113] observed slightly reduced paclitaxel release from PLGA-CS and PLGA-PEG NPs than from PLGA NPs, which is consistent with the results obtained by us.

2.3.2. In Vitro Characterization of the Different Polymeric NPs

The cytocompatibility with AT1 cells observed by us for gelatin NPs (~80% viability at 2 mg/ml) is similar to the value reported by Tseng et al. [114] using human fetal lung fibroblasts (HFL1). Our chitosan NPs maintained greater than 80% cytocompatibility up to a concentration of 1 mg/ml which is in agreement with studies by Grenha et al. [115] that showed ~80% viability for human bronchial Calu-3 cells and A549 alveolar epithelial cells viability at an NP concentration of 1 mg/ml. Similarly, our alginate NPs showed a comparable cell viability (92% cell viability at 250 µg/ml concentration) as reported in previous studies using T47D breast cancer cells (~90% viability at 50 µg/ml NP concentration, 24h incubation) [116]. The higher cytocompatibility observed for PLGA-based NPs in our studies agrees with results by Mura et al. [117], which showed more than 80% viability of Calu-3 cells incubated with PLGA and PLGA-CS NPs up to a concentration of 5 mg/ml for 24 hours. These results indicate that all of our NP

formulations are compatible with lung cells up to a high concentration of 1 mg/ml (Figure 2.4 A, B).

These findings were confirmed using Picogreen dsDNA assays. More than 90% of the total cell DNA was retained following incubation with PLGA- based NPs at all concentrations (Figure 2.4D) while ~ 80% of control DNA content was obtained following treatment with gelatin and chitosan NPs up to 2 mg/ml concentration (Figure 2.4C). Incubation with alginate NPs resulted in a decrease in DNA content to 76% at 2mg/ml concentration. It should be noted, however, that more than 80% of the DNA content was observed in all samples following incubation with all particles up to 1 mg/ml concentration

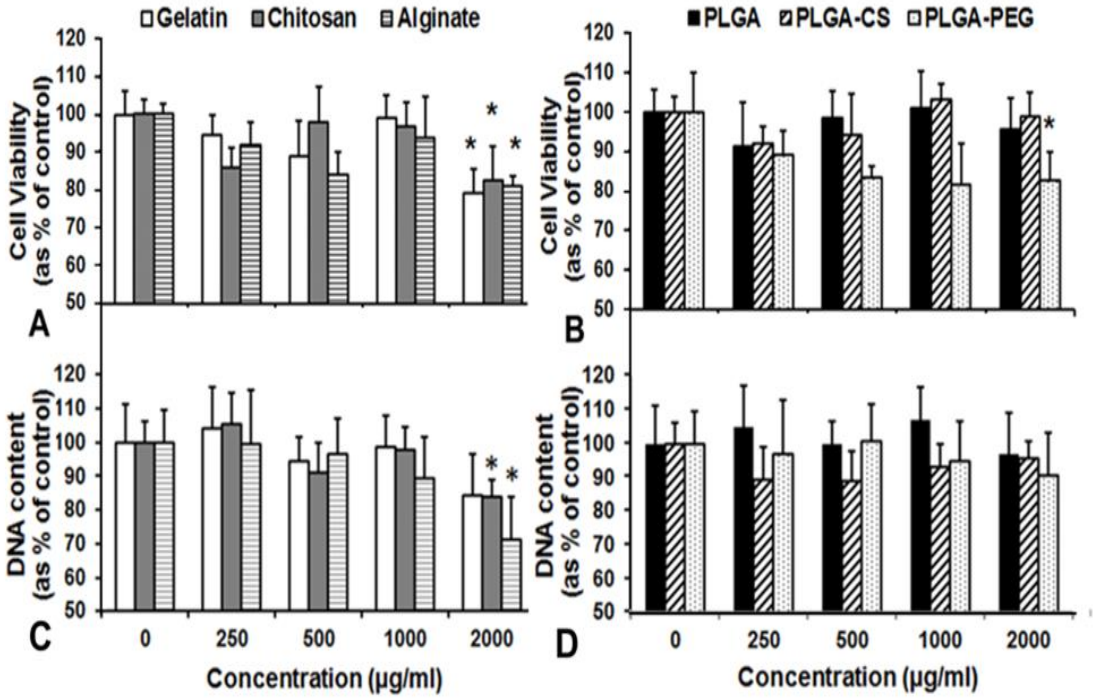

Figure 2.4 Cell viability studies on AT1 epithelial cells using (A, B) MTS assay and (C, D) Picogreen ds DNA assay indicated that gelatin, chitosan, alginate and PLGA-PEG NPs maintained cytocompatibility up to a concentration of 1000 µg/ml. All NPs except alginate showed greater than 80% DNA content at 2000 µg/ml concentration. (n=3, *p<0.05 w.r.t cell viability at 0 µg/ml MDNP concentration)

indicating that these particles are cytocompatible up to 1mg/ml. This indicates that all the NP formulations are cytocompatible at high concentrations with AT1 cells *in vitro.*

The uptake of all NPs by AT1 cells following a 2 h-incubation with increasing NP concentrations was studied. All of our NP formulations exhibited concentration-dependent uptake by human AT1 cells. These results are in keeping with reports by other groups that tested various NP formulations on different cell lines. For example, complexes of gelatin NPs and biotinylated epithelial growth factor (EGF) conjugated with NeutrAvidin^{FITC} demonstrated increasing NP uptake by A549 cells up to a concentration of 200 µg/ml [114]. Nam et al. [118] observed a similar dose-dependent uptake of hydrophobically modified glycol chitosan NPs by HeLa cervical cancer cells up to 200 µg/ml concentration. The dioctylsodium sulfosuccinate (AOT)-sodium alginate NPs formulated by Chavanpatil's group [119] also showed dose-dependent uptake when incubated with MCF7 breast cancer cells and MCF7-ADR cells (a multidrug resistant sub-line of MCF7). Chen et al. [120] demonstrated concentration-dependent uptake of PLGA-PEG NPs by MCF7 cells. Further, the dose-dependent uptake of PLGA and chitosan-modified PLGA NPs by A549 cells observed by Tahara et al. [89] is comparable to our results using PLGA and PLGA-CS NPs. However, contrary to our results, this group observed greater PLGA-CS uptake than PLGA NP uptake. This difference may have occurred due to differences in the chitosan concentration used for preparation as well as variations in formulation techniques (Figure 2.5).

We observed a higher *in vitro* NP uptake of natural polymer-based NPs than synthetic-polymer based NPs by lung cells grown in culture. This disparity could have occurred due to differential uptake rates of different polymer-based NPs by cells over time. We previously demonstrated variation in uptake rates of PLGA-based NPs by different cells in a concentration and incubation time-dependent manner [88, 121].

Interactions between the cell membrane and polymers could affect the uptake of NPs by human AT1 cells [122]. For example, the negatively-charged cell membranes would favor the positively-charged chitosan NPs, resulting in higher cellular uptake of these particles [123].

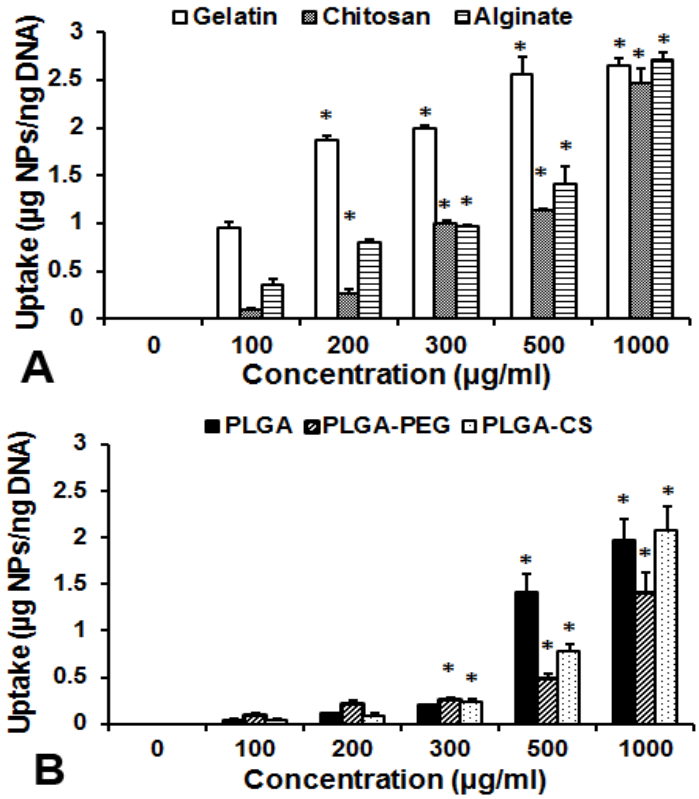

Figure 2.5 Cellular uptake of all NP formulations by alveolar Type 1 epithelial cells was studied using BCA protein assay and fluorescence readings from NPs after 2h incubation with increasing NP concentrations. Dose-dependent increase in cellular uptake was observed with increasing NP concentration (n=3, *p<0.05 w.r.t to cellular uptake at 100 µg/ml)

Finally, cell activation study was conducted to determine whether NP uptake by AT1 cells can cause oxidative stress. ROS are factors and free radicals known to cause

oxidative stress and eventual apoptosis in cells. Inhalation of toxic substances can result in overproduction of ROS by the cells which in turn can cause inflammation in the lung [124]. In this study, ROS produced by cells cultured in media only served as a control. We observe that chitosan and PLGA-PEG NPs showed greater ROS production (172 and 175 % of the control respectively) at 1000 µg/ml concentration among all the formulations (Figure 2.6). Treatment with Alginate NPs also triggered ROS production (132% and 147% w.r.t control at 250 µg/ml and 1000 µg/ml concentrations respectively). Gelatin and PLGA NPs on the other hand triggered minimal ROS production (127 and 122 % of the control respectively at 1000 µg/ml concentration). LPS initiated ROS production that was

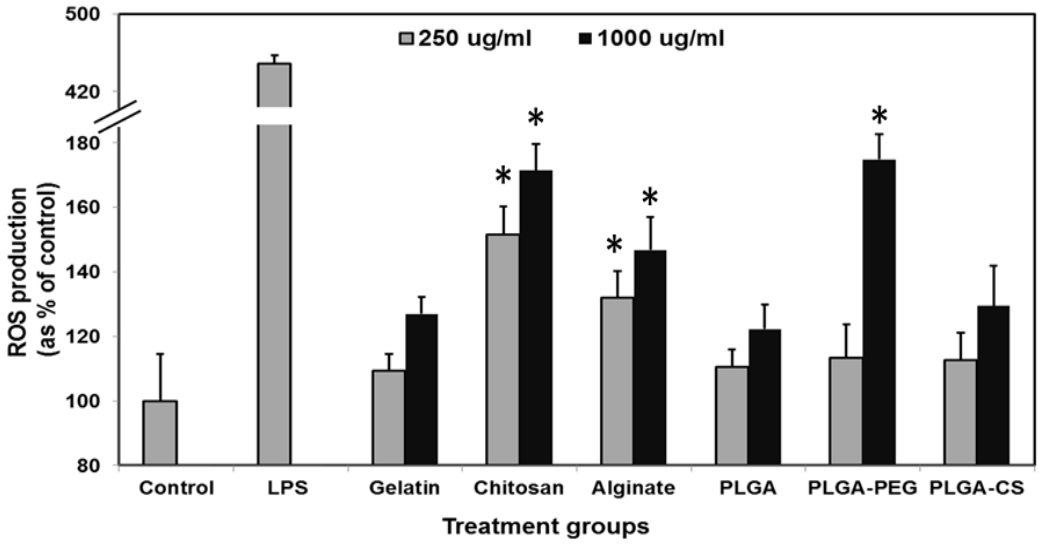

Figure 2.6 The effect of NPs on ROS production by Alveolar Type 1 cells following a 24 hour exposure. ROS production was calculated as a percentage of control (cells grown in media only). Significant ROS production was seen in cells exposed to both concentrations of chitosan and alginate NPs compared to the control samples. Significant ROS production was also observed on treatment with 1 mg/ml PLGA-PEG NPs (*$p<0.05$ w.r.t control)

425% of the control. Previous studies on BALB/c mice have reported the moderately proinflammatory properties of PEGylated nanocarriers 48h following instillation, which is in keeping with our *in vitro* study [125]. The inflammatory effects of chitosan observed by us also concur with previously published *in vivo* reports where chitosan microparticles caused dose-dependent inflammatory effects in rat lungs following inhalation [126, 127]. However this inflammation was reported to be mild compared to that induced by LPS, as also observed by us.

Taken together, our results imply that gelatin and PLGA NPs possess the most promising characteristics as nanocarriers for pulmonary delivery of biological agents (Table 2.2). Both nanocarriers were within the appropriate size range for alveolar deposition with minimum clearance by alveolar macrophages. Further, they showed excellent stability, good cytocompatibility and dose-dependent uptake by AT1 cells. Due to their overall promising features, both PLGA and gelatin NPs were chosen for our preliminary *in vivo* studies.

Table 2.2 Comparison of physical-chemical, in vitro and in vivo characteristics of the formulated NPs

Nanoparticle	**Natural polymer-based**			**Synthetic polymer-based**		
	Gelatin	**Chitosan**	**Alginate**	**PLGA**	**PLGA-CS**	**PLGA-PEG**
Size <200 nm	Yes	No	No	Yes	Yes	No
Stability at 5 d	Yes	No	No	Yes	Yes	Yes
Burst core release (2 d)	<40%	>40%	<40%	>40%	<40%	<40%
Sustained core release (3 wk)	>80%	>80%	<80%	>80%	>80%	>80%
Time and concentration dependent cell uptake	Yes	Yes	Yes	Yes	Yes	Yes
Cytocompatibility	Up to 1 mg/ml	Up to 1 mg/ml	Up to 1 mg/ml	Up to 2 mg/ml	Up to 2 mg/ml	Up to 1 mg/ml
Pulmonary distribution of delivered or expressed protein following nebulization	Less uniform or sustained	-	-	More uniform and sustained	-	-

2.3.3. In Vivo Properties of Gelatin and PLGA NPs

A single dose of gelatin or PLGA NPs incorporating YFP DNA or recombinant human EPO nebulized to the lungs of anesthetized and intubated rats resulted in widespread and increasing fluorescence throughout lung tissues up to 7 days. The pattern of distribution observed in lung slices and histological sections increased from punctate (day 3) to diffuse (days 5 and 7) in all lobes, consistent with persistent gene

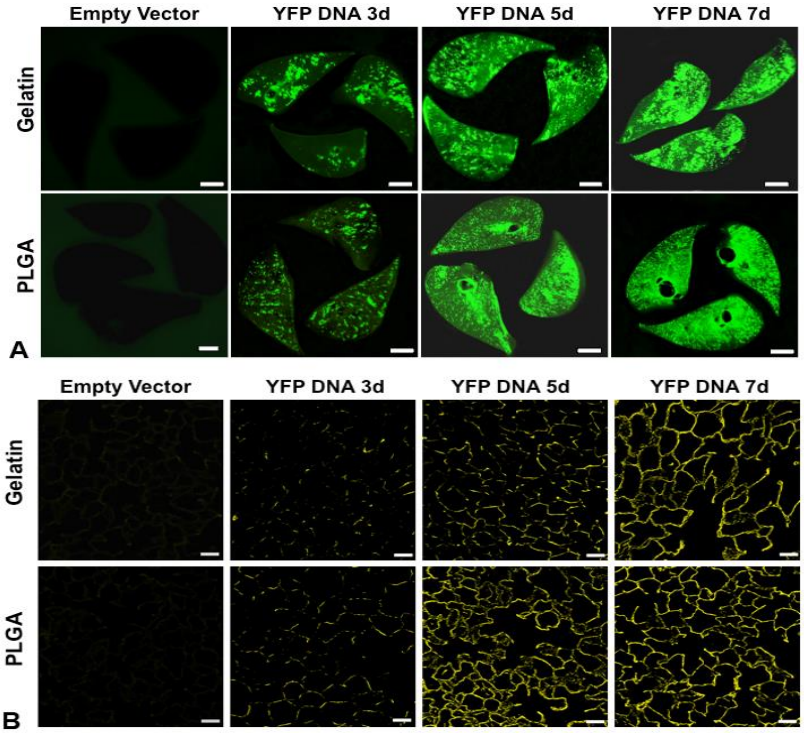

Figure 2.7 Panel A*:* Biofluorescence of rat lung slices fixed at 3, 5 and 7 d after nebulization of gelatin or PLGA based NPs loaded with YFP cDNA, compared to control lungs following nebulization of the corresponding NPs loaded with empty vector (bar=0.5 cm). The panels show increasing YFP expression up to 7 d following nebulization; expression was greater and more uniform using PLGA than gelatin NPs. Panel B*:* Confocal fluorescence microscopy of histological sections taken from the corresponding lungs shows increasing and widespread YFP expression up to 7 d post-inhalation compared to the respective controls (bar=50 µm).

expression and YFP production by lung cells (Figure 2.7A and 2.7B).

Similarly, a single inhalational dose of gelatin or PLGA NPs incorporating EPO-rhodamine resulted in widespread fluorescence in lung tissue that persisted for at least 10 days (Figure 2.8A and 2.8B). At the same delivered dose of cDNA or protein, tissue expression was uniform following inhalation of both protein and cDNA-loaded PLGA and gelatin NPs. However, uniform protein expression was observed for a longer time following inhalation of PLGA NPs than that following gelatin NP inhalation.

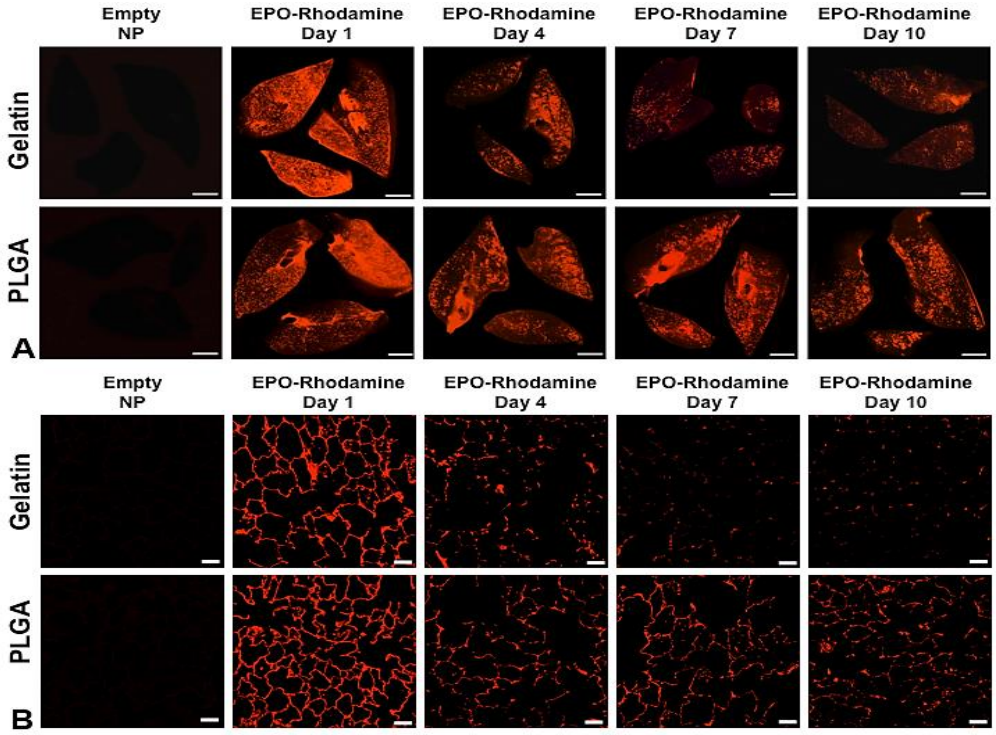

Figure 2.8 Panel A*:* Biofluorescence of rat lung slices fixed at 1, 4, 7 and 10 d following nebulization of gelatin or PLGA-based NPs loaded with rhodamine-conjugated recombinant human erythropoietin (EPO-Rhodamine) compared to control lungs following nebulization of the corresponding empty NPs (bar=0.5 cm). Panel B*:* Confocal fluorescence microscopy of histological sections taken from the corresponding lungs. These panels show more sustained fluorescence up to 10 days post-inhalation using PLGA NPs compared to those of gelatin NPs (bar=50 µm)

Although AT1 cells showed greater uptake of gelatin NPs than PLGA NPs *in vitro*, the *in vivo* lung tissue distribution profile was relatively similar for both PLGA and gelatin NPs loaded with YFP cDNA. Greater fluorescence was observed with time in lung slices of animals administered Rhodamine-tagged EPO encapsulated PLGA NPs than gelatin NPs containing the same protein. Studies have shown that cellular uptake decreases with increasing size and hydrophilicity of the polymeric NPs [128]. Therefore, the observed variation between *in vitro* and *in vivo* results could potentially be explained by the slightly larger size of gelatin NPs following drug encapsulation (~260 nm), which could result in more rapid clearance by alveolar macrophages. The inherent hydrophobicity of PLGA may have contributed to its greater uptake *in vivo* compared to the hydrophilic gelatin NPs. Additional factors in intact lung, such as the amount and physical properties of alveolar lining fluid as well as various extracellular and intracellular clearance mechanisms, could also have differentially influenced the distribution, penetration and retention of nebulized NPs in tissues. These data thus illustrate the importance of verifying *in vitro* test results with *in vivo* results. Our results suggest that PLGA and gelatin NPs can be used as potential nanocarriers for inhalational delivery of proteins and DNA are about equal, but PLGA NPs are more effectively retained in the distal lung under physiological conditions.

Further biodistribution studies were conducted to determine the fate of the NPs following nebulization. PLGA NPs containing green fluorescent protein (GFP) encoding human erythropoietin receptor (EPOR) cDNA was nebulized into anesthetized and intubated animals. Fluorescence was observed in kidney and liver slices of the nebulized animals from day 4 until day 21 indicating that some of the NPs entered the systemic circulation from the lung following nebulization and were expressed in other organs

including the liver and kidneys (Figure 2.9). Further studies would need to be done to determine the route of elimination of these NPs from the body.

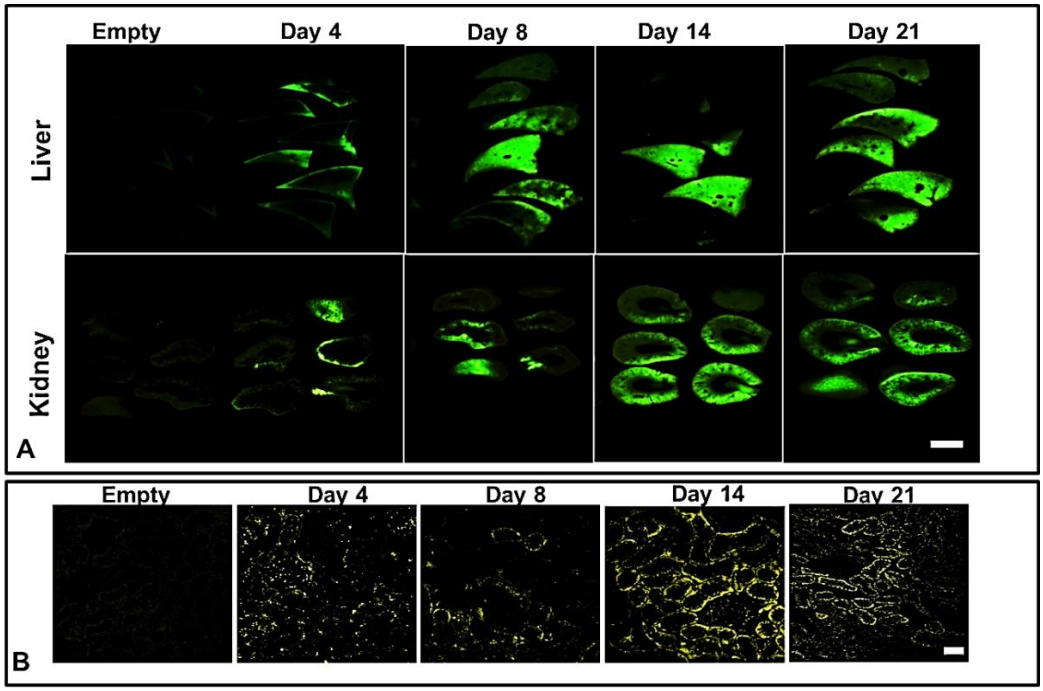

Figure 2.9 Biodistribution of NPs following nebulization. Panel A*:* Biofluorescence of rat liver and kidney slices fixed at 4, 8, 14 and 21 d following nebulization of gelatin or PLGA-based NPs loaded with Green fluorescent protein (GFP)-tagged human EPOR cDNA compared to those of control samples (nebulization of the corresponding empty NPs) (bar=0.5 cm). Panel B*:* Confocal fluorescence microscopy of the kidney cortex showing fluorescence up to 21 days (bar=50 µm).

2.3.4. Characterization of PLGA-SPIO NPs

Our PLGA-SPIO NPs had an average size of 250+97 nm and polydispersity of 0.22±0.01, indicating minimal particle size variation. The zeta potential of -38±0.5 mV imply that these particles are highly stable. Although PLGA NPs had a smooth spherical

morphology, PLGA-SPIO NPs had a rough, speculated shape due to the presence of iron oxide which was distributed on the particle surface (Figure 2.10A, B). Iron assay results indicated that the PLGA-SPIO NPs contain 11.8% iron by weight.

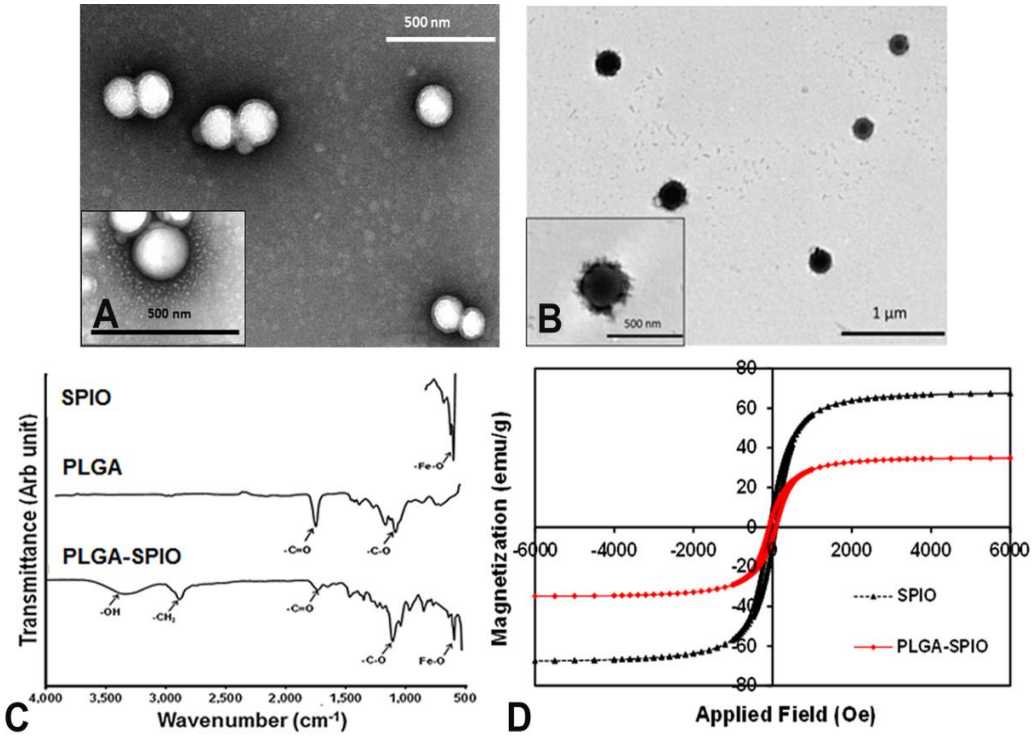

Figure 2.10 TEM image of (A) PLGA and (B) PLGA-SPIO NPs. (C) FTIR spectra of SPIO, PLGA and PLGA-SPIO NPs (D) Comparison of hysteresis loops of bare SPIO and PLGA-SPIO NPs indicating a decrease in magnetization in polymer-bound iron oxide NPs. The coercivity and remanence values remain within the range suitable for magnetic-based drug delivery

FTIR spectra of PLGA-SPIO NPs (Figure 2.7C) show characteristic –OH stretching by the carboxylic acid groups in PLGA at 3320 cm^{-1}. Other peaks representative of bare iron oxide NPs (Fe-O peak at 590 cm^{-1}) and PLGA (C=O stretching at 1735 $cm^{-1}$and C-O stretching at 1072 cm^{-1}) was also observed. Magnetic

property of PLGA-SPIO NPs studied using SQUID magnetometry (Figure 2.7D) showed a decrease in saturation magnetization of PLGA-SPIO NPs compared to bare SPIO. This decrease occurred due to the diamagnetic property of the polymer coating [104, 129]. Magnetic NPs with saturation magnetization as low as 7-8 emu/g have shown attraction towards small magnets, which supports their experimental use as targeting contrast agents [130]. Further, a remanence of 0.022 and coercivity of 69.8 was observed demonstrating that our PLGA-SPIO NPs exhibit similar properties as bare SPIO which has a remanence of 0.0028 and a coercivity of 75.4.

Stability study in DI water, FBS, saline and Gamble's solution showed that PLGA-SPIO NPs maintained their initial particle size with minimal aggregation for over 5 days (Figure 2.11A). These results are consistent with previous studies in our lab showing good stability of PLGA NPs in water and serum with no variation in particle size for up to 5 days at 37^{o}C [88].

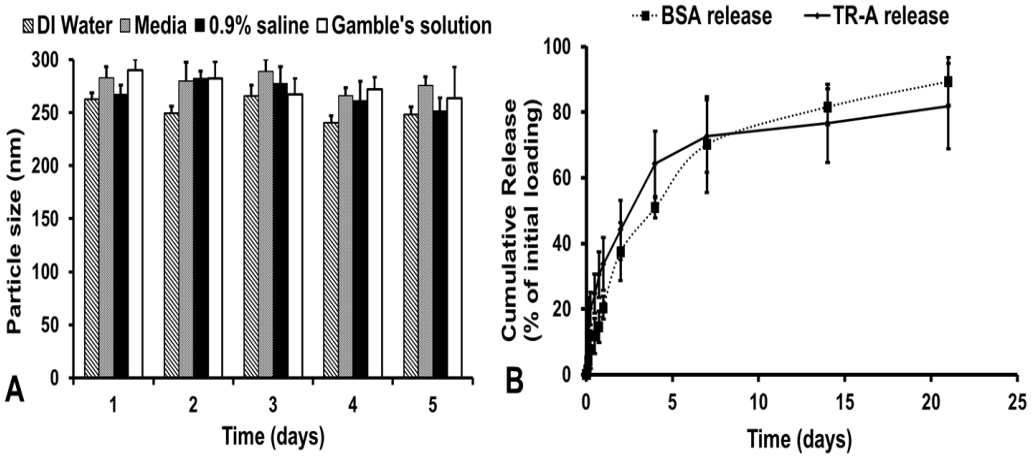

Figure 2.11 (A) Stability studies in DI water, FBS, 0.9% saline and simulated lung fluid (Gamble's solution) (n=4 each) indicating good stability of PLGA-SPIO NPs over 5 days with minimal aggregation (B) Release of TR-A and BSA from PLGA-SPIO NPs indicating a bi-phasic release involving an initial burst release of 40% of encapsulated agent within 2 days followed by sustained release for 21 days (n=4)

Drug release analysis showed that both BSA and TR-A-loaded PLGA SPIO particles showed a burst release of about 38% of the loaded BSA and 44% of the loaded TR-A within 2 days. This was followed by a characteristic sustained release of 89% of loaded BSA and 82% of TR-A over 21 days (Figure 2.11B). Release occurs via bulk erosion of PLGA by the hydrolysis of its ester bonds. Previous studies have shown a burst release of ~68% of FITC from PLGA-iron oxide NPs within 3 hours. This was followed by sustained release of almost 86% FITC by 168 hours [131]. Similarly, dexamethasone acetate-loaded PLGA (75:25) superparamagnetic microparticles have shown a burst core compound release of ~60% within 1 day and sustained release of 80% within 8 days [132].

2.3.5. In Vitro Cell Studies on PLGA-SPIO NPs

Human dermal fibroblasts and AT1 cells maintained >90% viability when incubated with PLGA-SPIO particles up to a concentration of 500 µg/ml. Cell viability was >80% at 1000 µg/ml concentration (Figure 2.12A). Factors such as the cell line tested, polymer composition and SPIO concentration may contribute to differential cytocompatibility. Concentration dependent uptake of PLGA-SPIO NPs by AT1 cells was observed within 2h of incubation with saturation of uptake occuring at 300 µg/ml NP concentration (Figure 2.12B). This is in keeping with previous reports of PLGA nanoparticle uptake by airway, gut and renal epithelial cells [133] as well as by human umbilical vein endothelial cells (HUVECs) [134], and the uptake of poly(dl-lactic acid-co-*α*,*β*-malic acid)-magnetite composite NPs by human mesenchymal stem cells [135]. Uptake by AT1 cells was also found to saturate within 2 hours of incubation, indicating time-dependence of uptake (Figure 2.12C).

To observe the bioactivity of released therapeutic agent, EPO released from the NPs was studied for its activity on EPO-sensitive Ba/F3 cell lines. Ba/F3 cells showed poor viability in control medium (Figure 2.12D). While empty PLGA NPs had no significant effect on cell viability, the EPO in the media helped keep the cells viable. The

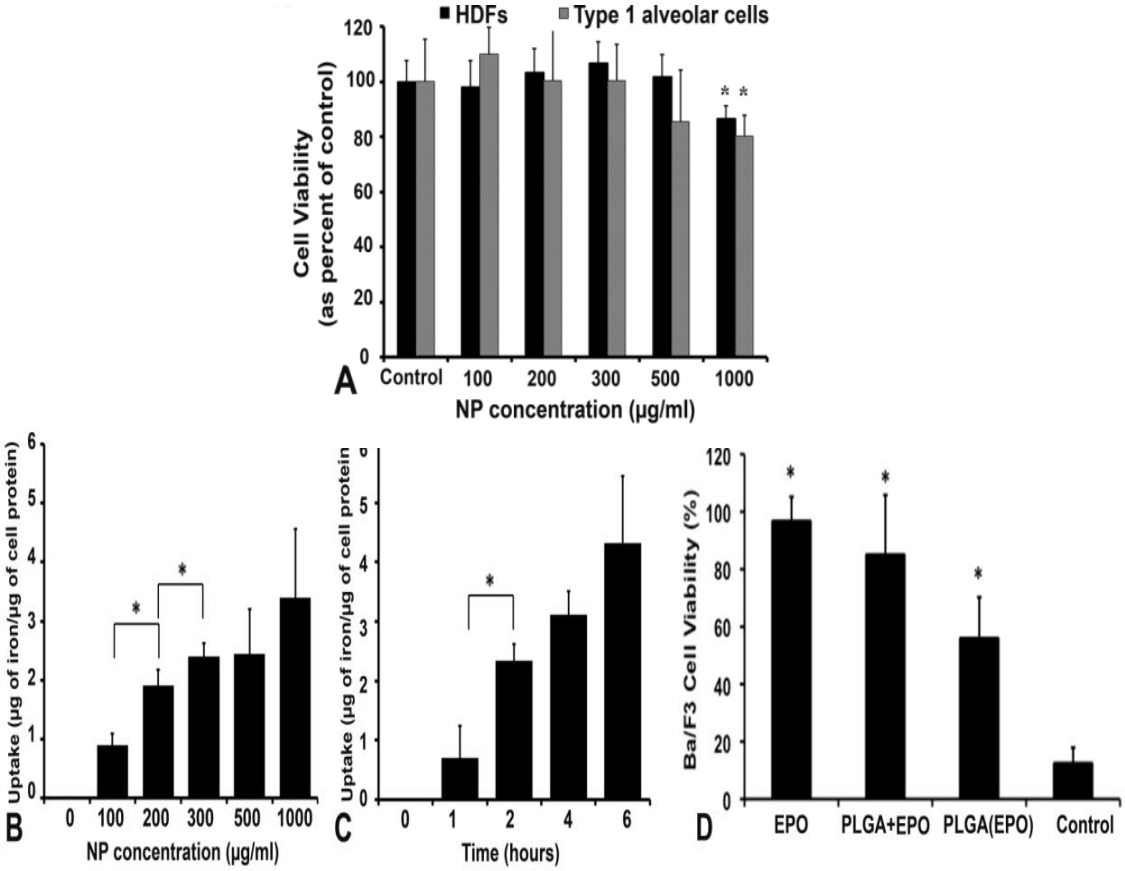

Figure 2.12 (A) Cell viability studies demonstrating that PLGA-SPIO at a concentration of 500 µg/ml were compatible with human AT1 cells (n=4, *p<0.05 w.r.t Control). (B) Dose-dependent uptake of PLGA-SPIO NPs by human AT1 cells up to a nanoparticle concentration of 300 µg/ml was observed (n=4, *p<0.05). (C) Time-dependent uptake of PLGA-SPIO NPs (100 µg/ml) by AT1 cells over 6 h (n=4, *p<0.05) (D) Viability of EPO-dependent Ba/F3 cells was poor in EPO-free (RPMI) medium (control), but rescued in medium containing EPO, EPO plus empty PLGA NPs, or medium incubated for 5 days with PLGA NPs encapsulating EPO [PLGA(EPO)] (n=3, * p<0.05 vs. control)

EPO-containing supernatants obtained after 5 days' release from the NPs also significantly improved Ba/F3 cell viability (56±6%) compared to the control group (<20%).

2.3.6. In Vivo Studies on PLGA-SPIO NPs

Following a single inhalation dose of PLGA-SPIO NPs, the normalized MR signal intensity (SI) of lung parenchyma became much lower than SI of simultaneous saline-treated or untreated control lungs. SPIO has been used as a "negative" MRI contrast agent, in the liver [136], owing to its effect of shortening the proton spin-spin relaxation time (T2) and causing a reduction of signal intensity on MRI. Our results demonstrate this effect of SPIO encapsulated in the PLGA NPs using UTE MRI (Figure 2.13).

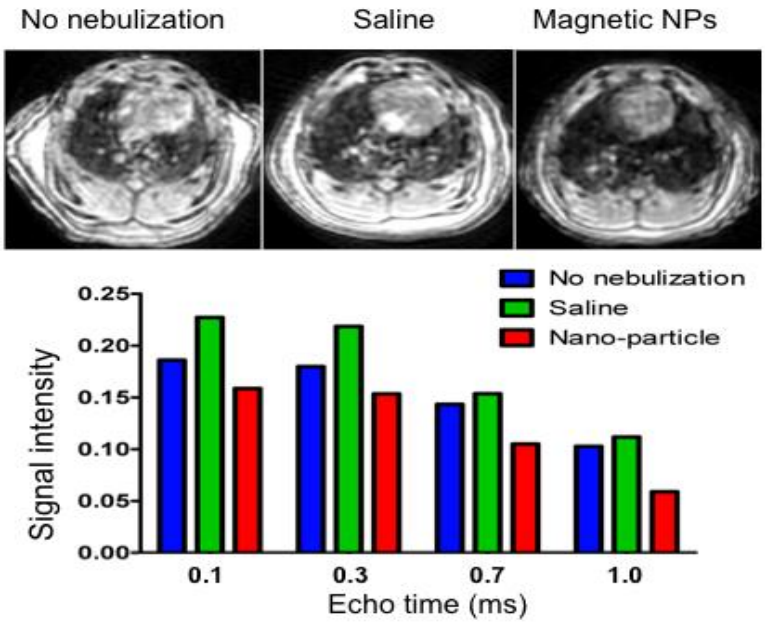

Figure 2.13 Signal intensity changes following inhalation of PLGA-SPIO nanoparticles, using UTE MRI. *Upper panel:* The lung in rats administered PLGA-SPIO via nebulization showed significant darkening compared to control untreated rats or rats that received nebulized saline. *Lower panel:* At any given echo time, the normalized SI of lung parenchyma was lower following PLGA-SPIO inhalation when compared to SI of control and untreated animals

Additionally, light microscopy images of Prussian Blue tissue staining showed scattered distribution of iron oxide within alveolar septal cells as well as alveolar macrophages under light microscopy (Figure 2.14: upper panels). PLGA-SPIO NPs distribution within the lung cells was also visualized using TEM. (Figure 2.14: lower panels).

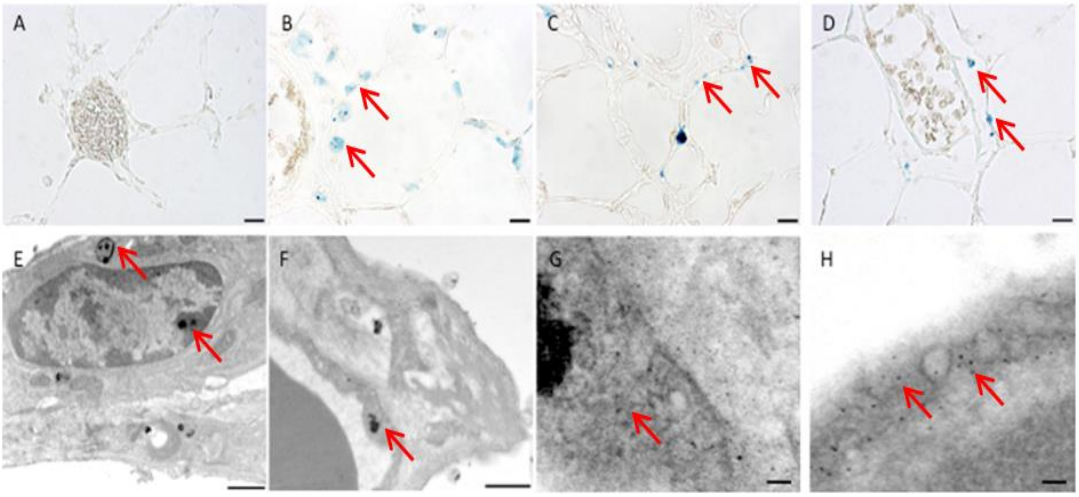

Figure 2.14 Distribution of inhaled PLGA-SPIO NPs in rat lung. A to D: Prussian blue staining was negative for (A) control lung (saline inhalation) while scattered blue stains (arrows) were seen in the alveolar septa of animals given the nanoparticle formulation (B, C, D) Bar=25 µm. E to H: TEM images show the presence of NPs (arrows) in (E) alveolar interstitial fibroblasts (bar=1 µm), the (F) interstitium and an endothelial cell (bar=1 µm). Images at higher magnification show dispersed free iron particles (~5 nm) within the (G) interstitium and endothelium (G, bar=50 nm), and (H) within alveolar type-1 epithelium (bar=50 nm)

.

The distribution of nebulized NPs was observed in lung slices (Figure 2.12: upper panels) and histological sections (Figure 2.15: lower panels). The control lung (saline)

showed no distinct fluorescence while, a single inhalation of NPs containing NIR dye resulted in diffuse fluorescence throughout the lung 3 d after administration. A single inhalation of GFP-containing NPs also showed extensive peribronchial and peribronchiolar fluorescence up to 5 days. A previous report of inhalational delivery of insulin-loaded PLGA nanospheres, had similarly demonstrated a sustained insulin release in the lung and hypoglycemic effect for up to 48 hours [137]. Further, a single inhalation of NPs encapsulating YFP cDNA resulted in diffuse and increasing fluorescence atleast up to 7 d. This is consistent with persistent gene expression and YFP production by lung cells seen by us previously following PLGA NP uptake. Our results are also consistent with published in vitro studies using DNA-containing PLGA-

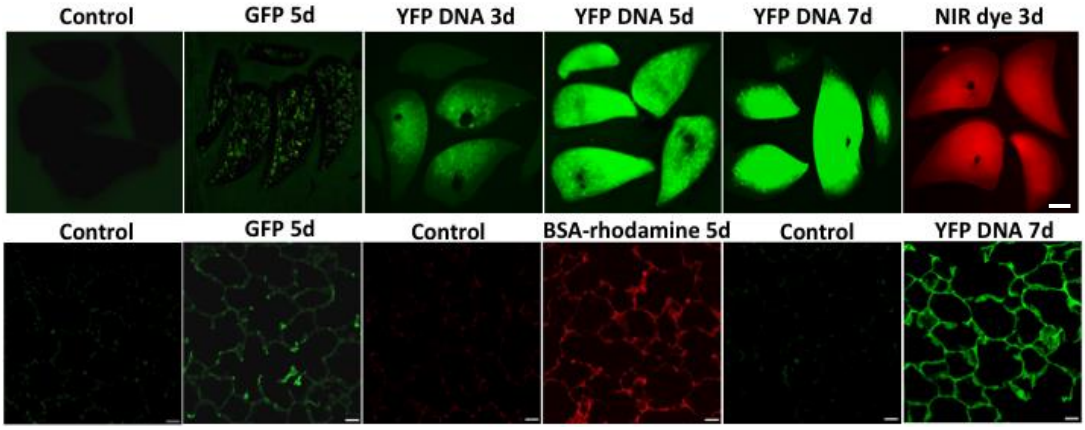

Figure 2.15. *Upper row:* Biofluorescence of fixed rat lung slices at different times following PLGA-SPIO NP nebulization. Encapsulated compounds include : GFP or BSA-rhodamine protein, YFP cDNA, and near-infrared (NIR) dye, compared to control (saline nebulization). The scattered GFP expression (5 d), increasing YFP expression (from 3, 5, to 7 d), and diffuse NIR dye (3 d) indicate that the particles were successfully delivered to the lung and released their payloads at the site (bar=0.5 cm). *Lower row:* Confocal fluorescence microscopy shows scattered GFP and diffuse BSA-rhodamine expression at 5 d, and widespread YFP expression at 7 d after inhalation, compared to their respective controls (bar=50 µm)

polyethyleneimine (PEI) NPs (207-211 nm), which were localized to the endo-lysosomal compartment of lung epithelial cells within 6 hours of treatment, indicating their potential as gene carriers [138].

2.4. Summary

To summarize, we have successfully synthesized and characterized six different polymeric NPs and characterized them in terms of their physical and chemical properties, in vitro cytocompatibility and cellular uptake as well as in vivo deposition and action of the core compound. Gelatin and PLGA NPs showed the smallest sizes of 187 and 160 nm respectively and also maintained consistent particle sizes in water, serum, saline and Gamble's solution. Further they showed a bi-phasic drug release profile, although PLGA NPs had the highest burst release within 2 days. PLGA-based NPs showed the highest cytocompatibility with AT1 cells while natural polymeric NPs showed the highest uptake at a given concentration. Based on the results from *in vitro* characterization, PLGA and gelatin NPs showed the most favorable characteristics for pulmonary delivery. Following inhalational delivery of PLGA NPs, more sustained and uniform distribution of encapsulated proten was seen compared to those of gelatin NPs. We can thus conclude that PLGA NPs demonstrate the most favorable set of characteristics as carriers for pulmonary delivery of therapeutic agents. Further, the feasibility of PLGA-SPIO NPs as vehicles for *in vivo* inhalational administration of active biological compounds such as DNA and proteins was also established. These particles were characterized in terms of their distribution and expression within lung tissue following delivery, both by MRI and fluorescence imaging. Our results thus provide a proof-of-concept for the further development of PLGA-based nanocarriers for various pulmonary drug delivery applications.

Chapter 3

Development of Multi-Functional Core-Shell NPs for Targeted Lung Cancer Dual Therapy

3.1. Introduction

Lung cancer is one of the leading causes of cancer-related mortality in the United States with a quarter of cancer-related deaths in 2014 expected to be attributed to this disease [14]. Factors contributing to lung cancer include excessive tobacco use, air pollution, genetic aspects and environmental factors [139, 140]. Up to 40% of non-small lung cancer (NSCLC) patients present with locally advanced and mostly inoperable disease. Conventional treatments are limited by temporary remission [16] and systemic toxicity due to non-specificity of these therapies [19, 20]. Poor overall survival rates in NSCLC patients may also be attributed to the intrinsic radiation resistance of many tumors due to increased ability to repair DNA damage after radiation therapy. Therefore, it is crucial to develop a system that that can provide targeted and controlled therapy for effective lung cancer treatment for these patients.

Nanomedicine has been recently gaining widespread attention for cancer treatment due to its multiple advantages including improved drug solubility and bioavailability, site-specific targeting, reduced systemic toxicity due to the use of lower drug dosages as well as multi-functionality for diagnosis and therapy [141, 142]. Specifically, stimuli-responsive or ‘smart’ polymer-based nanoparticle systems are capable of undergoing rapid and reversible phase transitions in response to external stimuli such as temperature or pH changes, thereby releasing their contents at the site of interest “on demand” [143]. These NPs are a stepping stone towards the development of highly accurate and site-specific drug delivery systems. For example, a pH- responsive polymer- based nanoparticle can be used in a wide array of medical applications ranging

from delivering drugs to the acidic stomach lumen and tumor microenvironment, to intracellular drug delivery [144]. A temperature-sensitive polymer, on the other hand, could be used to deliver and release drugs in response to induced temperature changes at the disease site. PNIPAAm and chitosan are two commonly used thermo-responsive and pH-responsive polymers, respectively. However, PNIPAAm is limited by its non-biodegradability [145]. Therefore in this project, PNIPAAm was copolymerized with the biodegradable carboxymethyl chitosan (CMC) to form a semi-interpenetrating network, in order to impart pH- and temperature-sensitivity and degradability to the final product. This material could incorporate with PLGA and iron oxide NPs to provide multi-functionalities for drug delivery applications. As discussed in Chapter 2, PLGA-based NPs are promising nanocarriers that can deliver the encapsulated therapeutic agent to the lung and provide a sustained release of drugs over a period of time. Also, superparamagnetic iron oxide can be incorporated in the NPs for MR imaging and to induce hyperthermia therapy [146].

Therefore in this project, a novel multi-functional dual responsive nanoparticle (MDNPs) system was developed consisting of a PLGA-SPIO core and a PNIPAAm-CMC shell. In order to sensitize the cancer cells for effective radiation therapy, the PLGA-SPIO core will be encapsulated with 8-dibenzothiophen-4-yl-2-morpholin-4-yl-chromen-4-one (NU7441) – a highly potent radiosensitizer known to selectively inhibit DNA-dependent protein kinase (DNA-PKcs). As a result of the DNA-PKcs inhibition, cells are unable to successfully repair DNA damage and die through various mechanisms [147]. The NU7441 is expected to release gradually over one month from the core preventing repair of DNA double strand breakage by cancer cells following radiation therapy. The PNIPAAm-CMC shell will contain gemcitabine hydrochloride - an FDA approved chemotherapeutic lung cancer drug. The burst release of gemcitabine hydrochloride from

the PNIPAAm-CMC shell in response to increase in surrounding temperature and acidic tumor environment (low pH) will aid in chemotherapy. Further, the MDNPs will be surface conjugated with folic acid to actively target folate receptor-α known to be overexpressed in a number of human tumor cells including lung cancer cells [148]. The glycosylphosphatidylinositol-anchored folate receptor is known to show high affinity for folic acid, which it usually captures to feed the fast-dividing tumor cells [149]. Therefore, the innovation of this project lies in the development of a biodegradable multi-functional nanocarrier that can actively target lung cancer cells followed by controlled release of two different therapeutic agents for non-invasive and effective lung cancer therapy. The theranostic aspect of this nanocarrier system lies in the fact that they can also be tracked using MRI following administration to ensure precise delivery.

3.2. Experimental section

3.2.1. Western Blot Analysis of Folic Acid Receptors on Lung Cancer Cells

For this project we have compared two different lung cancer cells - A549 and H460 for expression of folic acid receptors. First the cells were lysed using a lysis buffer consisting of Tris (50 mmol/l) of pH 7.5, 1% NP40, EDTA (1 mmol/l) and a protease and phosphotase inhibitor cocktail (phenylmethylsulfonylfluoride (1mmol/l), sodium orthovanadate (0.2 mmol/l), sodium fluoride (0.1 mmol/l), aprotinin (10 µg/ml), and leupeptin (10 µg/ml). The lysates were sonicated, incubated in ice for 15 mins and then centrifuged at 12000 rpm for 10 min. Following quantification of cell protein by Bradford assay (Bio-Rad, Hercules, CA), 20 µg of protein was subjected to a 10% SDS-Poly acrylamide gel electrophoresis (SDS-PAGE) and transferred to polyvinylidene difluoride membranes and probed with Anti-folate binding protein antibodies (Abcam, Cambridge, MA) as per manufacturer's instructions. Actin was used as loading control.

3.2.2. Analysis of Binding Efficiency of Folic Acid to Cellular Folate Receptors

The binding of folic acid to folate receptors was studied using Resonant Sensors Bioassay system (Resonant Sensors Inc.(RSI), Arlington, TX). A549 and H460 lung cancer cells as well as AT1 cells were seeded at a density of 10,000 cells/well in RSI sensor 96-well plates, which were then incubated at 37^{o}C for 24 hours to allow cell attachment. For folic acid binding efficiency studies, the cells were incubated with folic acid at varying concentrations (0, 0.1, 1, 5, 10, 15 µM) for 3 h in the RSI system and peak shift with cell binding over time was studied. The results were plotted as peak shift vs time where greater binding of folic acid to cells resulted in greater peak shifts.

3.2.3. Development of PLGA-SPIO NPs

The PLGA-SPIO NPs were prepared similar to the procedure described earlier. Briefly, 20 mg of SPIO was added to 90 mg PLGA (50:50) solution in 5 ml DCM (oil phase) and sonicated for 8 mins at 20 W power. This emulsion was then added dropwise to 20 ml of 5% (w/v) PVA solution and sonicated for another 10 mins at 50 W. Following overnight stirring to allow solvent evaporation, the particles were centrifuged at 1000 rpm for 1 min to remove unencapsulated SPIO, and the NPs in the supernatant were then collected via lyophilization. To carry out drug loading, NU7441 was dispersed well in the DCM solution containing SPIO and PLGA (oil phase). This mixture was then added to PVA solution as described above.

3.2.4. Surface Modification of PLGA-SPIO NPs with Allylamine (AH)

20mg of PLGA-SPIO NPs was dispersed in MES buffer (pH 4.8) by sonication at 30W, 10 mins. This suspension was then kept for stirring and equal parts of *N*-(3-

dimethylaminopropyl)-*N*′-ethylcarbodiimidehydrochloride (EDC) and N-hydroxy succinimide (NHS) were added to it. Then 130 µl of Allylamine, and 14mg of SDS were added consecutively every 20 minutes. The reaction was allowed to continue for 4-6 h and the particles were washed and isolated by centrifugation at 15,000 rpm for 20 min.

3.2.5. Development of MDNPs

The final step of the nanoparticle formulation involves formation of the PNIPAAm-CMC shell followed by folic acid conjugation. 28mg of PLGA-SPIO-AH particles was dispersed in DI water by sonication at 40W for 20 mins. 58mg of NIPA, 6mg of CMC, 13mg of *N*,*N*′-methylenebisacrylamide (BIS) and 50mg of Sodium dodecyl sulfate (SDS) were added consecutively every 2 mins during sonication. Then the particle suspension was transferred to a 125ml flask and purged with Nitrogen gas for 30 mins. Following addition of 0.08% (w/v) of Ammonium persulfate (APS) and 50 µl of TEMED, the reaction was allowed to continue in Nitrogen gas for 4-6 h. The particles were then isolated by centrifugation at 15,000rpm for 20min.

For folic acid conjugation, 0.1 % w/v folic acid solution in 5 ml MES buffer (pH 4.7-5) was prepared. Then 20 mg of EDC and NHS was added to it every 30 mins. EDC activates the surface carboxyl groups on folic acid [150] and NHs stabilizes it to form an active ester intermediate [151]. This intermediate then covalently binds to the amine groups of CMC present on the PNIPAAm-CMC shell. 5 mg of the prepared MDNPs was then added and sonicated for 2 mins at 20 W. Shaking was continued for 24 hours followed by centrifugation at 15,000 rpm, 20 mins and lyophilization to obtain the MDNPs.

For drug loading, 1mg of gemcitabine hydrochloride was incubated with 5 mg MDNPs at 4^{o}C under shaking conditions for 3 days. Since the polymeric shell is

hydrophilic below LCST, the drug will be loaded into the particles by diffusion. Following drug loading, the MDNPs were washed multiple times by centrifugation and the drug loaded MDNPs were collected via lyophilization. The supernatant following centrifugation was collected and stored for drug loading efficiency determination.

3.2.6. Characterization of MDNPs

3.2.6.1. Physical Properties

The MDNPs were characterized extensively to observe their particle size and surface charge, stimuli-responsive and magnetic properties, stability as well as drug release characteristics. The MDNP size, polydispersity and zeta potential values were obtained using DLS as mentioned in Chapter 2. Briefly, 3 ml of DI water was taken in a transparent cuvette and 20 µl of MDNP suspension (1mg/ml) was added to it. Following insertion of the cuvette in the DLS instrument, readings were taken based on scattering of laser light by Brownian motion of the particles. TEM (TEM, FEI Tecnai G2 Spirit BioTWIN, Hillsboro, OR) was used to observe the size as well as morphology of the particles. A drop of 1 mg/ml nanoparticle suspension was added to a Formvar-coated 200-mesh copper grid (Electron Microscopy Sciences, Hartfield, PA) and air-dried. The grid was then inserted into the holder within the TEM instrument and particle morphology was observed. In order to confirm the incorporation of all components used during synthesis, FTIR was also conducted on individual components as well as at different stages of nanoparticle preparation.

3.2.6.2. Magnetic and Stimuli-Responsive Properties

Following characterization of their surface properties, the MDNPs were further studied for their magnetic as well as stimuli-responsive properties. In order to determine

iron content within the particles, an iron assay was conducted as mentioned in Chapter 2.. Additionally, the magnetic property of the particles was analyzed using a SQUID magnetometer. For this study, the MDNPs were well dispersed in epoxy resin beads and inserted into the instrument. Their response to varying magnetic fields at room temperature was recorded and plotted. Finally, agarose phantoms (0.5% w/v) containing varying concentrations of MDNPs (0, 0.25, 0.5, 1, 2 mg/ml) were prepared to determine whether the SPIO within MDNPs can be visualized using MRI. All images were done on a 7T Agilent (Varian) MRI Scanner with a build in fsems sequence. Some major parameters are as follows: TR=5000ms, TE = 8.58 ms, FOV = 35 x 35mm, slice thickness = 1mm.

In addition to observing magnetic properties, the temperature- and pH-responsiveness of the MDNPs were also studied. To study pH-responsiveness, the particles were dispersed in solutions of varying pH at room temperature and the size was observed using DLS. Temperature responsiveness of the sample was also studied. Briefly, 5 mg/ml MDNP solution was placed in a quartz cuvette (Starna Cells, Atascadero, CA) and submerged in a transparent water tank. The temperature of the water in the tank was varied using a temperature controller with a heater and a temperature feedback probe. A laser light of 609 nm wavelength was then shed on the MDNP sample and the scattered light captured by a photomultiplier (PMT) at 90 degree angle. A 594 nm long-pass filter was used as the captured-light filter. The signal was averaged 100 times following which the peak intensity of the emission decay curve was used to calculate the intensity. Photographs of the nanoparticle suspension were taken before and at LCST to observe cloudiness of the polymer network.

3.2.6.3. Stability, Drug Release and Degradation Characteristics

Variation of MDNP size on incubation with DI water, 10% FBS, saline and Gamble's solution at body temperature over time was studied. Briefly, 20 µl of MDNP suspension of 1 mg/ml concentration was added to a cuvette containing the respective solution. The cuvette was incubated at 37^{o}C and DLS readings were taken every 24h to observe changes in nanoparticle size with time. In order to perform drug release studies, the drug loaded particles were dispersed in 4 different solutions (37^{o}C and pH 7.4, 37^{o}C and pH 6, 45^{o}C and pH 7.4, and 45^{o}C and pH 6) and kept shaking at the respective temperatures. At pre-determined timepoints, the particles were collected using an external magnet and the supernatant saved for analysis. Then the particle were re-dispersed in fresh solutions of appropriate pH and incubated at the designated temperatures. The amount of gemcitabine released was detected at 234 nm absorbance using a spectrophotometer. NU7441 release was detected at λ_{ex} 470 nm and λ_{em} 520 nm using a spectrophotometer. Further, degradation studies were conducted on the MDNPs. Briefly, 4 mg/ml of nanoparticle suspension was prepared in DI water and incubated at 37^{o}C. At each time point, the particles were collected using a 1.3T magnet and the supernatant was removed. Following air-drying, the particle weight was measured to determine decrease in weight over time.

3.2.7. In Vitro Cell Studies

3.2.7.1. Cytotoxicity Studies

With the intention of studying the cytocompatibility of our formulated MDNPs, a 24 hours cell viability study was conducted. Human dermal fibroblasts (HDFs) and AT1cells were seeded at a density of 5000 cells/well in a 96 well plate and allowed to attach at 37^{o}C and 5% CO_2 for 24 hours. Then the cells were incubated with varying

concentrations of folic acid (0 [control], 0.1, 1, 5, 10, 15 μM) as well as MDNPs (0 [control], 100, 250, 500, 1000, 2000 μg/ml) for 24 hours. Following incubation, the cells were washed with 1X sterile PBS and cell viability was assessed using MTS and Picogreen dsDNA assays (Life Technologies, Grand Island, NY) according to manufacturer's instructions. MTS assay gives us the percentage of cells alive in each well compared to the controls. These findings were validated using Picogreen dsDNA assay which gives us the amount of total cell DNA present in each well compared to the control.

3.2.7.2. Cellular Uptake Studies

The effect of MDNP concentration and external magnetic field on cellular uptake was also studied. A549 and H460 lung cancer cells were seeded at a density of 12,000 cells/ well in a 48 well plate and incubated overnight at 37^{o}C and 5% CO_2 to allow cell attachment. Then MDNPs at different concentrations (0, 100, 200, 300, 500 μg/ml) were added to each well and the wellplate was incubated at 37^{o}C for 2 h. Uptake by cells treated with particles in the presence and absence of a 1.3 T external magnet was also studied. This study was also repeated with human AT1 cells as well as human bronchial epithelial cells (HBECs). At the end of the uptake studies, the cells were washed thrice with 1X PBS and lysed using 1% Triton X-100. The contents in each well were analyzed using iron assay to detect amount of NPs internalized by the cells. This was normalized against the amount of cell protein per well, determined using BCA Assay. The cellular uptake was also visualized using Prussian blue iron staining and fluorescence imaging with ICG-loaded MDNPs. For this study, the cells were first incubated with the MDNPs for 2 h following which they were washed and fixed using 1ml of 4% paraformaldehyde solution. For Prussian blue iron staining, a solution consisting of equal parts of 20% v/v

hydrochloric acid and 10% w/v potassium ferrocyanide was freshly prepared and added to the fixed cells for 20 mins. The cells were then washed thrice with PBS and immersed in eosin stain. Then the samples were further dehydrated in 95% and 100% ethanol respectively following which they were observed under a bright field microscope. To visualize uptake of ICG-loaded particles, the fixed cells were washed following a 2 h incubation with the NPs and then visualized using an enhanced fluorescent optical microscope (Nikon Eclipse TI, Nikon Instruments Inc., Melville, NY)

A mechanism of uptake study was also conducted to determine the pathway used for uptake of the MDNPs by A549 and H460 cells. Following cell attachment by overnight incubation, the cells were first exposed to different endocytic inhibitors –10 µg/ml chlorpromazine to inhibit clathrin-dependent endocytosis, 1 µg/ml filipin III to inhibit caveloae-dependent endocytosis and 50 µM amiloride to inhibit micropinocytosis. Following 1 h incubation with these inhibitors, the cells were washed and treated with 500 µg/ml MDNP suspension for 2 h. This NP concentration was chosen based on the concentration at which saturation of cellular uptake had occurred in A549 and H460 cells.

3.2.7.3. Cell Activation Studies

The *in vitro* ROS production and cellular cytokine expression of AT1 cells in response to treatment with MDNPs was studied using methods described in Chapter 2, Section 2.2.6. To study cytokine production, the concentration of interleukin-1 alpha (IL-1∞), interleukin-1 beta (IL-1β), interleukins 2, 4, 6, 8, 10, 12, 10A, and tumor necrosis factor-alpha (TNF-α) in the medium was measured using Multi-Analyte ELISAArray Kit (SA Biosciences, Frederick, MD) according to the manufacturer's directions.

3.2.7.4. *In Vitro* Clonogenic Assays

In order to study the *in vitro* therapeutic efficacy of MDNPs, A549 and H460 cells were first seeded in 60 mm petridishes and *in vitro* clonegenic assays were performed similar to the procedure described previously [152]. A clonogenic or colony formation assay is highly sensitive and cost efficient compared to LDH, DNA and MTT assays, especially when studying monolayer cultures *in vitro* [153]. Three treatment groups (Control, MDNPs without drug and MDNPs with drug) and two temperatures (37^{o}C and 43^{o}C) were used for this study. Following cell seeding, the cells were exposed to either media (control) or the respective MDNP suspensions. Then the dishes assigned to the 37^{o}C group were placed at 37^{o}C undisturbed for 10 days. Dishes assigned to 43^{o}C group were placed at this temperature for 1 hour following which they were moved to 37^{o}C and incubated for 10 days undisturbed. This was done as the cells would die due to hyperthermia if exposed to 43^{o}C for long periods of time. At the end of the 10-day timepoint, the cells were washed well with PBS, fixed and stained using crystal violet staining. The number of colonies in each dish was then counted using a light microscope.

3.2.8. Hemocompatibility Studies

3.2.8.1. Hemolysis Analysis

In order to assess blood compatibility, a hemolysis assay was conducted on the MDNPs. Human whole blood in acid citrate dextrose anticoagulant (ACD) tubes was used for the studies. First two tubes of blood were taken and 0.9% saline and distilled water was added to prepare the negative and positive controls respectively. Distilled water is hypotonic to RBCs and this causes them to rupture. MDNPs at varying concentrations (0, 100, 200, 300, 500 µg/ml) were placed in 1.5 ml Eppendorf tubes and 200 µl of the saline-diluted blood was added to them. The tubes were then shaken gently

at 37^{o}C for 2h. Following centrifugation at 1000 g and 10 mins, 200 µl of the supernatants were added to a 96 well plate and absorbance readings were taken at 545 nm to compare percentage of hemolysis for the experimental groups in comparison with the positive and negative controls. The percentage of hemolysis was calculated using the equation below:

$$\%\ hemolysis = \frac{Sample\ OD - Negative\ OD}{(Positive\ control\ OD - Negative\ control\ OD)} \text{x } 100\%$$

3.2.8.2. Whole Blood Clotting

The kinetics of whole blood clotting when exposed to our MDNPs was studied. First 0.1M of calcium chloride ($CaCl_2$) solution was added to 8.5 ml of ACD blood to initiate blood coagulation. 50 µl of this activated blood was then added to MDNP samples of varying concentrations (0 [control], 100, 200, 300, 500 µg/ml) and incubated at room temperature. At pre-determined time points (10, 20, 30, 50 mins), 1.5 ml of DI water was added and the samples were incubated for 5 mins more. This step was performed to lyse red blood cells (RBCs) that had not been involved in clot formation. The supernatant thus obtained contained lysed RBCs which were measured at an absorbance wavelength of 540 nm using a spectrometer. The blood clotting kinetics was also observed visually.

3.2.9. In Vivo Investigation

3.2.9.1. Acknowledgements

The intratumoral injections and histology following the MRI studies were done by Elizabeth Hernandez and Leah Gandee respectively from Dr. J.T. Hsieh's laboratory at UTSW. MRI was performed by Dr. Shanrong Zhang from Dr. Masaya Takahashi's laboratory at UTSW. For the study on therapeutic efficacy of MDNPs, the intratumoral

injections were performed by Dr. Zhang Zhang while tumor irradiation and excision were done by Dr. Debabrata Saha at UTSW.

3.2.9.2. *In Vivo* Imaging

All animal procedures were approved by the Institutional Animal Care and Use Committee (IACUC) at the UTSW. For our preliminary *in vivo* study, H460 tumors were induced in the hind limbs of female athymic nude mice. The animals were monitored in terms of their weights, and tumor volume. When the tumor volume reached about 100mm^3, they were imaged using non-invasive MRI with a 4.7T Varian small animal scanner. Multi-echo multi-slice T2 images (TR = 2500 ms; TE = 10 ms; field of view of 40 mm × 40 mm; matrix = 256 × 256; slice thickness = 1 mm) were obtained. Then the animals were randomly assigned to different groups: control, unconjugated MDNPs, folic acid-conjugated MDNPs. Intratumoral injection of MDNPs was done to mimic the localized delivery of particles seen following nebulization to the lungs. 24 hours post particle injection, the animals were imaged again using MRI. Then the animals were sacrificed and Prussian blue staining done on the tumor sections to detect the presence of iron oxide. The MR imaging of animals was also used to confirm if more folic acid-conjugated MDNPs will be retained in the tumor region compared to the unconjugated MDNPs.

3.2.9.3. *In Vivo* Therapeutic Efficacy

The animal procedure for this study was approved by the IACUC at UTSW. In order to establish the therapeutic efficacy of the MDNPs, female athymic nude mice were injected with 1 x 10^6 H460 cancer cells in the hind limbs and tumor volume and weight were measured over time. Once the tumor reached 100 mm^3 volume, the mice were

randomly assigned to the different groups (Sham control, Drug cocktail, Drug cocktail + Radiation, MDNPs without drugs, MDNPs with drugs + Radiation). All animals were anesthetized by 1% isoflurane inhalation following which they were administered the different solutions by intratumoral injections. Intratumoral injections have also been adopted previously by other research groups to study the localized therapeutic efficacy of NPs for inhalational drug delivery [19, 154, 155]. Therefore this method of administration was chosen to mimic localized delivery of NPs which will be seen following inhalation. The injections were given on alternate days for 2 weeks. Tumors requiring radiation were treated with a radiation dose of 2 Gy per treatment day (Source to Surface Distance – 20cm, Dose rate – 16.64 Gy/min) using an X-RAD320 (Precision X-Ray, North Branford, CT) biological irradiator. 24 hours following injection, for the duration of the study. Tumor volumes and animal weights were measured and recorded prior to the injections at each timepoint.

3.3. Results and Discussions

3.3.1. Western Blot and Folic Acid Binding Efficiency

Western blot results demonstrated that the folate receptors are overexpressed on both A549 and H460 lung cancer cells (Figure 3.1A). This is in concurrence with previous studies which had also confirmed folate receptor expression on H460 cells using Western blot [156]. However, A549 has previously shown only low levels of folate receptor expression [157]. This is in concurrence with folic acid binding results obtained by us using the RSI system. Our studies with the RSI instrument indicated minimal peak shift on incubating AT1 cells with folic acid (Figure 3.1 B). This peak shift was also not dependent on the concentration of folic acid. On the other hand, H460 cells had comparatively larger peak shifts than both A549 and ATI cells (Figure 3.1C, D). The

larger peak shifts of H460 compared to A549 and AT1 cells indicate that H460 cells have more affinity for binding to folic acid. When the components within the RSI sensor well plates are illuminated with an incident broadband light, light of a specific wavelength gets reflected or transmitted back from it. When folic acid binds to H460 and A549 cells, a shift occurs in the resonance wavelength emitted from the plate. This shift is used to quantify the binding of folic acid onto the cells.

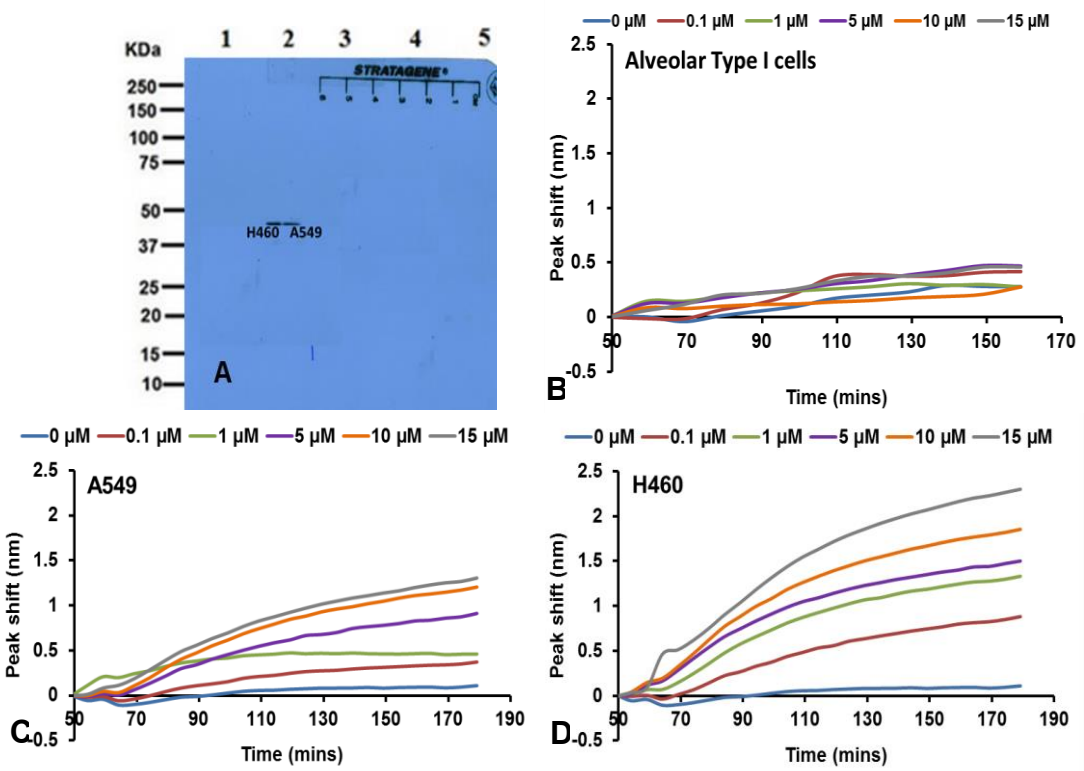

Figure 3.1 (A) Western blot results indicating the overexpression of folate α receptors on both H460 and A549 lung cancer cells. RSI bioassay system results demonstrating that (B) there is no dose-dependent increase in peak shift on treatment of human AT1 cells with folic acid. An increase in peak shift was observed for both (C) A549 and (D) H460 cells compared to their respective controls (0 µM) indicating folic acid binding to cell surface receptors. H460 cells showed a comparatively larger peak shift indicating greater affinity for folic acid (n=4)

3.3.2. Characterization of MDNPs

DLS results at each step of nanoparticle formulation indicate that PLGA-SPIO NPs had a hydrodynamic diameter of 230 ± 98 nm while NPs following AH surface modification, and MDNPs had an average size of 262 ± 79 nm and 289± 49 nm respectively. The NPs were highly stable at all steps of synthesis, which is evident from the high zeta potential values of -12, -18 and -36 mV observed for PLGA-SPIO NPs, AH-modified PLGA-SPIO NPs and MDNPs respectively. The polydispersity ranging from 0.12 to 0.32 indicate that the particles are well-dispersed (Table 3.1).

Table 3.1: Size, surface charge and polydispersity values of the NPs at different stages of preparation

	Diameter (nm)	Polydispersity	Zeta potential (mV)
PLGA-SPIO NPs	230 ± 98	0.22± 0.40	-12
AH-modified PLGA-SPIO NPs	262 ± 79	0.12 ± 0.23	-18
MDNPs	289 ± 49	0.32 ± 0.31	-36

The TEM images established that the particles were in the 250-280 nm size range and had smooth, spherical morphology (Figure 3.2A). The core-shell structure of MDNPs and their expected behavior at LCST and acidic pH have been represented in Figure 3.2B.

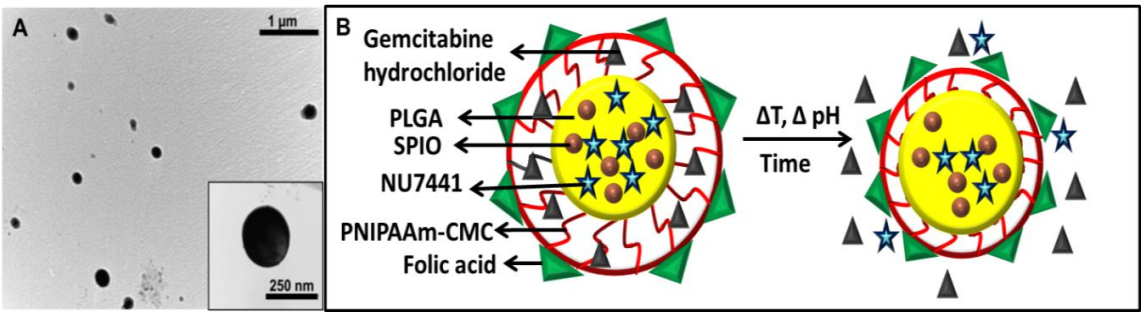

Figure 3.2 (A) TEM image of MDNPs showing smooth spherical morphology in the range of 250-280 nm. (B) A schematic representation of the MDNPs demonstrating their behavior in response to changes in surrounding temperature and pH and over time. The gemcitabine hydrochloride encapsulated within the shell was released promptly with temperature and pH change while slow, sustained release of NU7441 occurs from the PLGA core over time

The successful incorporation of all components within the MDNPs was confirmed using FTIR as shown in Figure 3.3. The OH stretching characteristic of COOH groups in

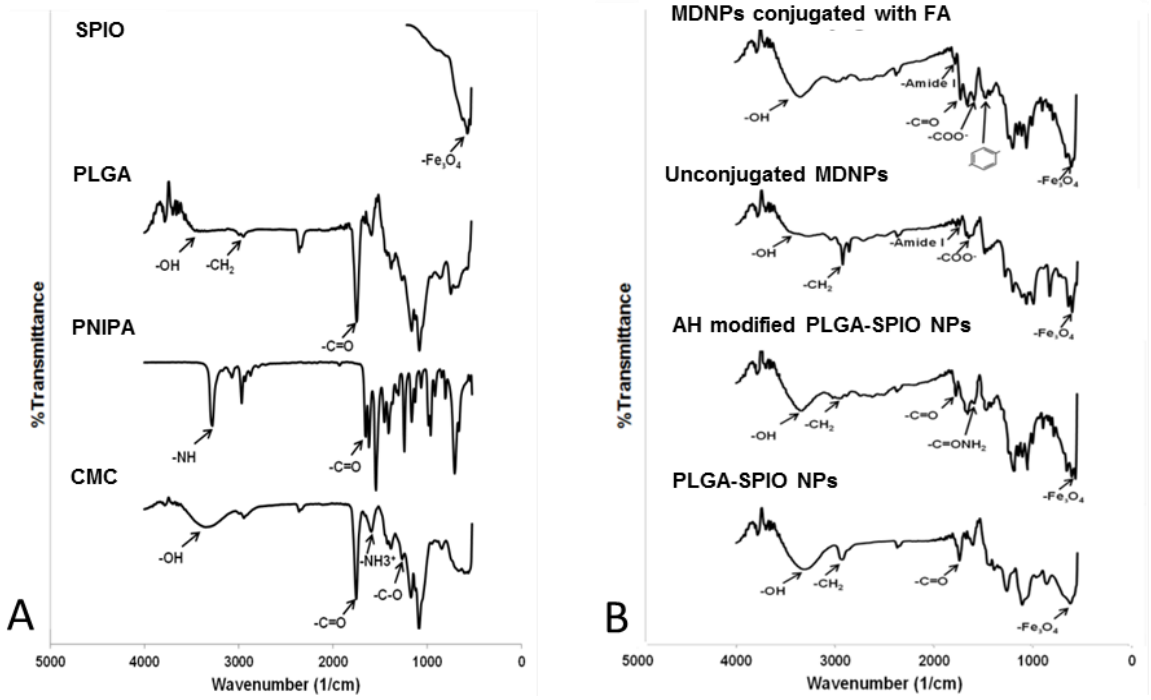

Figure 3.3 FTIR spectra of (A) individual components and (B) each step of nanoparticle synthesis demonstrating that all the components have been incorporated in the final nanoparticle system

PLGA can be seen in PLGA-SPIO NPs as well as AH-modified PLGA-SPIO NPs between 3200–3300 cm^{-1}. The incorporation of SPIO was confirmed at all stages of synthesis by the distinctive peak observed between 530 to 570 cm^{-1}. Further, the peaks at 1720 cm^{-1} for PLGA-SPIO NPs and 1750 cm^{-1} for AH represent the carbonyl groups seen in ester linkages within PLGA. The FTIR spectra for AH-modified PLGA-SPIO NPs also shows a distinct peak at 1560 cm^{-1} for $C{=}ONH_2$ which represents successful coupling of Allylamine with the PLGA surface. The amide peaks at around 1670 cm^{-1} for both MDNPs and folic acid-conjugated MDNPs are characteristic for both chitosan and PNIPAAm. Further, peaks at around 1590 cm^{-1} indicate asymmetric stretching vibrations of COO^- due to the presence of carboxymethyl groups on the chitosan component. CH_2 peaks of PNIPAAm are also visible at 2920 cm^{-1}. Folic acid conjugation was confirmed by the presence of an aromatic ring stretch at 1430 cm^{-1}.

3.3.3. Magnetic Property and Stimuli-Responsiveness of MDNPs

The iron content of MDNPs was observed to be about 47%. The magnetic properties were studied both visually as well as using a SQUID magnetometer. It was observed that the NPs dispersed in DI water could rapidly move in the direction of the applied 1.3T magnet as evident from Figure 3.4A (inset). The hysteresis loop for MDNPs showed that the particles retained their magnetic properties with a remanence of 6.45 (M_r/M_s) and coercivity of 52.6 Oe. Bare SPIO on the other hand showed a remanence of 7.16 (M_r/M_s) and coercivity of 66.7 Oe (Figure 3.4 A). This decrease in magnetic properties could be due to the generation of a diamagnetic moment by the polymer coatings [104]. However, particles with similar or lower magnetization have been successfully used previously for MRI and drug delivery [158], indicating the feasibility of

our NPs in magnetic field-based drug delivery applications such as magnet-based targeting and MRI.

Further, T2-weighted images of MDNPs-containing agarose phantoms showed darker negative contrast with increasing concentration of MDNPs (Figure 3.4 B). The percentage drop in MR signal intensity of the phantom with increasing MDNP concentrations was calculated and compared to the control (agarose only). It was observed that there was almost 87% decrease in signal intensity in the case of agarose

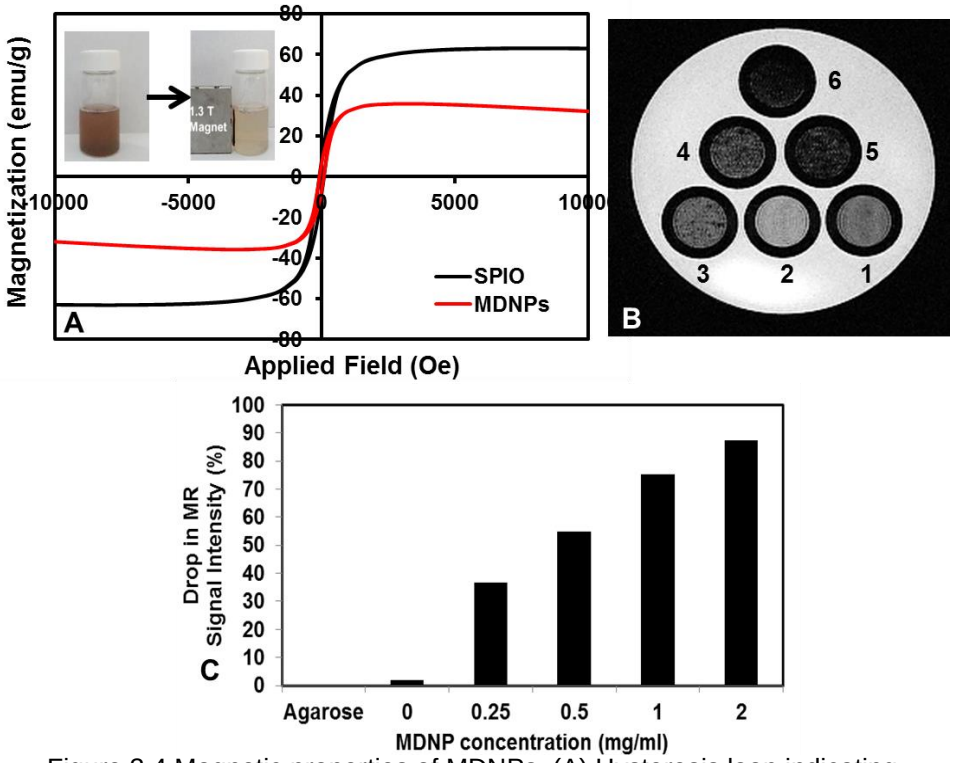

Figure 3.4 Magnetic properties of MDNPs. (A) Hysteresis loop indicating superparamagnetic property of MDNPs. Magnetic behavior of MDNPs on application of 1.3 T magnet could be observed visually (inset) (B) MR images of agarose phantoms containing (1) Agarose only (2) MDNPs without iron oxide, (3) 0.25 mg/ml MDNPs, (4) 0.5 mg/ml MDNPs, (5) 1 mg/ml MDNPs, (6) 2mg/ml MDNPs (C) MR signal intensity drop observed with increasing concentration of MDNPs compared to the control (agarose only)

phantoms containing 2 mg/ml MDNP while 0.25mg/ml, 0.5 mg/ml and 1mg/ml MDNP concentrations caused the signal intensity to drop by 36%, 55% and 75% respectively compared to the control (agarose phantom only) (Figure 3.4C). This is in agreement with previous results from our lab where an SPIO containing core-shell NP formulation showed drops in signal intensity as the NP concentration increased from 0.3 mg/ml to 0.6 mg/ml [104].

In order to ascertain the stimuli-sensitive properties of our NPs, two studies were performed. DLS studies performed to determine pH sensitivity showed a significant decrease in particle size from pH 7 to pH 5 indicating that the particles shrink in response to acidic pH environment (Figure 3.5A). This is in keeping with the findings of Li et al.[159], who had synthesized chitosan-graft-PNIPAM hollow spheres which demonstrated significantly smaller sizes between pH 4.5 and 6.5 and larger sizes at more acidic and basic solutions. The ionization of chitosan chains at low pH and their rapid deprotonation at basic pH could result in instability in the system leading to possible swelling and eventual aggregation [160]. Further, LCST measurements confirmed that

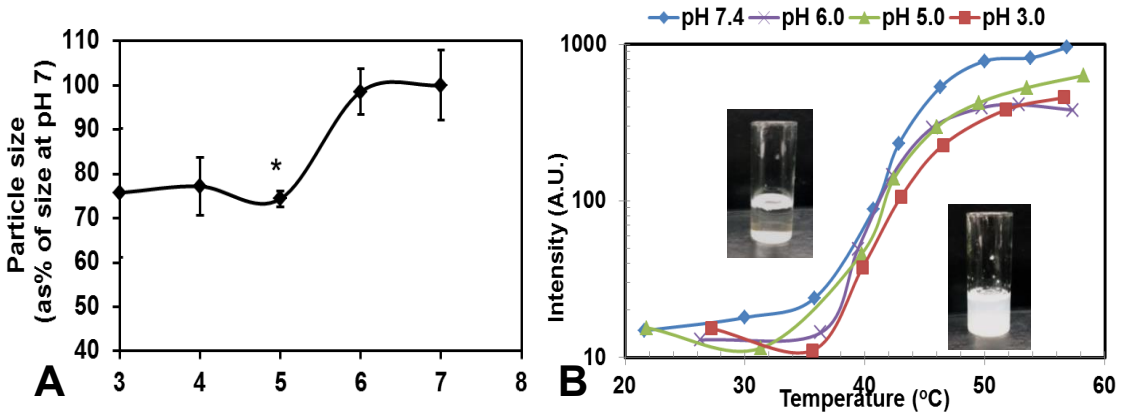

Figure 3.5 (A) Significant decrease in MDNP size observed with change in environmental pH from 7 to 5 (n=4, *p<0.05 w.r.t particle size at pH 7) (B) MDNPs demonstrated temperature-sensitive behavior with LCST at 40^{o}C. No significant variation in LCST was observed with pH. LCST changes could be observed visually (in set)

the PNIPAAm-chitosan shell can undergo rapid, reversible phase transition at an LCST of 43^{o}C. In addition, a distinct cloudiness in the PNIPAAm-CMC NP suspension was observed at around 43^{o}C while it remained clear below this temperature (Figure 3.5B). Therefore it was confirmed that the LCST of PNIPAAm-CMC is achieved at 43^{o}C. pH was found to have no effect on the LCST of the particles.

3.3.4. Stability, Degradation and Drug Release Kinetics of MDNPs

Particle size measurements over a period of 5 days indicated that the MDNPs remained relatively stable in DI water, media containing 10% FBS, 0.9% saline and Gamble's solution (Figure 3.6A). There was only about 30% decrease in particle size by the end of the experiment (day 5). About 25% reduction in particle size was observed in all solutions by day 3. This was consistent with our degradation study results where 20% decrease in particle weight was observed by day 3 (Figure 3.6B). This indicates that the MDNPs would remain stable in various solutions including body fluids without undergoing

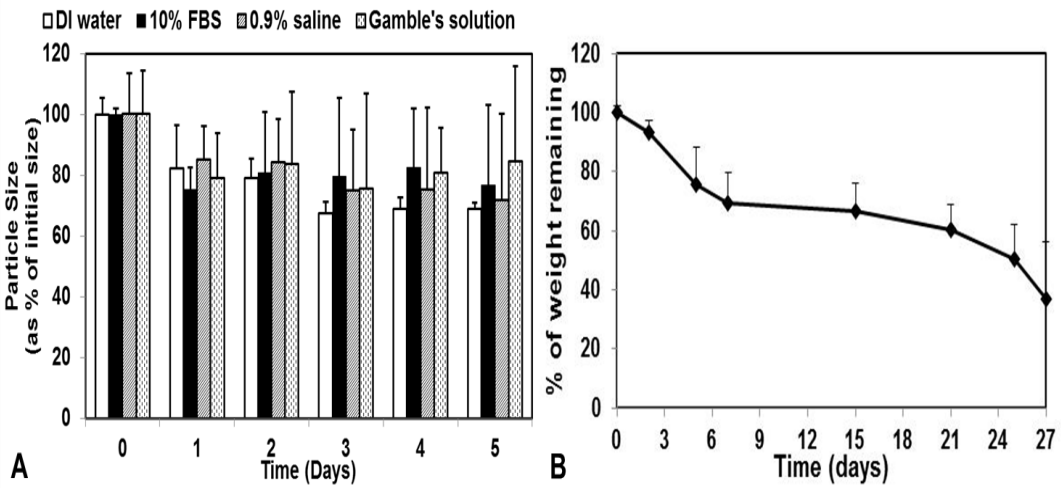

Figure 3.6 (A) Stability studies indicating minimal particle size variations for MDNPs incubated in DI water, media (10% serum), 0.9% saline and Gamble's solution over a period of 5 days. (B) MDNP degradation studies showing decrease in particle weight by 63 % in 27 days. (n=4)

significant aggregation. Further degradation studies showed that the MDNP weight had decreased to 76 % of its initial weight in 5 days. There was a gradual decrease in weight to 37% of its initial weight by day 27. This indicates that the particles had undergone slow and gradual degradation with time.

Further, drug release kinetics of the MDNPs was tested at different temperatures - 37oC (physiological temperature) and 45oC (hyperthermia temperature) and at solutions of different pH – 7.4 (physiological pH) and 6.0 (pH prevalent in acidic tumor microenvironment). The loading efficiency observed for NU7441 and gemcitabine hydrochloride was 52% and 88% respectively. The gemcitabine hydrochloride loaded in the PNIPAAm-CMC shell showed temperature- and pH-dependent release and achieved 100% release at 45^{o}C, pH 6 within 2 days. At 45^{o}C and pH 7.4, only 85% of the encapsulated gemcitabine was released. Release under 37^{o}C (pH 6 and 37oC, pH 7.4 and 37^{o}C) conditions was found to be 82% and 52% respectively (Figure 3.7B). There was sustained release of NU7441 from the core with about 70% release at 37^{o}C and

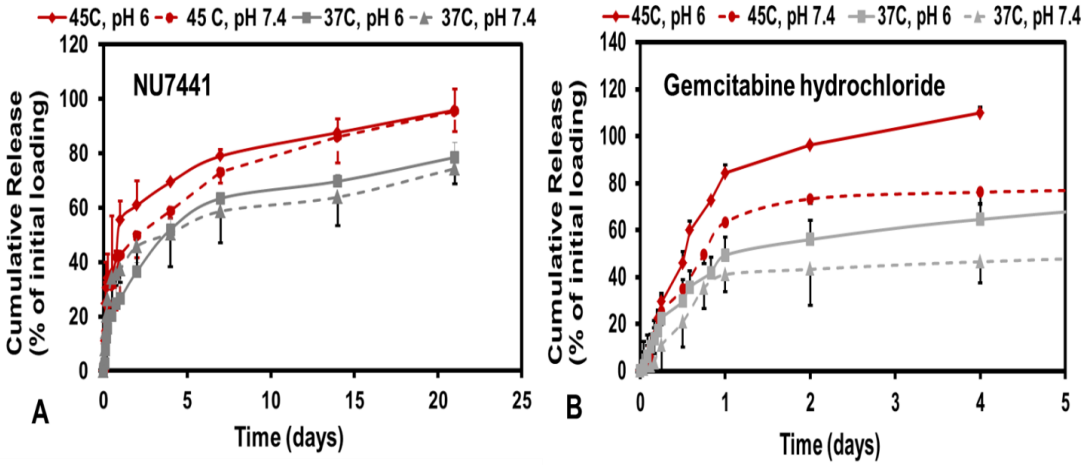

Figure 3.7 (A) Sustained release of NU7441 was observed from the PLGA core for 21 days. This bi-phasic release is characteristic of PLGA. (B) Gemcitabine hydrochloride loaded in the PNIPAAm-CMC shell showed temperature- and pH-dependent release with maximum release at 45^{o}C and pH 6

about 90% release at 45^{o}C (Figure 3.7A). However the bi-phasicNU77441 release pattern observed is characteristic of PLGA NPs [88] indicating that the release was dependent chiefly on PLGA degradation and subsequent drug diffusion rather than on the stimuli-sensitiveness of the PNIPAAm-CMC shell.

3.3. 5. In Vitro Cell Studies

In vitro cytocompatibility studies using MTS assays on HDFs and AT1 cells indicated folic acid was non-toxic even at high concentrations of 10 µM (Figure 3.8A).

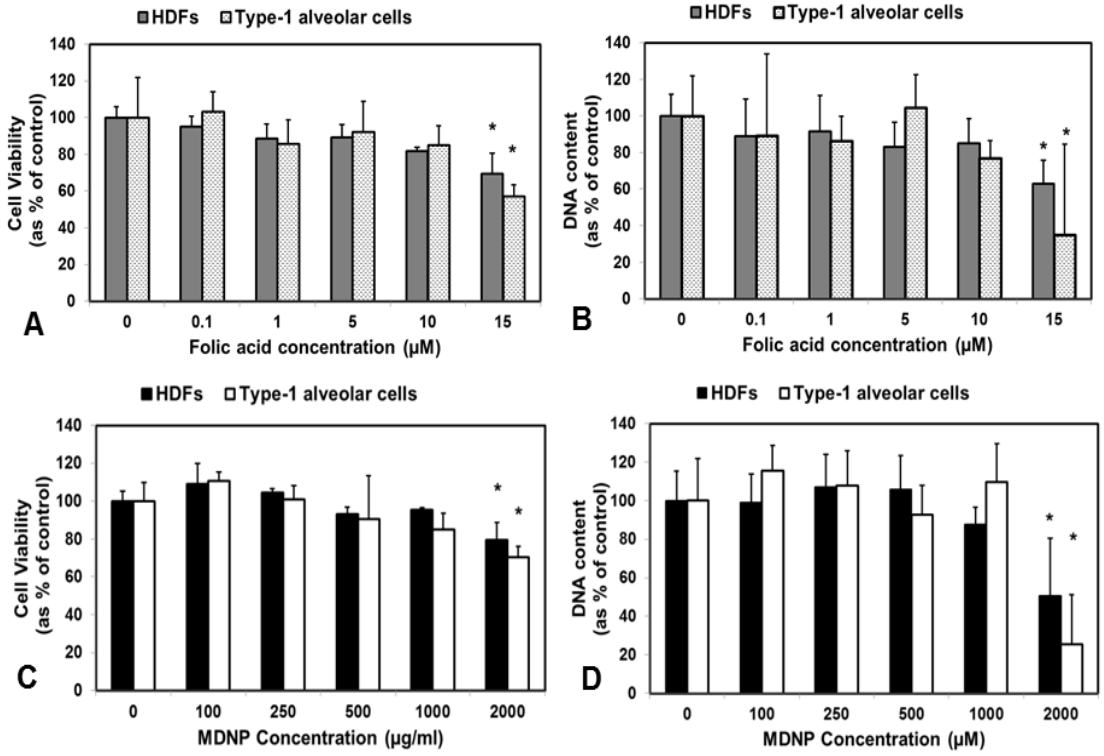

Figure 3.8 *In vitro* folic acid cytocompatibility studies on HDFs and AT1 cells using (A) MTS assays (B) Picogreen dsDNA assays indicating good cell viability up to10 µM concentration. *In vitro* cytocompatibility of MDNPs using (C) MTS and (D) Picogreen dsDNA assay also demonstrated that cells were viable up to a high concentration of 1 mg/ml (n=4, *p<0.05 w.r.t cell viability in 0 µg/ml group [Figures 3.8 A and C] or DNA content in 0 µg/ml group [Figures 3.8 B and D])

This was confirmed using Picogreen dsDNA assay which showed that the total DNA content in samples treated with 10 μM folic acid was similar to that of control samples (0 μM) (Figure 3.8C). The MDNPs also showed cytocompatibility with HDFs and AT1 cells up to 1 mg/ml concentration. At all concentrations, 80% or more of the cells were viable indicating that the particles are relatively non-toxic (Figure 3.8B). DNA assay results also demonstrated that >80% DNA content in each well was retained up to 1 mg/ml MDNP concentration. However a decrease in DNA content was observed in samples treated with 2 mg/ml MDNP concentration. (Figure 3.8D). These results confirm that the MDNPs are cytocompatible *in vitro* up to 1 mg/ml concentration.

Cellular uptake studies were conducted using normal lung cells (AT1 cells and HBECs) as well as A549 and H460 lung cancer cell lines to determine the optimal MDNP concentration that can be taken up by the cells. Our results demonstrated that for AT1 cells and HBECs, there is magnetic-field dependent uptake and dose-dependent concentration of 300 μg/ml and 200 μg/ml respectively. However, this uptake is much smaller than what was observed in the case of A549 and H460 cells. In the case of both cancer cell lines concentration-dependent uptake was observed. Further, dependence of cellular uptake on applied external magnetic field was also studied. It was observed that a significantly higher cellular uptake of MDNPs occurred in the presence of a 1.3 T magnet for both A549 and H460 cells. Thus this study verified that cellular uptake of MDNPs by A549 and H460 cells was both concentration- and magnetic field-dependent (Figure 3.9A, B). On the other hand, uptake by healthy alveolar and bronchial epithelial cells was observed to be minimal with greater uptake occurring under the influence of an externally applied 1.3 T magnetic field.

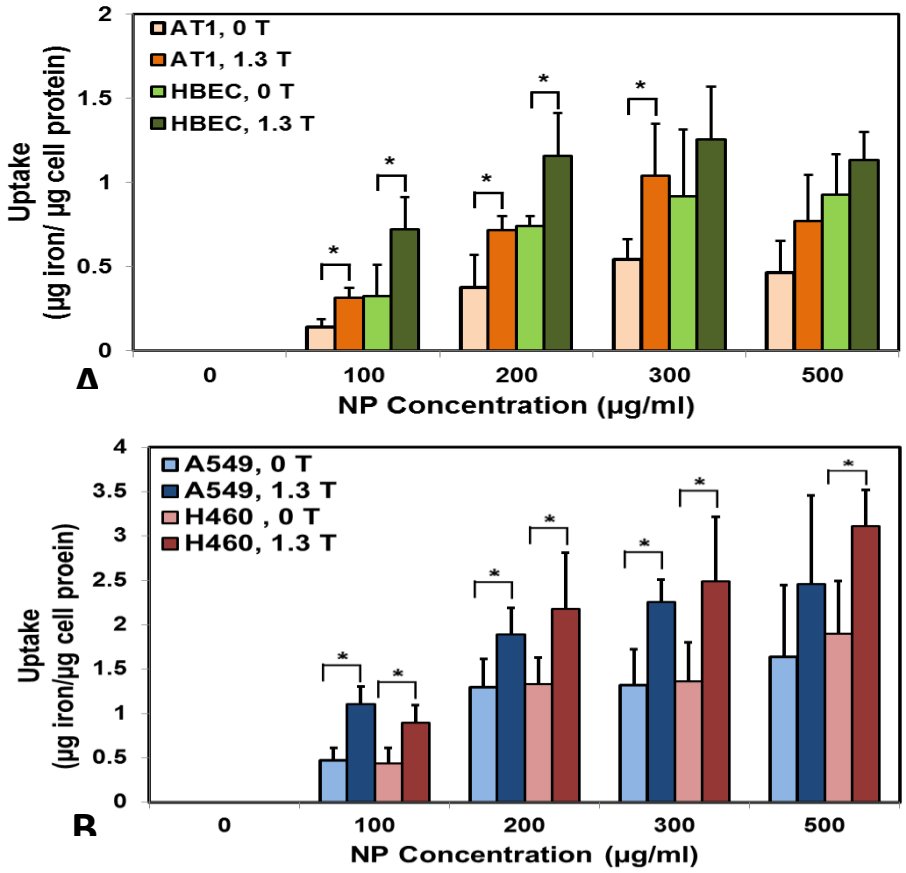

Figure 3.9 *In vitro* cellular uptake of MDNPs by (A) AT1 cells and Human bronchial epithelial cells (HBECs) demonstrating magnetic field-dependent uptake of MDNPs up to 300and 200 µg/ml MDNP concentration respectively. The MDNP uptake by (B) A549 and H460 lung cancer cells was dependent on NP concentration and on externally applied magnetic field (1.3T) (n=4, *p<0.05)

In addition, a mechanism of uptake study was conducted to determine the route of uptake of our MDNPs by A549 and H460 cells. As shown in Figure 3.10, it was observed that MDNP uptake was significantly reduced when A549 and H460 cells were treated with filipin (60% and 45% reduction respectively). This indicates that caveolae-mediated endocytosis played a key role in the uptake of our particles. Our results are in accordance with previous findings which show that folic acid binds to folate receptors, which are thought to be clustered around invaginated caveolae on the cell surface.

Following ligand binding, the caveolae pinches the neck region and releases the folic acid into the cytosol. Then it reopens at the cell surface to enable further ligand binding. This method of endocytosis is also known as potocytosis [55]. Significant decrease in uptake was also observed in cells treated with chloropromazine indicating that clathrin-mediated endocytosis also plays a role in MDNP uptake. However greater inhibition of MDNP uptake occurred on cells treated with filipin than with chlorpromazine. This is similar to the results obtained previously by our lab where RGD-conjugated core-shell NPs were primarily taken up by caveolae mediated endocytosis in B16F10 skin cancer cells, although other uptake pathways also played some role in particle uptake [104].

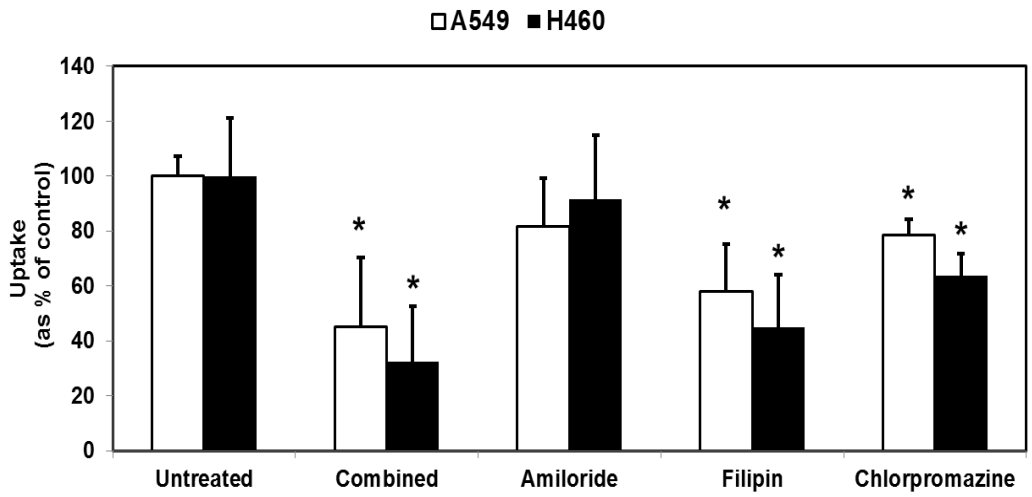

Figure 3.10 Mechanism of MDNP uptake by A549 and H460 cells. Significant reduction in MDNP uptake was observed in cells treated with filipin inhibitor suggesting that caveolae-mediated endocytosis played a key role in the uptake. Also some decrease in cellular uptake was observed in H460 and A549 cells treated with chlorpromazine suggesting that clathrin-mediated endocytosis may have also played a role in MDNP uptake(*$p<0.05$ compared to Untreated group)

3.3.6. In Vitro Clonogenic Studies

To assess the therapeutic efficacy of our MDNPs, a colony forming study was also conducted. The number of cell colonies in each group was counted at the end of the study. No significant cell death was observed when compared to the controls, when A549 and H460 cells were incubated with MDNPs not loaded with drugs at both 37 and 43^{o}C. Some cell death was observed in the control and MDNPs (no drug) groups exposed to 43^{o}C and this might be due to hyperthermia (~80% cell death for H460 cells and ~60% cell death for A549 cells). However drug-loaded MDNPs showed significant reduction in cell proliferation at 43^{o}C with only 10% colonies compared to control group at 37^{o}C in the case of A549 cells and only 7% colonies compared to control at 37^{o}C for H460 cells. On the other hand, A549 and H460 cells treated with drug-loaded MDNPs at 37^{o}C showed 19% and 14% colonies respectively compared to the control at 37^{o}C (Figure 3.11).

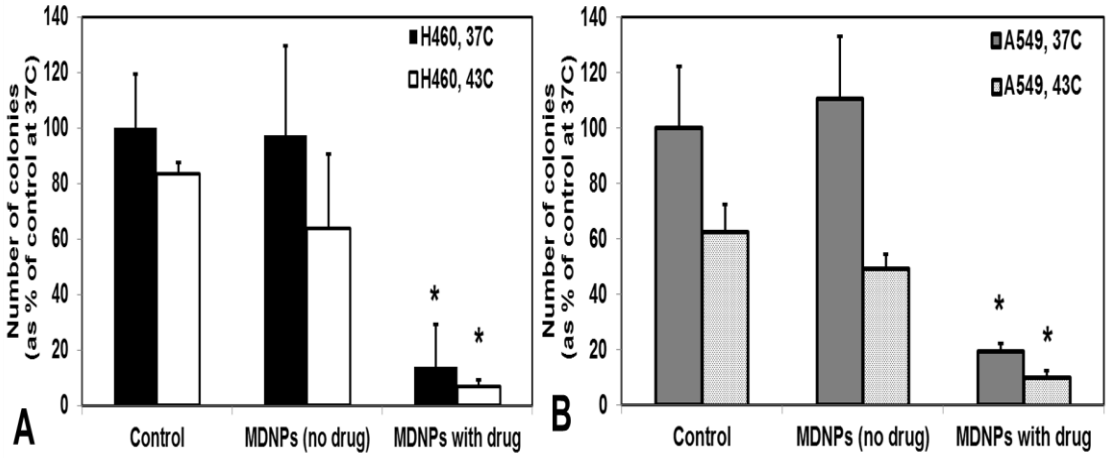

Figure 3.11 Colony forming study indicating that MDNPs not loaded with drugs did not have significant effects on (A) H460 and (B) A549 cell viability. Drug-loaded MDNPs on the other hand significantly reduced cell proliferation especially at 43^{o}C (LCST of the MDNP shell) indicating the chemotherapeutic effect of MDNPs on the cancer cells (n=4, *p<0.05 w.r.t control at 37^{o}C)

3.3.7 Visualization of MDNP Uptake by H460 cells

Based on all the results obtained so far, H460 cells seemed to show greater affinity towards uptake of MDNPs. Greater folic acid binding was observed on H460 cells using RSI system. Also these cells showed greater dose- and magnetic-field dependent uptake. Therefore H460 cells were chosen for our further studies. In order to visualize *in vitro* uptake of MDNPs by H460 cells, Prussian blue and eosin staining was done. The particles could be clearly visualized within the H460 cells using bright microscope (Figure 3.12A). Further ICG-loaded particles were internalized by H460 cells and clearly visualized using a fluorescence microscope (Figure 3.12B)

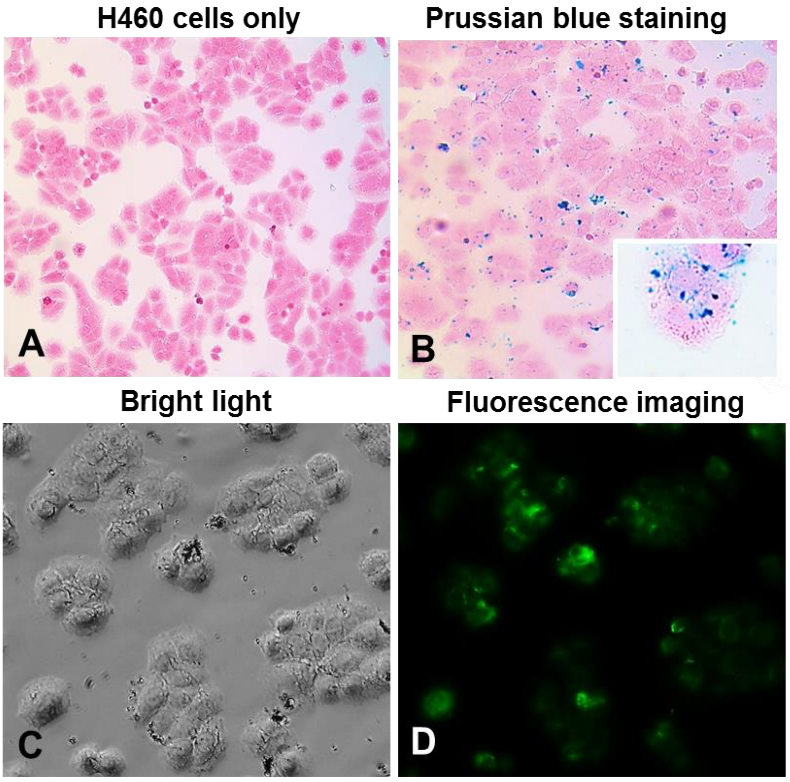

Figure 3.12 Visualization of MDNP uptake by H460 cells by (A,B) Prussian blue and Eosin staining and (B) Fluorescence imaging using ICG-loaded MDNPs

3.3.8 Cell Activation Studies

Cell activation studies were conducted by incubating MDNPs with AT1 cells for 24 hours following which cytokine and ROS production from the exposed cells was analyzed. The media from each tested group (i.e., control, 0.25 mg/ml MDNPs, 1 mg/ml MDNPs) was collected for the cytokine ELISA. The cells stimulated using LPS (positive control) produced 0.25 ng/ml IL-6, 1.27 ng/ml IL-8, 0.24 ng/ml IL-10 and 0.11 ng/ml TNF-α inflammatory cytokines. In comparison, 0.25 mg/ml MDNPs showed significantly lower amount of, IL-6, IL-8 and IL-10 production and negligible amounts of TNF-α was released (Figure 3.13A). Even at a high MDNP concentration of 1 mg/ml, only 0.07 ng/ml IL-6, 0.73 ng/ml IL-8, 0.05 ng/ml IL-10 and 0.02 ng/ml TNF-α cytokines was produced by the cells, which was significantly lower than the amounts produced by LPS stimulation.

The selected cytokines were studied in our research as they play major roles in inflammatory reactions. For example, IL-6 is known to be produced on exposure to acute air pollutants while IL-10 is a regulatory cytokine known to decrease inflammatory responses by inhibiting production of other inflammatory cytokines [161]. In addition, IL-8 is known to be released in response to airway inflammation although the mechanism is unknown [162], while TNF-α is also commonly produced by alveolar epithelial cells in the case of acute inflammation and injury [163]. Our results agree with previously published works on PLGA core-PNIPAm shell NPs which did not stimulate TNF-α production in THP1 monocytic cell line at a high concentration of 5 mg/ml [162]. Significant TNF-α production was observed in the THP1 cells treated with LPS in this study, which was also observed by us in our study [164]. Similarly, the ROS produced by the cells on exposure of 1 mg/ml MDNPs was only 16% of the ROS produced by them on LPS treatment (Figure 3.13B). These results indicate that MDNP uptake does not cause significant cell activation or initiate significant inflammatory reactions in the cells.

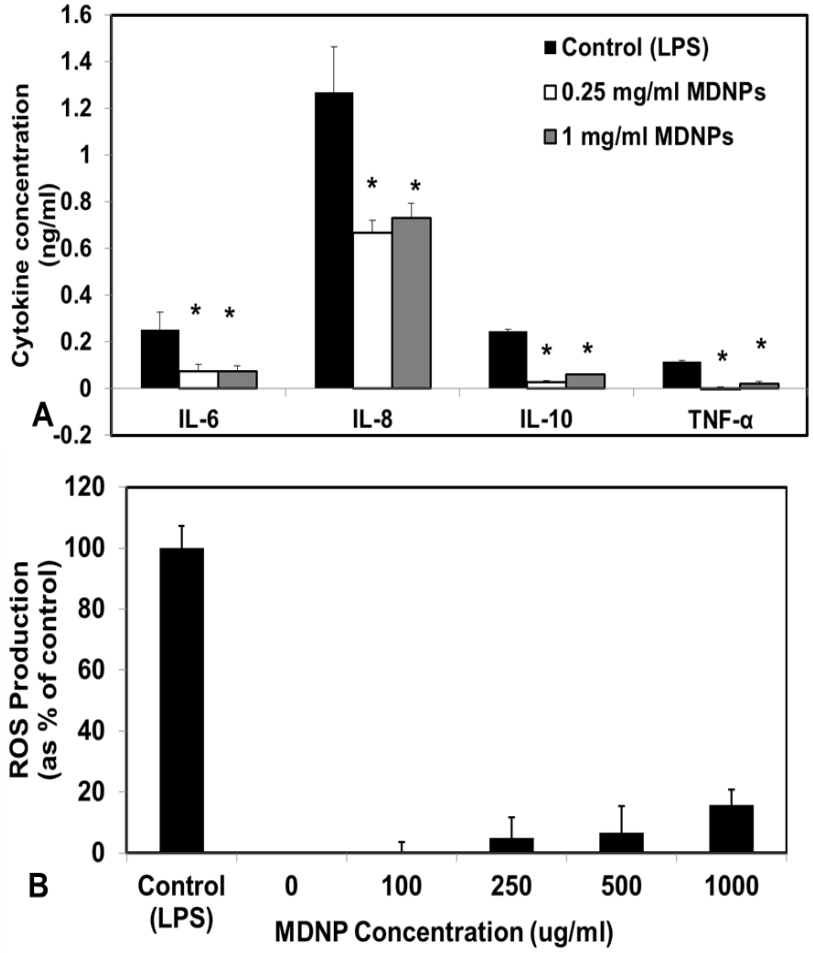

Figure 3.13 Cell activation study using AT1 cells. (A) Inflammatory cytokine release from cells following 24h exposure to MDNPs at two concentrations: 0.25 mg/ml and 1mg/ml. Significantly smaller quantities of IL-6, IL-8, IL-10 and TNF-α were produced compared to the positive control (LPS stimulated cells) (n=4, *p<0.05 w.r.t cytokine production by LPS-treated cells) (B) ROS production from cells was found to be about 16% compared to LPS control even at a high MDNP concentration of 1000 µg/ml

3.3.9 Hemocompatibility Studies

Due to the presence of alveolar-capillary interface in the lungs, a few of the administered NPs could enter the blood stream over time. Therefore it is essential that

they maintain good blood compatibility to avoid clot formation or other adverse inflammatory reactions. The hemolytic property of administered drug carriers should be studied extensively to ensure that they do not lyse RBCs resulting in hemoglobin release. This release could result in several critical consequences including development of anemia, jaundice, acute renal failure and eventual death [165, 166]. Studies have shown that formulations causing <10% hemolysis is considered to be non-hemolytic [165]. Our hemolysis study results showed that less than 2% hemolysis occurred even at 500 µg/ml MDNP concentration, indicating that these particles were non-hemolytic. Visual observation also showed reddening of the solution for the positive control indicating hemolysis while no visual indication of hemolysis could be seen for the negative control and experimental groups (blood exposed to 100, 200, 300 and 500 µg/ml MDNP concentration) (Figure 3.14A, B).

Further, blood clotting studies were conducted to ensure that the MDNPs will not promote clot formation on entering the blood stream. DI water addition causes lysis of unclotted RBCs in the samples. The hemoglobin released from these lysed RBCs can be quantified at 540 nm absorbance wavelength using a spectrometer. Therefore, the absorbance readings obtained at 540 nm is inversely proportional to clot formation. As seen in Figure 3.14C, the absorbance values for all experimental samples decreased gradually indicating clot formation in the tubes aligning with time. The MDNPs at varying concentrations ranging from 100 to 500 µg/ml showed the same blood clotting rate as the control group (whole blood not exposed to NPs). This was visually confirmed as shown in Figure 3.14D, where the solution for control group and 500 µg/ml group had comparatively clearer supernatants at 60 mins than at other time points. The clot formation is clearly visible in both experimental groups during the 30 and 60 min timepoint.

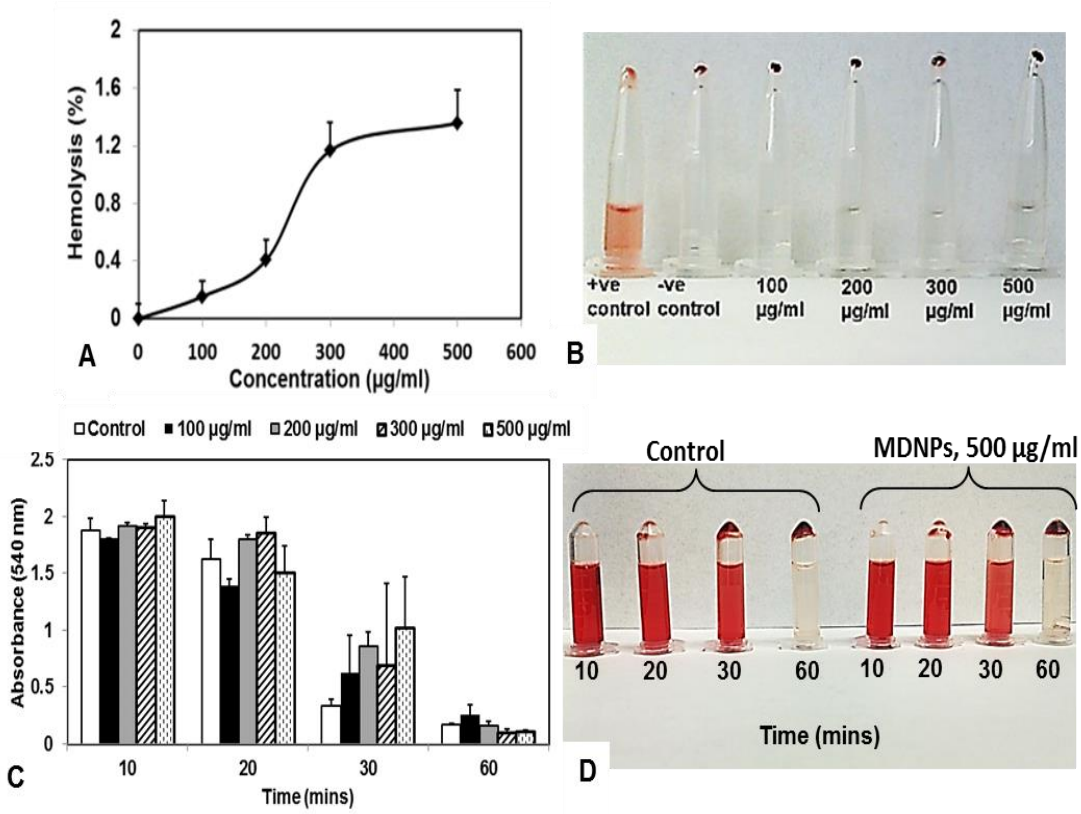

Figure 3.14 (A) Hemolysis study showed that less than 2% hemolysis occurred even at an MDNP concentration of 500 µg/ml indicating that the particles are non-hemolytic. (B) Visual observation confirmed that minimal hemolysis occurred in negative control and other experimental groups while distinct reddishness was seen in the positive control group. (C) Blood clotting studies indicated that the amount of hemoglobin in the blood exposed to varying MDNP concentration decreased at the same rate as the control (blood not exposed to MDNPs). (D) Visual observation of the blood clotting study

3.3.10. In Vivo Investigation

3.3.10.1 *In Vivo* Imaging

Tumors were visualized before and 24 hours after intratumoral injection of MDNPs into H460 tumor bearing mice. The darkening of the tumor region 24 hours

following injection of the folic acid-conjugated MDNPs can be clearly visualized (Figure 3.15 A,B,C, D). T2 signal intensity in the tumors was found to drop significantly by 30% in animals treated with folic acid-conjugated MDNPs compared to the tumor signal intensity before treatment. On the other hand, control (untreated) animals and the animals treated with unconjugated MDNPs showed signal intensity drops of about 3.5% and 12%

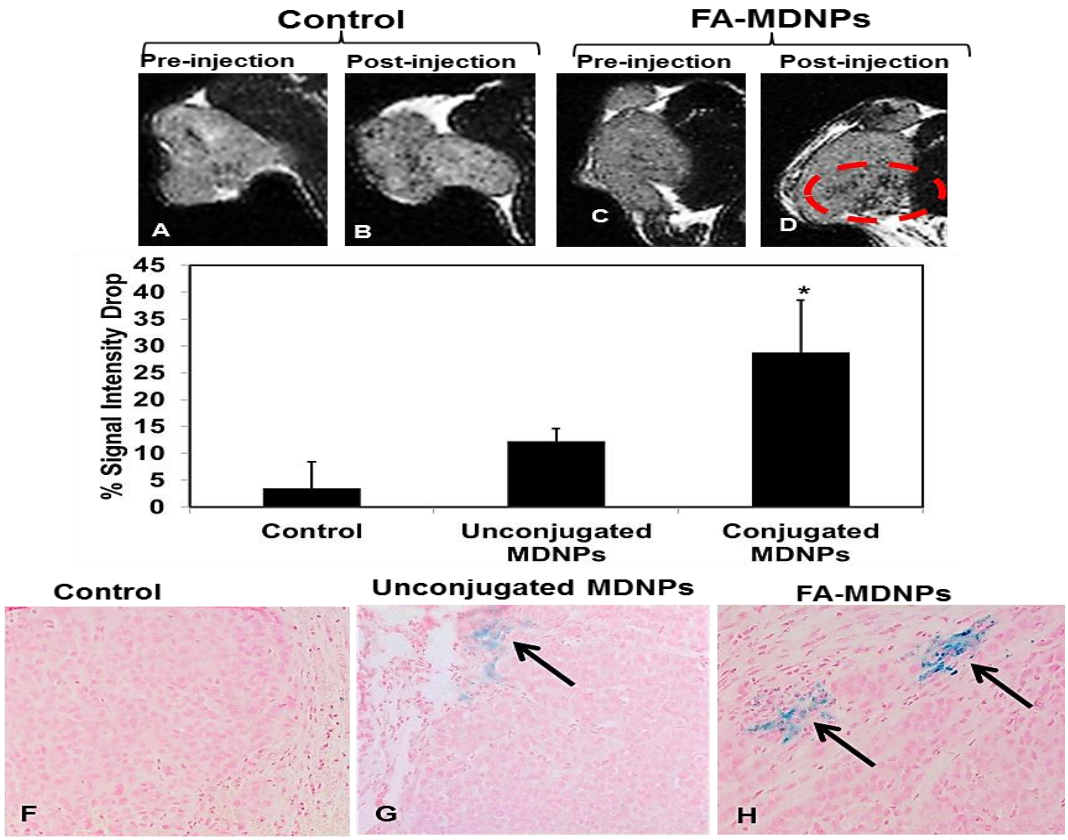

Figure 3.15 (A,B) MR images of the control group before and after saline injection. (C,D) MR images of animals treated with folic acid-conjugated MDNPs before and after injection. A distinct darkening of the tumor was observed post injection. (E) Significant T2 signal intensity drop was observed in the case of folic acid-conjugated MDNPs indicating that there was greater negative contrast compared to the pre-injection scans, due to the presence of iron oxide in the tumor. (F,G,H) Prussian blue staining on the tumors (10x magnification). More blue regions (arrows) seen in the folic acid-conjugated MDNPs group indicating presence of greater amount of iron oxide as the MDNPs contained iron oxide

respectively compared to the intensity before treatment (Figure 3.15 E). These results are in agreement with previous studies done in our lab where R11-conjugated thermosensitive NPs showed greater retention in prostate tumors *in vivo* than unconjugated NPs, 24 hours after administration [167].

Prussian blue staining of the tumors was carried out and the sections were visualized at 10x magnification. More iron could be seen in the tumor sections treated with folic acid-conjugated MDNPs compared to sections treated with unconjugated MDNPs (Figure 3.15 F, G, H), 24 hours post treatment. This indicates that the folic acid-conjugated MDNPs were retained longer in the tumor following administration.

3.3.10.2. *In Vivo* Therapeutic Efficacy

Further, the efficacy of drug-loaded MDNPs was studied in H460-tumor bearing athymic nude mice. For RT, the mice were placed under anesthesia in the X-RAD320 chamber and a probe was used to deliver the radiation dose specifically to the tumor. In this preliminary proof-of-principle study, the external tumor volume of all animals was measured prior to the injections for the duration of the study and plotted as a percentage of initial tumor volume (Figure 3.16 B, C). It was observed that the tumors in control (sham) group grew exponentially to 6000% of their initial volume within 12 days. On the other hand, tumors in 'MDNPs only' (not drug-loaded) group and 'drug cocktail' (NU7441+Gemcitabine) group grew to ~2400% and ~1200%of their initial volumes respectively. The comparatively slower tumor growth rate in the 'MDNPs only' group compared to the sham control group could be due to possible release and subsequent toxicity of SPIO from the particles. This can be overcome by replacing SPIO with FDA-approved Feraheme or other MR contrast agents such as manganese or gadolinium for future studies. The tumor inhibitory effect of the drug cocktail can be attributed to

therapeutic effect of gemcitabine hydrochloride which was released from the shell. On providing RT only, the tumor growth on day 12 was only 535% of the initial volume.

However significant inhibition of tumor growth was observed in 'drug cocktail + RT' group and 'drug-loaded MDNPs+RT' groups whose tumor volumes at day 12 were 506% and 377% of their initial tumor volumes respectively (Figure 3.16 C). This indicates that the drug-radiosensitizer combination used in our study is effective in slowing down tumor growth when used in combination with RT. Our particles could potentially overcome the systemic side effects that may occur on administering the free drug cocktail [168]due to its controlled release properties and targeting capabilities. The targeting capabilities of the MDNPs have already been confirmed using *in vivo* MRI were folic acid-conjugated particles were retained longer in the tumor. Following treatment, the animals were sacrificed and the tumors excised for *ex vivo* volume measurements (Figure 3.16 D) and visual observation (Figure 3.16 E). It could be clearly seen that tumors of animals treated with drug loaded particles + RT were significantly smaller than tumors from animals in the other treatment groups at the end of the study. Our preliminary results thus indicate the potential of our MDNPs as carriers of therapeutic agents for controlled and localized lung cancer therapy.

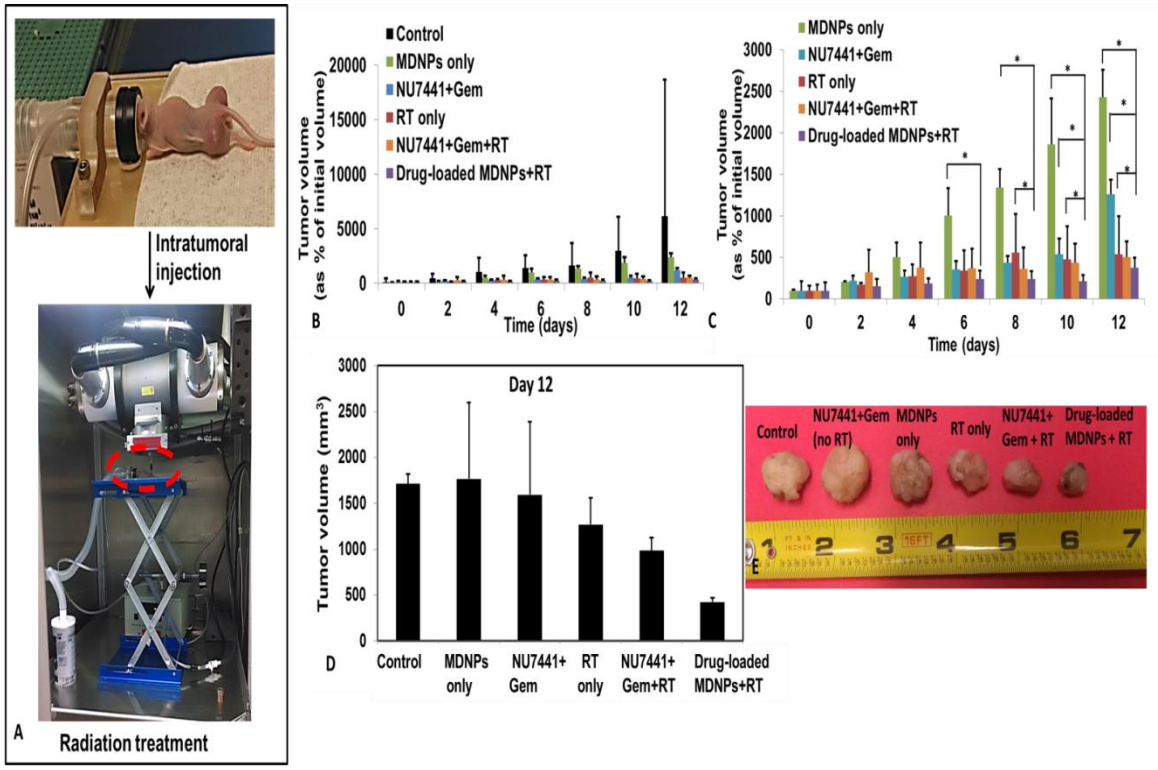

Figure 3.16 (A) Representative images showing the anesthesia set up for the *in vivo* studies (top) and the set up for radiation treatment (bottom). The circled area shows the mouse under anesthesia inside the X-rad320 biological irradiator. (B) Graphical representation of the changes in tumor volume for each group as a percentage of their initial volume at the beginning of the study. (C) Tumor volumes for each group excluding the Control group showing significant slower tumor growth rate in the case of 'NU7441+Gem+RT' group and the 'Drug-loaded MDNPs+RT' group compared to other treatment groups at days 8, 10 and 12 (n=4, *p<0.05 for 'Drug-loaded MDNPs+RT' group compared to other treatment groups) (D) *Ex vivo* tumor volumes of the different treatment groups at day 12 demonstrating the much smaller tumor size of 'Drug-loaded MDNPs+RT' group compared to the other groups (n=2) (E) Representative images of tumors from the different treatment groups

3.4 Summary

To summarize, multi-functional core-shell NPs responsive to environmental changes in temperature and pH were successfully synthesized. The particles had an average hydrodynamic diameter of 289 nm and zeta potential of -36 mV indicating good stability. They also showed minimal particle size variations in DI water, serum, saline and body fluids over a period of 5 days indicating that they are stable. In addition, these particles maintained the magnetic property of encapsulated SPIO which was demonstrated both visually as well as using a hysteresis loop. Further these multi-functional particles showed distinct temperature- and pH-responsiveness at 43^{o}C and pH 5 respectively. Drug release studies showed temperature and pH-dependent release of the encapsulated agents. *In vitro* cell studies demonstrated that our multi-functional particles were cytocompatible with HDFs and AT1 cells up to a concentration of 1 mg/ml and showed dose and magnetic field-dependent uptake chiefly by calveolae-mediated endocytosis. Colony forming studies established that our drug-loaded particles caused significant cell death at 43^{o}C. Furthermore, our particles showed excellent hemocompatibility and did not accelerate hemolysis and blood clotting at high MDNP concentrations of 500 µg/ml. *In vivo* studies confirmed that our particles can be visualized by MRI and showed good therapeutic efficacy by slowing down tumor growth when administered in combination with radiation treatment.

Chapter 4

Preliminary Investigation on the Use of Porous PLGA Microparticles as *In Vitro* 3D Tumor Models for Lung Cancer Drug Screening

4.1. Introduction

Two-dimension (2D) cell culture has been in existence as early as 1885 when Wilhelm Roux demonstrated that the medullary plate of a chick embryo can be maintained on glass plates with warm saline solution [169, 170]. Since then, cells have been traditionally cultured *in vitro* in 2D polystyrene or glass surfaces. With the advent of the field of drug delivery, there have been numerous works making use of 2D cell culture models for drug screening and cytocompatibility studies. However, these conventional 2D systems differ from *in vivo* tissues in cell surface receptor expression, extracellular matrix synthesis, cell density and metabolic functions [171]. They are also unable to develop hypoxia or demonstrate the different rates of cell proliferation seen in different parts of the tumor [172]. Further, studies have shown that tumor cell monolayers grown on tissue culture plates develop a non-natural morphology which could be a major factor affecting their responses to drugs as well [173].

Recent studies have demonstrated that the promising effects of therapeutic agents in *in vitro* 2D cell culture systems have not translated into successful results *in vivo* in animal models and humans. Only about 5% of the chemotherapeutic agents that showed promising preclinical activity have demonstrated good therapeutic efficacy in phase III clinical trials [174].Therefore the need for an *in vitro* three-dimensional (3D) cell culture model that attempts to mimic *in vivo* tissues more closely for cancer drug screening and other tissue engineering applications becomes vital.

The tremendous progress in the field of tissue engineering as well as enhanced knowledge of cell physiology has recently led to the development of biodegradable polymeric scaffolds for 3D cell cultures. Considerable interest has been shown towards the development of microparticles as scaffolds for 3D cell cultures, particularly due to the large surface area available for cell attachment and growth [175]. Previously, spheroids, gels and scaffolds have been used in the development of 3D tissue models. However spheroids are limited by the difficulty in controlling the size of cell aggregates – variations in diameter ranges from 20-1000 μm. On the other hand Gels are usually not adequately porous to support long term cell growth and proliferation and well as ECM deposition [176]. Scaffolds on the other hand are limited by uneven distribution of cells on its structure. The cells adhered to the outside would be exposed to nutrients and oxygen while cells within the scaffold may become necrotic quicklydue to limited availability of resources essential for their growth [177].

Porous microparticles have attracted attention recently as substrates for forming 3D tumor models for *in vitro* drug screening. These particles provide greater surface area for cell growth, facilitates EMC production [171] and allow nutrient and oxygen diffusion through them, thereby simulating an *in vivo* tumor microenvironment better than a 2D model [78, 175]. In this project, three types of PLGA-based porous microspheres were synthesized and compared for *in vitro* lung cancer drug screening applications. The long-term motivation of this project is to develop *in vitro* tumor models for comparatively more accurate testing of the therapeutic efficacy of drugs and drug delivery systems such as the MDNPs developed in Chapter 3. These tumor models could be used to study the activity of therapeutic agents before conducting *in vivo* studies, thereby potentially reducing the cost and time spent on optimizing and investigating drugs *in vitro*. This research could also contribute towards the development of personalized medicine where

the patient's owns cells can be used to form *in vitro* tissue or tumor models which can aid in tailoring the medication more accurately according to the disease of the patient, for effective therapy.

As mentioned before, PLGA is an FDA-approved biocompatible and biodegradable polymer used in several drug delivery applications. Gelatin and Sodium bicarbonate (SBC) were used as porogens in this study. In addition, a novel method of porous microparticle formation involving the use of PNIPAAm particles (PMPs) as porogens has been introduced. Following optimization of their properties, the 3D tumor models prepared using these porous microspheres will be used for screening different FDA-approved lung cancer drugs in terms of their therapeutic efficacy.

4.2. Experimental Section

4.2.1. Materials Used

Poly(lactic-co-glycolic acid) (PLGA, 50:50) was purchased from Lakeshore Biomaterials while Type B gelatin and sodium bicarbonate were obtained from Sigma-Aldrich and Invitrogen respectively. Poly vinyl alcohol (PVA, 87-89%), Dicholoromethane (DCM) and all other chemicals were purchased from Sigma-Aldrich. The A549 lung adenocarcinoma cell line was kindly given by Dr. Debabrata Saha's laboratory at the UT Southwestern Medical Center. RPMI media, trypsin-EDTA and penicillin-streptomycin were purchased from Invitrogen while Fetal Bovine Serum (FBS) was bought from Atlanta Biologics.

4.2.2. Preparation of Non-Porous PLGA Microparticles

Non-porous PLGA microspheres were fabricated as control to observe differences in cell attachment and proliferation between porous and non-porous

microparticles. Cells cultured in a well plate (2D cell culture) will serve as another control for the *in vitro* experiments. A standard single emulsion solvent evaporation technique was employed for the particle preparation. Briefly, 100mg of PLGA was dissolved in 5 ml of DCM to form the oil phase, which was then added drop-wise to 60 ml of 0.5% (w/v) PVA solution (water phase). The resulting emulsion was stirred overnight at 450 rpm to allow solvent evaporation. The particles were then isolated by centrifugation at 4000 rpm for 5 mins and lyophilized to obtain non-porous PLGA microparticles.

4.2.3. Preparation of Porous PLGA Microparticles

As mentioned earlier, three batches of porous microspheres were prepared using gelatin, SBC and PMPs as porogens respectively. A double emulsion technique was used for particle fabrication. The preparation technique for gelatin porogen-based particles was modified from a previously published work by Huang et al. [178]. Initially, 37.5 mg of gelatin was dispersed in 60 ml of 1% (w/v) PVA to form the first water phase. This solution was then added dropwise to 2% (w/v) PLGA in DCM (oil phase) and vortexed. The resulting emulsion was then added to the second water phase consisting of 1% (w/v) PVA solution placed in ice water bath. The double emulsion thus formed was gently stirred overnight to allow solvent evaporation. In order to facilitate gelatin leaching, the particle suspension was kept in a warm water bath at 45^{o}C under gentle stirring for 4 hours. The porous particles were then isolated by washing thrice with water, followed by centrifugation at 4000rpm for 5min and lyophilization.

The SBC porogen-based particles were prepared by modifying the protocol of Ke et al.[179]. Briefly, 500µl of 1% (w/v) SBC solution (first water phase) was added dropwise to the oil phase consisting of 5% (w/v) PLGA solution in 2ml DCM. This emulsion was then added dropwise to 60 ml of 0.1% (w/v) PVA solution and gently stirred

overnight. SBC leaching was done by centrifuging the obtained particles in PBS solution at a pH of 3-4 at a speed of 1500 rpm for 30 min. Subsequently, the particles were washed twice in DI water, isolated by centrifugation (1500 rpm, 30 min) and lyophilized to obtain porous PLGA microspheres.

To prepare the PMPs porogen-based particles, first the PMPs were prepared by free radical polymerization. Briefly, 1.54 mg of NIPA, 26.2 mg BIS and 43.8 mg SDS were allowed to disperse in 90 ml of DI water by stirring. The solution was then purged with nitrogen gas for 30 mins following which APS and 500 µl of TEMED was added. The reaction was allowed to occur in a nitrogen atmosphere for 5 hours and the particles were purified by dialysis and collected by lyophilization. In order to prepare the PMP porogen-based PLGA microspheres, 0.5 ml of 0.3% w/v PMP suspension in DI water was added in a dropwise manner to 2ml of 5% (w/v) PLGA solution in chloroform. This oil-in-water emulsion was vortexed and dispersed well following which it was added dropwise to a 0.1% (w/v) PVA solution. Following overnight stirring, the particles were collected by centrifugation at 1500 rpm and 30mins, and lyophilization. For porogen leaching, the microparticle suspension was kept shaking at 37^{o}C for 2 hours following which the particles were centrifuged at 2000rpm for 5 mins to allow the heavier microparticles to settle down. The lighter PMPs that were leached out of the particles remained in the supernatant. The pellet containing the microparticles was then lyophilized to obtain porous PLGA microspheres.

4.2.4. Physical Characterization

Particle size, poly dispersity and surface charge measurements were carried out using the DLS instrument. 20 µl of 1mg/ml microparticle suspension was taken and 20µl was added to a transparent cuvette containing 3 ml of DI water. Particle size readings

were taken by scattering of laser light within the instrument by the Brownian motion of the suspended particles in the suspension. Further, the morphology of the prepared porous and non-porous microspheres was observed using Scanning electron microscopy (SEM, Hitachi S-3000N, Hitachi, Pleasanton, CA). Briefly, 10µl of the microparticle suspension was added onto a coverslip and air-dried overnight. This coverslip was then silver sputter-coated and inserted into the SEM instrument. Further, Energy dispersive X ray spectroscopy (EDS) was conducted to identify atomic compositions at the porous and non-porous sites of the particles. Additionally, the average pore size of the particles was also measured from the SEM images using Image J software.

4.2.5. Particle Stability and Degradation Kinetics

Stability of particles was investigated in DI water and media containing 10% serum over a period of 5 days. Briefly, 20µl of prepared particle suspension (1 mg/ml) was added to a transparent cuvette containing 3ml of serum/ water. Particles were incubated for 5 days at 37^{o}C and their size evaluated at predetermined time points using DLS.

In addition to stability, the degradation kinetics of the particles was also studied over a period of 4 weeks. Pre-weighed microparticles (1mg) were dispersed in 1 ml of PBS and incubated while shaking at 37^{o} C. At fixed time intervals (0, 1, 4, 7, 14, 21 and 28 days), the particles were collected by centrifugation (4000rpm, 5 min), and then lyophilized. The degradation profile was determined by calculating the weight loss of the particles over time, compared to their initial weight at day 0.

4.2.6. In Vitro Cell Studies

4.2.6.1. Cell Attachment Study

Multiple *in vitro* studies were done on the particles in order to optimize them for development of 3D tumor models. Before beginning the studies, the porous PLGA particles were first sterilized by overnight via UV light exposure following which they were immersed in 70% EtOH. They were subsequently washed with sterile 1X PBS and cell culture media. The serum proteins in the cell culture media were expected to be adsorbed onto the porous microparticles, which would provide a suitable surface for cell adhesion and proliferation [180]. Further, the wellplates were coated with 100 µl of 0.5% w/v agarose to ensure that cells do not adhere to the bottom of the wells. Studies were first conducted to determine the optimum cell seeding density onto the microparticles. A549 lung adenocarcinoma cells were seeded at varying densities such as 15, 25, 35, 45 and 55 cells/mg of particles into 48 well plates. These wellplates were incubated at 37^{o}C in alternating shaking (30 rpm, 25 mins) and static conditions (25 mins) for the first 2 hours of incubation following which they were left undisturbed. After 24 hours, the wells were washed well with PBS to remove unattached cells and the particles were transferred to a new 48-well plate. MTS assay was performed on the particles following the manufacturer's instructions and absorbance was read at 490nm using spectrophotometer. Greater absorbance readings indicated that more number of cells have attached onto the particles.

In order to study the effect surface coating on cellular attachment and proliferation, the microparticles were further coated with fibronectin. Briefly, 5 mg of porous particles were sterilized and placed in 48 well plates and 5 ml of serum-free media containing 10 µg/ml fibronectin was added to it. These particles were then shaken

at 37^{o}C for 2 hours at 30 rpm following which cell seeding studies were conducted as described above.

In order to visualize the cell growth on our particles, Live/Dead staining (Invitrogen, Grand island, NY) was used. Briefly, the particles containing cells were washed with PBS in a 48 well plate and 100µl of media was added to it. Then 100ul of working dye (EtD1 and Calcein in 2ml of PBS) was added to the particle-cell complexes. Following incubation at 37^{o}C for 30 mins, the particles were washed with PBS and 100 ng/ml DAPI solution was added to the cells and incubated at room temperature for 5 mins. Then the cells were washed and imaged using an Enhanced fluorescent optical microscope (Nikon Eclipse Ti, Nikon Instruments Inc., Melville, NY).

4.2.6.2. Cell Proliferation Study

Based on the optimized cell seeding density observed in the cell attachment study, a cell proliferation study was conducted to determine the number of days up to which A549 cells can proliferate on our microparticles. Briefly, cells were seeded at 250,000 cells/mg of particles seeding density on fibronectin-coated particles and these particles were incubated while shaking at 37^{o}C. At pre-determined timepoints (1, 3, 5, 7 and 9 days), MTS assay was carried out using a spectrophotometer and the absorbance values were normalized against a cell standard. The cells were further visualized using Live/Dead staining with the procedure mentioned above. Further cell attachment on the particles was also observed using SEM. For this procedure, the particle-cell complex was fixed using 2.5% glutaraldehyde followed by incubation at room temperature for 30 mins. Then the complexes were washed using PBS following which they were incubated with 1% osmium tetroxide for 1 hour. The samples were again washed and then dehydrated in

50%, 75%, 95% and 100 % ethanol. Hexamethyldisilazane (HMDS) was added to the samples which were then air-dried and visualized using SEM following sputter-coating.

4.2.6.3. *In Vitro* Drug Screening Study

The difference in therapeutic efficacy of cancer drugs on 2D and 3D tumor models *in vitro* drug screening study was studied. First the PLGA-SBC particles were sterilized and coated with fibronectin as described previously. The wellplates used for this study were coated with 100 µl of 0.05% agarose solution as described previously in order to prevent cell attachment to the bottom of the wellplates. Then A549 cells at a seeding density of 250,000 cell/mg of particles was added. The well plate containing the particles and cells were kept shaking for 3 days to ensure cell attachment and proliferation. For this study six chemotherapeutic drugs were chosen. Three of them – gemcitabine hydrochloride, paclitaxel and cisplatin have been approved by the FDA for treatment of lung cancer. Three other drugs not approved by the FDA for lung cancer treatment (doxorubicin, 5-FU and curcumin) were also tested. All drugs were added at their previously reported IC_{50} concentrations to the cell-particle complexes as well as the 2D cell layers. The groups were then incubated for 2 d at $37^{o}C$ following which the samples were washed well to remove residual drugs. The number of cells viable in each group was tested with MTS assay and confirmed using LDH assay, following manufacturer's directions.

4.2.6.4. *In Vitro* Therapeutic Efficacy of MDNPs

An *in vitro* study was also conducted to establish the therapeutic efficacy of MDNPs developed in Chapter 3 on our porous microsphere-based tumor models, both under normoxic and hypoxic conditions. The purpose of this study was to confirm our

hypothesis that 2D monolayers and cells grown in a 3D environment may not respond im a similar manner to therapeutic agents. Results from this study could potentially lead to the development of more appropriate testing methods for drug delivery vehicles *in vitro* so that it can in turn speed up the time spent on clinical investigation and these products could be released faster in to the market to save people suffering from various critical ailments. Briefly, A549 cells were seeded at 250,000 cells/ mg of PLGA-SBC microparticles seeding density in 48 well plates and allowed to grow for 3 days to form the *in vitro* tumor model. Then the media was replaced using 200 µg/ml MDNP suspension in media and the wellplate was placed in a modular incubator chamber (Billups-Rothenberg, Inc. Del Mar, CA). The chamber was flushed with 0.1% O_2 for 20 mins following which it was sealed and placed in the incubator. 10 ml of sterile water was placed in the chamber in a beaker to prevent evaporation of cell culture media. At the end of the study, the cells were washed and viability was determined using MTS assays. The results were confirmed using LDH assays. This study was conducted under two conditions: 37^{o}C and 43^{o}C and also under normoxia (21% O_2) or hypoxia (0.1% O_2). A549 cells cultured as a 2D monolayer and exposed to MDNPs served as controls.

4.3. Results and Discussions

4.3.1. Microparticle characterization

Non-porous as well as large porous PLGA microparticles were successfully synthesized using gelatin, SBC and PMPs as porogens. SEM images indicated that non-porous PLGA particles (Figure 4.1A) had a smooth spherical surface while PLGA-Gelatin (Figure 4.1B), PLGA-SBC (Figure 4.1C) and PLGA-PMPs (Figure 4.1D) microspheres have spherical morphology with diameters of 62, 46 and 39 µm respectively.

ImageJ analysis was done to establish that the pore size of PLGA-Gelatin microspheres was around 0.5-10 µm while PLGA-SBC and PLGA-PMPs particles had pores in the size range 5-12µm and 1-4 µm respectively. The smaller pore size distribution range for the PLGA-PMPs was because of the use of PMP porogen, which was about 1-5µm diameter. The advantage of using this novel porogen was to obtain relatively uniformly sized pores throughout the microparticle so as to allow uniform nutrient diffusion. The SEM images confirm that the formed PLGA-PMPs had better uniform pore size compared to other porous microparticles.

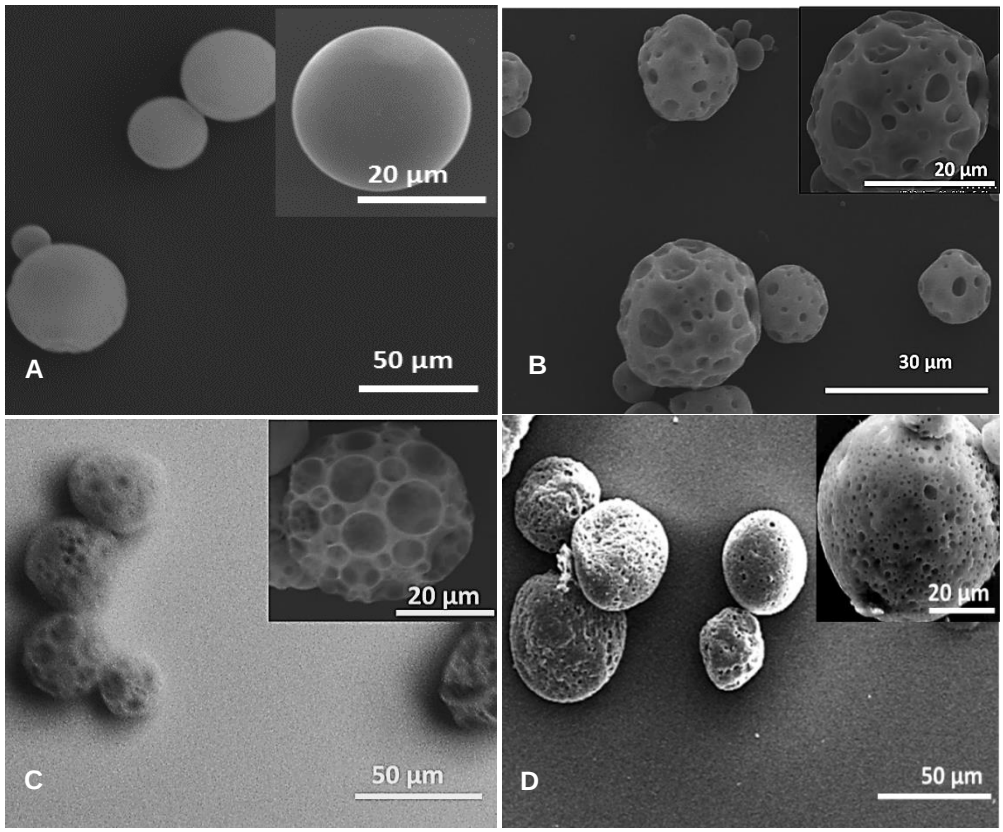

Figure 4.1 SEM images of (A) non-porous PLGA microparticles and porous microparticles prepared using (B) gelatin (C) sodium-bicarbonate, and (D) PMPs. The spherical morphology and porous nature of PLGA-Gelatin, PLGA-SBC and PLGA-PMPs can be clearly visualized

The physical characteristics including particle size, surface charge, polydispersity and pore size measured using DLS and ImageJ have been summarized in Table 4.1. Based on DLS readings, the hydrodynamic diameters of PLGA-Gelatin and PLGA-SBC microspheres are close to 50 µm while PLGA-PMPs had a size of about 39 µm. Previous published works have shown that A549 cells have an average diameter of 6-15 µm indicating that our particles will provide sufficient surface area for A549 attachment and growth [181, 182].

Table 4.1: Initial characterization of porous particles: PLGA-Gelatin, PLGA-SBC and PLGA-PMPs

Particle type	Diameter (µm)	Polydispersity	Zeta potential	Pore size (µm)
Non-porous PLGA	41	0.4	-19.3±0.3	-
PLGA-Gelatin	62	0.4	-26.3±0.9	0.5-10
PLGA-SBC	46	0.4	-37.5±1.6	5-12
PLGA-PMPs	39	0.3	-22.4±1.2	1-4

Prior to studying cell adhesion and growth *in vitro,* the porous PLGA microparticles were further analyzed using EDS to ensure that porogen leaching has occurred completely. Based on EDS spectrum given below, PLGA-SBC particles that have not undergone leaching of porogen shows a distinct Na peak suggesting the presence of SBC within the particle (Figure 4.2). On the other hand, PLGA-Gelatin and PLGA-PMPs does not show any distinct peaks as the components of gelatin and PNIPAAm are the same as the components of PLGA. Microspheres that have undergone porogen leaching show only the presence of carbon and oxygen, which represents the elemental composition of PLGA (data not shown).

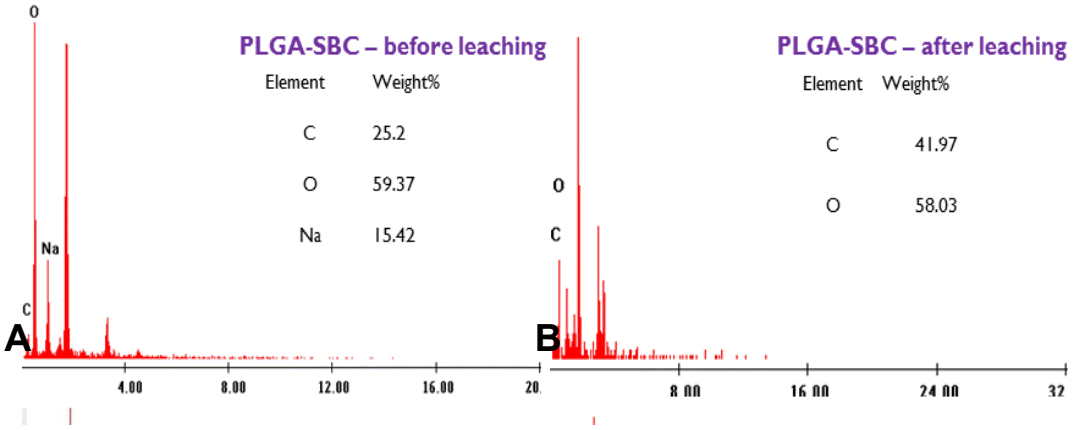

Figure 4.2 EDS spectrum showing the elemental compositions of PLGA-SBC (A) before and (B) after leaching. The absence of Na peak in figure B indicates that the SBC has been leached out successfully

4.3.2. Stability and Degradation Kinetics

The porous microparticles were further characterized and compared with non-porous PLGA microparticles in terms of their stability in media containing 10% serum and in DI water. It was seen that the particles maintain their size in DI water with minor variations, indicating that they are stable and undergo minimal aggregation. In media, all three types of particles were relatively stable and underwent minor fluctuations by about 20-30% of their original size, over a period of 5 days (Figure 4.3 A, B). This suggests that the non-porous as well as porous particles were fairly stable in serum and DI water and will not undergo major aggregation or clumping which could possibly reduce the surface area available for cell attachment and growth.

Prior to developing *in* vitro 3D tumor models, it is essential that the degradation rates of the scaffolds be properly characterized. This study is necessary to confirm that the polymeric microparticles will maintain their integrity long enough for the cells to attach, proliferate and infiltrate into them thus eventually replacing the polymer to form a

tissue model that is representative of tumors seen in the body. The degradation study conducted under physiological conditions for 4 weeks showed that the porous microspheres using gelatin and SBC porogens degraded 60% and 50% of their original weight respectively, as shown in Figure 4.3C. PLGA-PMPs also degraded about 50% of their weight within 4 weeks.

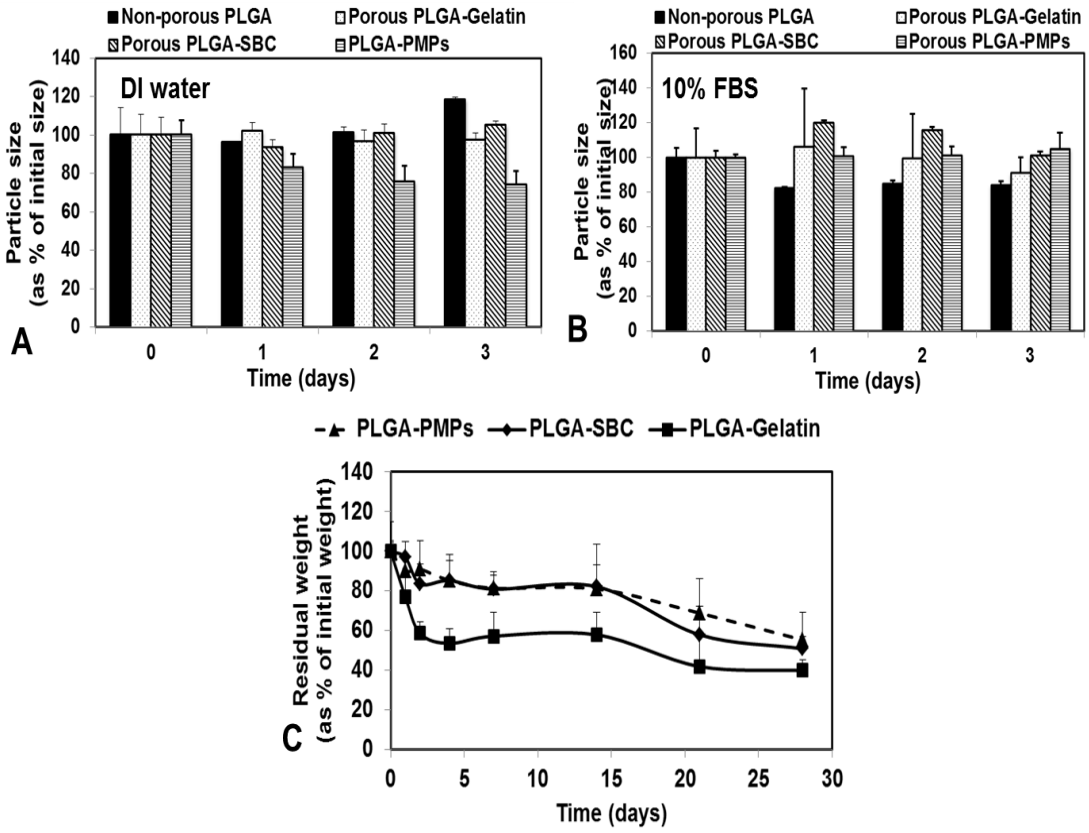

Figure 4.3 Particle stability in (A) water and (B) 10% serum indicating that non-porous PLGA, PLGA-SBC, PLGA-Gelatin and PLGA-PMPs maintained their size and granulometric properties for 3 days. (C) Degradation of porous PLGA microparticles investigated at 37^{o}C for 4 weeks. PLGA-Gelatin particles degraded 60% of their initial weight in 28 days while PLGA-SBC particles and PLGA-PMPs were reduced to 50% and 44% of their original weight respectively (n=4)

4.3.3. In Vitro Cell Studies

4.3.3.1. Cell attachment studies

In vitro studies were conducted to optimize the cell seeding density to be used on the microparticles. As shown in Figure 4.4 A and B, cell attachment saturated at a seeding density of 250,000 cells/ mg for all MPs (Figure 4.4 C). No significant increase in cell attachment was observed at higher densities. Significantly higher cellular attachment

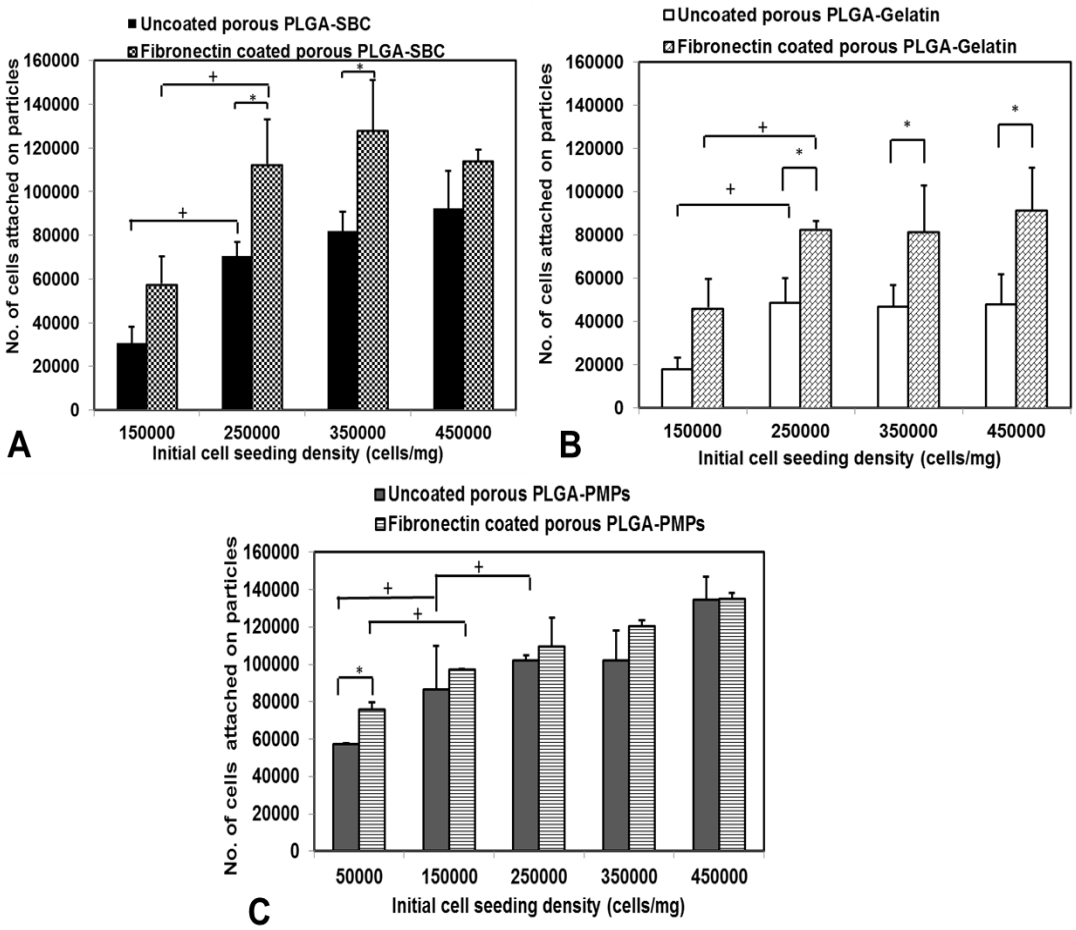

Figure 4.4 A549 cell attachment on uncoated and fibronectin-coated particles for 24h. Maximum cell attachment was observed at cell at 250,000 cells/mg of particles cell density for PLGA-SBC and PLGA-gelatin particles. Cell attachment saturated at 150,000 cells/mg density for PLGA-PMPs (*p<0.05 w.r.t cell attachment on uncoated particles, +p<0.05 w.r.t cell attachment between different cell seeding densities)

was observed on all particles following fibronectin coating and on dynamic cell seeding.

Further, cell attachment and viability on our porous microparticles was visualized using Live/Dead and DAPI staining in order to ensure that the cells are indeed viable following seeding and attachment onto the particles. It was observed that the cells attached onto all particles within 24 hours with minimal cell death. (Figure 4.5).

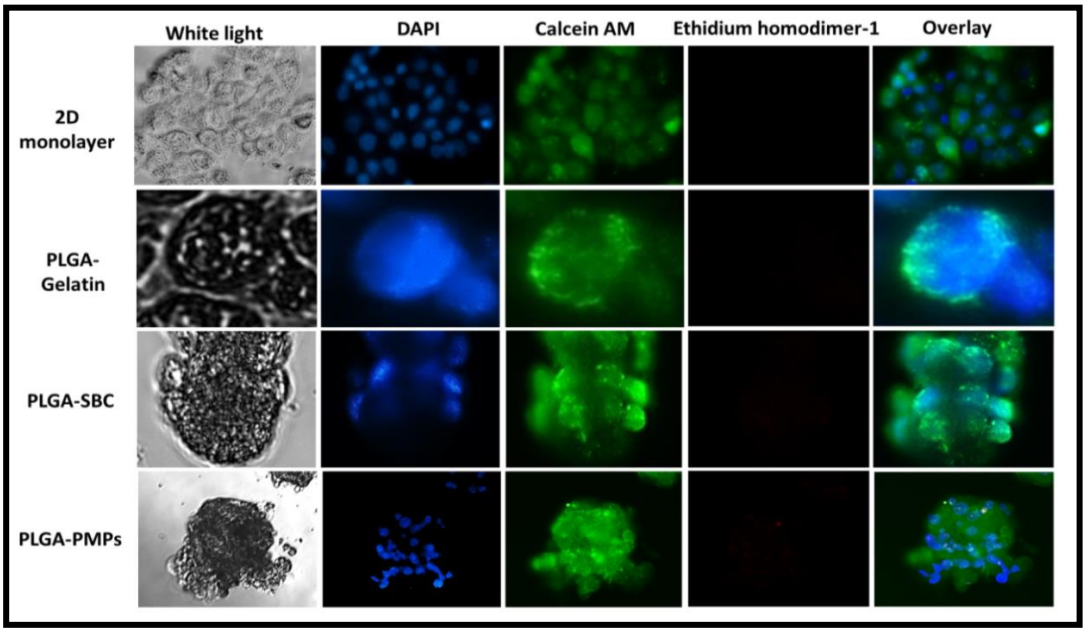

Figure 4.5 Live/dead and DAPI stained particles after 1d culture indicating that the A549 lung cancer cells could attach onto the particles within 24 hours and were viable (green = live, red = dead)

Cell attachment on the fibronectin-coated microparticles was further visualized using SEM. The arrows indicate regions where the A549 cells have adhered onto the particles. The cells appear to have retained their morphology and appendages can be seen indicating that the cells have spread out and begun to proliferate on the surface of all the particles (Figure 4.6). The protocol will be modified to incorporate critical drying in order to obtain better SEM images showing cell attachment on the particles, in the future.

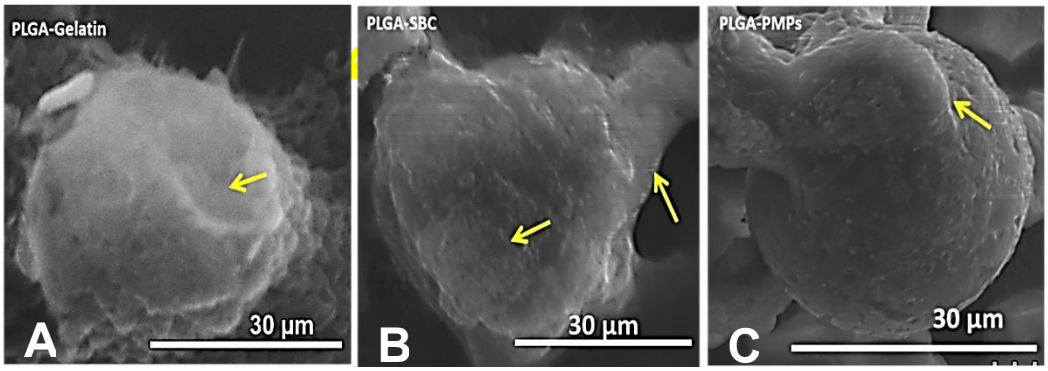

Figure 4.6 SEM images of cell attachment on (A) PLGA-Gelatin, (B) PLGA-SBC and (C) PLGA-PMPs following 2 days of culture. The cells are clearly seen attached on to the surface of the microparticles (arrows)

4.3.3.2. Cell Proliferation study

Cell proliferation study using A549 cells indicate that cell proliferation does occur on all three types of porous microparticles (Figure 4.7). However significantly higher cell proliferation occurred on the surface of porous PLGA-SBC microparticles. Cell number

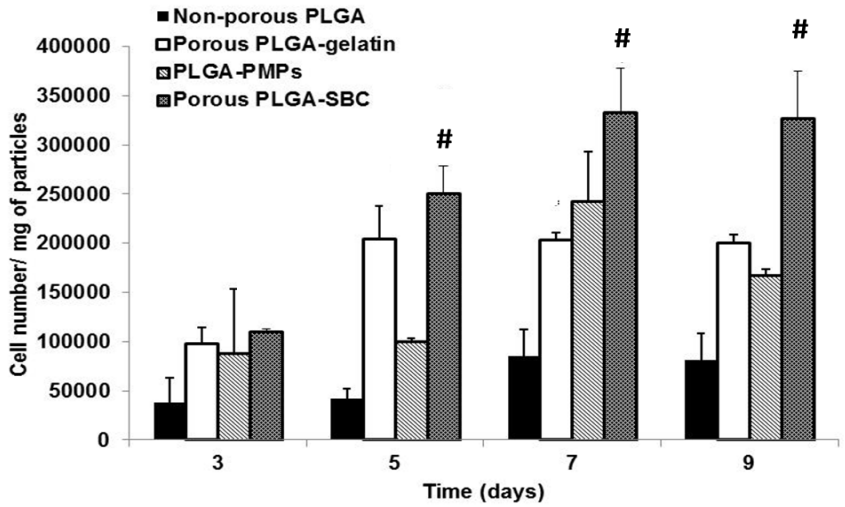

Figure 4.7 A549 cell proliferation on particles up to 9 days, showing significantly higher cell growth on PLGA-SBC porous particles compared to the non-porous control particles and other porous particles (Porous PLGA-SBC vs. porous PLGA-Gelatin and PLGA-PMPs (# $p<0.05$ w.r.t porous PLGA-Gelatin and PLGA-PMPs)

also appeared to saturate on all microparticles by day 7 of the study indicating that the cells may have covered the entire surface of the particles and did not have any further surface available for cell proliferation.

Further cell proliferation was visualized using Live/Dead assay. Cell death was observed at day 7 in the case of PLGA-Gelatin which could have occurred because of the lack of microparticle surface for cells to grow on. Similarly, cell death could be distinctly seen on PLGA-PMPs from day 5 as the particles are small and have less area available for cell attachment. On the other hand, no significant cell death could be observed on PLGA-SBC particles up to day 7 (Figure 4.8).

Based on all the studies conducted so far, it can be observed that PLGA-SBC particles were ideal for 3D tumor model formation as they demonstrated greater cell attachment, proliferation and viability than other particles. Therefore these particles were

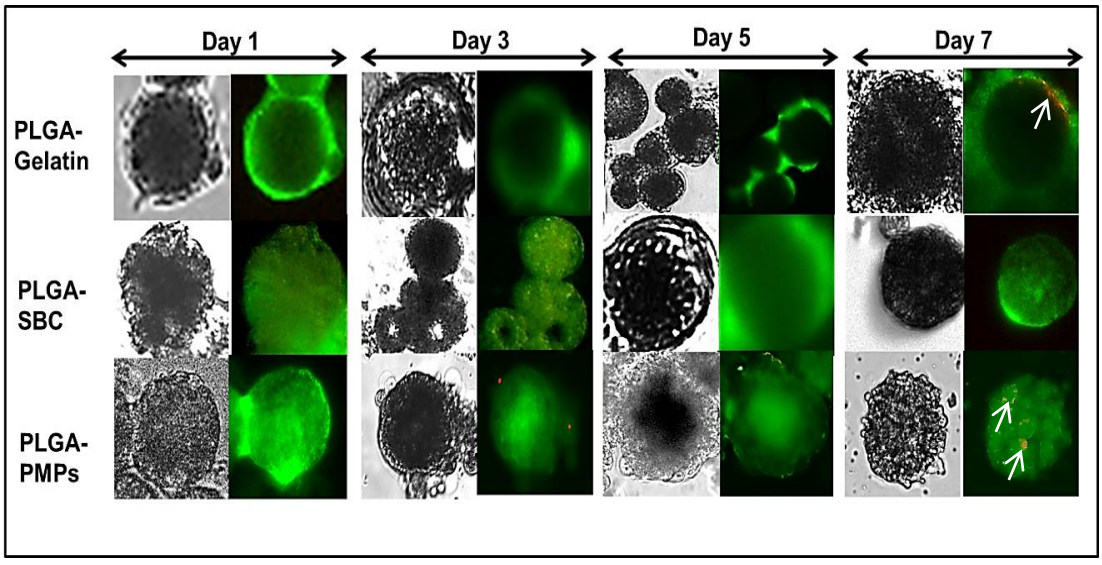

Figure 4.8 Live/Dead staining shows A549 lung cancer cells attached on porous PLGA micro particles are viable for up to 7 days with minimal or no cell death. PLGA-PMPs and PLGA-Gelatin showed minimal cell death (arrows) at around day 7; however PLGA-SBC microparticles remained viable throughout the study for 7 days

chosen to form A549 lung tumor models for our *in vitro* drug screening study.

4.3.3.3 In Vitro Drug screening

Six different drugs namely Gemcitabine, Paclitaxel, Cisplatin, Doxorubicin, 5-FU and Curcumin were screened *in vitro* for their therapeutic efficacy on 2D cell layers and 3D tumor models formed using PLGA-SBC particles. Both the monolayer and the 3D tumor model were treated with IC50 concentrations of all drugs (11nM Gemcitabine [183], 4.1nM Paclitaxel [184], 64 μM Cisplatin [185], 0.6 μM Doxorubicin [186], 13 μM 5-FU [187] and 17 μM curcumin [188]). As seen in Figure 4.9, the response of the 2D cell layer and the 3D tumor model to the same concentration of therapeutic drugs *in vitro* was significantly different. For example, gemcitabine, curcumin and cisplatin demonstrated significantly lower cell death on the 3D tumor model compared to control, than in the 2D cell layer at the same drug concentration.

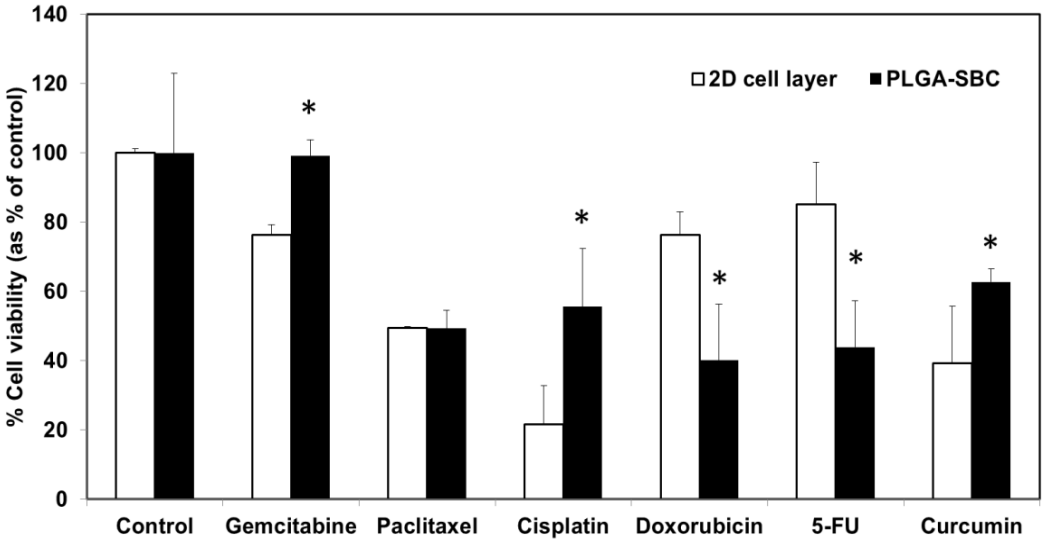

Figure 4.9 Drug screening study using A549 lung cancer 3D tumor model and 2D monolayer showed different responses to chemotherapeutic drugs of same concentration. There was no significant variation between the two groups in response to paclitaxel (n=4, *p<0.05 w.r.t % cell viability of 2D cell layer)

On the other hand, doxorubicin and 5-FU caused greater cell death on the 3D tumor model compared to the control, than in the 2D layer. Paclitaxel had no significant effect on cancer cell death both in 2D and 3D. This is different from results obtained by Nirmalanandhan et al.[189] who had tested the effect of chemotherapeutic drugs on *in vitro* 3D spheroids prepared using A549 and H358 lung cancer cells in collagen gel. This group observed no significant variation in the efficacy of doxorubicin and cisplatin between 2D and 3D models, while we observed less efficacy for cisplatin and greater efficacy for doxorubicin compared to the 2D monolayer. Also, the authors noticed greater therapeutic efficacy of paclitaxel in the 3D model while we observed no change in the response of our 2D and 3D monolayer when exposed to paclitaxel. The differential responses may have occurred due to the different types of 3D models used in both experiments. While we used porous microparticles as a substrate for cell growth, the aforementioned article used a collagen gel. However as mentioned earlier, the spheroids thus formed may have uncontrolled sizes/ cell aggregation and limited porosity to allow nutrient and oxygen diffusion. This may have resulted in the variable results observed. Detailed studies would have to be conducted and compared with *in vivo* results to select the most appropriate 3D tumor model for future studies.

Finally, drug screening was also conducted to study the *in vitro* therapeutic efficacy of drug-loaded MDNPs developed in Chapter 3 using our 3D tumor model and 2D cell layer *in vitro* under hypoxic and normoxic conditions. Cells grown in 2D and 3D but not treated with MDNPs were used as controls. It was observed that the 3D tumor model developed using PLGA-SBC particles and the 2D monolayer varied significantly in their responses to treatment using MDNPs. For example, PLGA-SBC tumor model demonstrated 52% and 82% cell viability compared to those of the control under normoxic and hypoxic conditions at 37^{o}C. The 2D monolayer on the other hand

demonstrated 23% and 34% viability respectively under the same conditions. At 43^{o}C, our 3D tumor model showed lower viability of 41% and 32% under normoxic and hypoxic conditions compared to those of 37^{o}C while the 2D monolayer showed 12% and 28% viability respectively. Cell viability under hypoxic conditions varied significantly from that observed under normoxia for both groups. Also, hypoxic cells in both groups showed resistance to the chemotherapeutic drugs at 37^{o}C while more cell death was observed at 43^{o}C due to the simultaneous effect of chemotherapy and sensitization of the hypoxic cells to hyperthermia (Figure 4.10). This is in concurrence with studies by Gerweck et al. [190] which demonstrated that *in vitro* cancer cell culture in conditions mimicking tumor microenvironment increased the sensitivity of these cells to hyperthermia at 42^{o}C. The

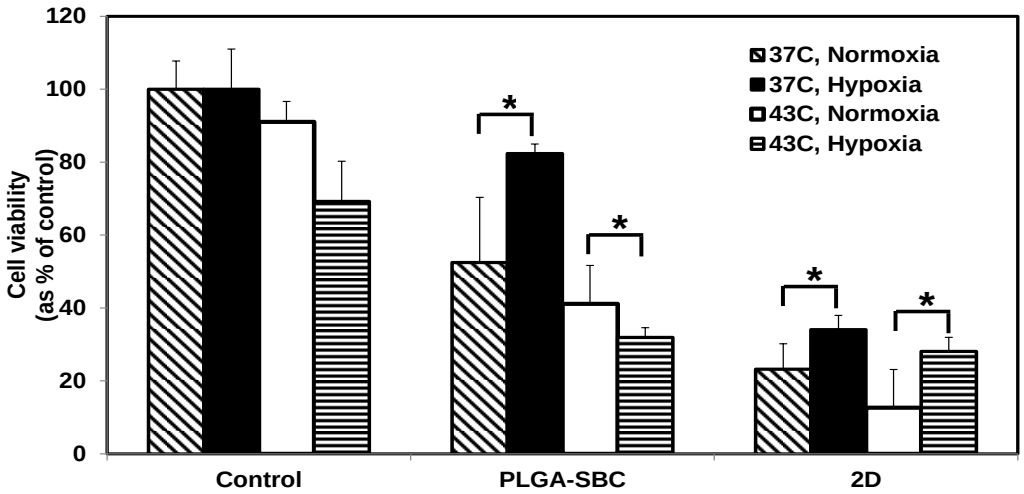

Figure 4.10 Comparison of therapeutic efficacy of drug-loaded MDNPs with 2D monolayer and 3D tumor model under hypoxic and normoxic conditions. Cell viability under hypoxia was significantly different from that observed under normoxia. Hypoxic cells at 37^{o}C demonstrated resistance to treatment while they showed significant death at 43^{o}C due to simultaneous hyperthermia and chemotherapy. 3D tumor model and 2D monolayer varied significantly in their response to treatment. Cells in 2D and 3D not exposed to MDNPs served as controls (n=4, *p<0.05)

greater resistance of hypoxic cells towards treatment also agree with findings by Jain et al.[191] who demonstrated that the *in vitro* uptake of their gold NPs was significantly lower in hypoxic DU145 cells than in normoxic cells. The lower MDNP uptake would have resulted in less drug release within the cells following endocytosis, which in turn would have caused lower cell death.

4.4. Summary

In summary, three biodegradable large, porous PLGA microparticles using gelatin, SBC and PMPs as porogens, for development of a 3D lung tumor model were synthesized. In addition, an innovative method of preparing porous microparticles with uniform pores, using PMPs was also been presented. These particles had average diameters 46-62 µm and showed high zeta potential of -26, -38 and -22 mV respectively for PLGA-SBC PLGA-Gelatin and PLGA-PMP microparticles. The PLGA-PMP particles showed a pore size of 1-4 µm while PLGA-Gelatin and PLGA-SBC had average pore sizes of 0.5-10 µm and 5-12 µm respectively. All three microparticle formulations particles were reasonably stable in DI water and serum up to 5 days and degraded up 60% (PLGA-Gelatin),44% (PLGA-SBC) and 50% (PLGA-PMPs) of their original weights respectively within 28 days. Moreover, saturation of cell attachment was observed at a seeding density of 250,000 cells/ mg of particles for all microparticles. Live/Dead staining and SEM images demonstrated that the cells were viable on all particles and had attached onto their surface within 24 hours of cell seeding. Cell proliferation studies conducted over a period of 9 days using MTS assays and Live/Dead staining indicate that all particles provided a good substrate for cell attachment and proliferation. However, PLGA-SBC showed maximum cell growth and viability while PLGA-Gelatin and PLGA-PMPs tend to show some cell death towards day 7. Based on these results PLGA-SBC

particles were chosen and optimized for further studies. Preliminary drug screening studies conducted to determine the therapeutic efficacy of various lung cancer drugs demonstrated that the 3D tumor model on PLGA-SBC microparticles responded differently compared to the 2D cell monolayer. This indicates that tumor architecture and dimension may play a significant role in the response of cells to different therapeutic agents. This is in keeping with previous published works that have shown differential drug responses between 2D and 3D models *in vitro* [173, 189]. Although drug screening using 3D models can be more time consuming, it may provide results with greater physiological relevance than a 2D model [192]. Therefore the 3D models should be further optimized to ensure high-throughput drug screening with reliable repeatable results. *In vitro* studies to evaluate the therapeutic efficacy of MDNPs also showed different responses in the 3D and 2D cancer models indicating that more studies are required to determine whether a conventional 2D tumor model is indeed the best option for evaluating *in vitro* therapeutic capabilities of different drugs prior to *in vivo* and clinical studies. Limitations of this work as well as other possible future studies have been explained in detail in Sections 5.2 and 5.3 respectively.

Chapter 5

Conclusions and Future Outlook

5.1. Conclusions

To summarize, seven different types of nanoparticle formulations and three porous microparticle formulations were developed in this project for various pulmonary-based applications. The first project involved the synthesis of gelatin, chitosan, alginate, PLGA, PLGA-PEG and PLGA-CS NPs which were extensively characterized and optimized to determine the most promising formulation apt for pulmonary delivery of biological molecules such as proteins and cDNA via nebulization. The PLGA and gelatin NPs showed promise in terms of optimal size, stability, *in vitro* cytocompatibility and uptake, as well as *in vivo* uptake and retention. However, PLGA NPs contained EPO-Rhodamine demonstrated greater retention *in vivo* indicating their potential as nanocarriers for inhalational delivery. The PLGA NPs were further modified to form a core-shell nanocarrier (MDNPs) for stimuli-responsive dual-drug delivery for targeted lung cancer therapy. These multi-functional NPs can be used for rigorous cancer treatment by stimuli-responsive burst release of encapsulated gemcitabine hydrochloride followed by radiosensitization of lung cancer cells by the controlled release of NU7441 – a potent radiosensitizer. The encapsulated SPIO successfully showed a decrease in signal intensity using MRI both *in vitro* and *in vivo*. Further the folic acid conjugated particles were successfully retained *in vivo* 24h after injection. Our formulated drug-loaded MDNPs also showed good therapeutic efficacy *in vivo* by significantly slowing down tumor growth when given in combination with RT. These results support our hypothesis that the MDNPs can be potentially used as nano-vehicles to provide simultaneous chemotherapy and radiation sensitization for lung cancer treatment.

Finally the PLGA polymer was also used in the development of porous microparticles (PLGA-Gelatin, PLGA-SBC and PLGA-PMPs) which could be used as substrates for cell attachment and proliferation to form *in vitro 3D* tumor/tissue models. These stable porous particles coated with fibronectin supported A549 lung cancer cell attachment and proliferation up to 9 days. PLGA-SBC supported greater cell proliferation and viability than the other two formulations and was hence chosen for further studies. Drug screening studies using six different chemotherapeutic drugs as well as drug-loaded MDNPs demonstrated varying therapeutic effects on the 2D monolayer and 3D PLGA-SBC models. These results support our hypothesis that a 2D cell layer would behave differently from a tissue/tumor model grown on a 3D platform. Extensive studies are required to confirm the feasibility of replacing the traditional 2D cell monolayers with 3D models for *in vitro* studies. However, these are only preliminary findings to support the use of 3D tissue/tumor models for drug delivery/screening as well as tissue engineering applications.

5.2. Limitations

Although the findings presented in this work are encouraging for pulmonary drug delivery and drug screening applications, a few limitations exist which have been detailed below. One of the limitations observed in Chapter 1was the comparatively larger size of PLGA-SPIO NPs (250 nm) compared to PLGA NPs (160 nm) alone. This large size could risk fast NP clearance from the lung by macrophages. However SPIO incorporation was done only for imaging purposes and will not be used eventually by us for drug delivery applications for later studies.

The PLGA NPs chosen after our extensive screening was used to develop the multi-functional MDNPs for delivery of therapeutic agents for lung cancer treatment. The

size of the particles (289 nm) is a limitation as this could result in rapid clearance from the lung. Efforts will be taken to further reduce and optimize the particle size by increasing the sonication power and/or surfactant concentration. Also, the use of multiple instruments for imaging (MRI) and treatment (Radiotherapy) using these particles could result in patient inconvenience. Another possible limitation is the use of iron oxide; many SPIO-based formulations have either been withdrawn by their manufacturers or by the FDA. Feraheme or Ferumoxytol is an ultrasmall superparamagnetic iron oxide nanoparticle (USPIO) that has been recently approved by FDA for treatment of anemia and could potentially be used in our MDNP and PLGA-SPIO NP preparation [193].

Although preliminary studies using our porous microparticles demonstrate good cytocompatibility, stability and cell adhesion following fibronectin coating, these particles may be limited by insufficient interconnecting pores. Also, our particles are only about 40-60 µm in diameter which would need to be increased to provide more area for cell attachment. Another limitation of this work is that the porous 3D models may not be an accurately represent the physiological environment seen *in vivo*. Further studies simulating the mechanical stresses seen in the lung as well as tumor angiogenesis may need to be done to study the effect of these factors on tumor cell proliferation and drug/ NP uptake. Also the response of the 3D model to drugs following development of necrosis needs to be studied. Further, co-culture of cancer cells on the 3D model with cancer-associated fibroblasts and other cells seen in a tumor region would potentially give more accurate responses to drugs than a 3D model of cancer cells alone.

5.3. Future Outlook

Based on the encouraging results obtained in this work, future studies will concentrate on the incorporation of various growth promoters into PLGA NPs for alveolar

remodeling, and determining the optimal dose and frequency of nanoparticle administration for treating lung diseases effectively. The local and systemic side effects of the encapsulated agents following delivery will also be studied in detail. In the case of MDNPs, future studies will concentrate on decreasing the particle size to facilitate greater retention in the lung following delivery. Further, SPIO could be replaced with other MR contrast agents such as ferumoxytol, gadolinium complexes and manganese oxide [194] and studied to ensure that the polymer coating does not affect imaging capabilities of these contrast agents. LCST and degradation rate can be also be controlled by varying the polymer ratios. Although our preliminary *in vivo* studies have demonstrated the therapeutic efficacy of MDNPs, future studies will involve nebulization of MDNPs to an orthotopic lung tumor model to study their effect and biodistribution following delivery.

In the case of porous microparticles, the particle size would need to be increased so that more surface area is available for cell adhesion and growth. The novel design of PLGA-PMPs can be used in the synthesis of uniformly porous microparticles for even distribution of nutrients and oxygen throughout the tumor model. Future studies will involve synthesizing larger PMPs so as to generate bigger pores on the PLGA-PMPs to support cell proliferation and infiltration. For detailed study on the effect of tumor necrosis on drug response, 3D cell culture may need to be conducted for longer periods of time to develop necrosis in the core, followed by drug screening. The response of non-porous and porous 3D tumor models to therapeutic agents can be compared to study the importance of porosity on the development of *in vitro* 3D models. Co-culture of cancer cells with fibroblasts can aid in providing better results for drug screening studies. Finally the optimized 3D tumor models can also be injected into animals to form tumors for *in vivo* studies. The response of animal models with these tumors as well as conventional animal tumor models, to varying therapeutic agents can then be compared.

The exponential growth in the field of nanomedicine and tissue engineering in the last few decades bears testimony to their immense potential in diverse medical applications. The particles presented in this work hold promise as theranostic carriers that provides innovative and high-throughput means of screening and delivering different agents with potential for clinical applications.

Appendix A

Related Manuscripts

Appendix A

Related Manuscripts

1. Menon JU, Ravikumar P, Pise A, Gyawali D, Hsia CCW, Nguyen KT. Polymeric Nanoparticles for Pulmonary Protein and DNA delivery. Acta Biomaterialia. http://dx.doi.org/10.1016/j.actbio.2014.01.033
2. Ravikumar P[‡], Menon JU[‡], Homayoni H, Gyawali D, Takahashi M, Moe OW, Nguyen KT, Hsia CCW. Feasibility study of Poly-(lactic co-glycolic acid) Nanoparticles for protein and DNA delivery to the lung by inhalation (‡ Equal contribution*, In preparation)*
3. Menon, JU, Kuriakose, AE, Saha, D, Nguyen, KT. Dual-responsive multi-functional magnetic-based NPs for targeted lung cancer treatment *(In preparation)*
4. Menon, JU, Tumati, V, Hsieh, J-T, Nguyen, KT, Saha, D. Efficacy of NU7441-encapsulated PLGA NPs in radiation sensitization of prostate cancer cells *(In preparation)*
5. Menon JU, Kuriakose AE, Nguyen KT. Porous PLGA-based microparticles as tumor models for lung cancer drug screening *(In preparation)*

References

1. Menon JU, Wadajkar AS, Xie Z, Nguyen KT. Nanomaterials for Management of Lung Disorders and Drug Delivery. In: Tiwari A, Tiwari A, editors. Nanomaterials in Drug Delivery, Imaging, and Tissue Engineering: John Wiley & Sons, Inc., 2013. p. 167-202.
2. Davies A. The evolution of bronchial casts. Medical history 1973 Oct;17(4):386-391.
3. West JB. A century of pulmonary gas exchange. Am J Respir Crit Care Med 2004 Apr 15;169(8):897-902.
4. Gonda I. The ascent of pulmonary drug delivery. Journal of Pharmaceutical Sciences 2000;89(7):940-945.
5. Verschakelen JA, Wever W. Basic anatomy and CT of the normal lung Computed tomography of the lung: Springer Berlin Heidelberg, 2007. p. 3-16.
6. Effros R. Anatomy, development, and physiology of the lungs. GI Motility Online 2006.
7. Fraser RS. Histology and gross anatomy of the respiratory tract. In: Hamid Q, Shannon, J, Martin, J, editor. Physiologic Basis of Respiratory Disease. Hamilton, Ontario, 2005. p. 1-14.
8. Wang S, Hubmayr RD. Type I alveolar epithelial phenotype in primary culture. Am J Respir Cell Mol Biol 2011 May 1, 2011;44(5):692-699.
9. West J. Respiratory physiology: The essentials Lippincott Williams & Wilkins, 2008.
10. Zarogoulidis P, Chatzaki E, Porpodis K, Domvri K, Hohenforst-Schmidt W, Goldberg EP, et al. Inhaled chemotherapy in lung cancer: future concept of nanomedicine. Int J Nanomedicine 2012;7:1551-1572.
11. Singh S, Soni N. Restrictive lung disease. In: Pollard B, editor. Handbook of Clinical Anaesthesia. Boca Raton, FL: CRC Press, 2012. p. 114.
12. Hsia CC. Signals and mechanisms of compensatory lung growth. J Appl Physiol 2004 Nov;97(5):1992-1998.
13. Athey VL, Suckling RJ, Tod AM, Walters SJ, Rogers TK. Early diagnosis of lung cancer: evaluation of a community-based social marketing intervention. Thorax 2012;67(5):412-417.
14. Siegel R, Ma J, Zou Z, Jemal A. Cancer statistics, 2014. CA: A Cancer Journal for Clinicians 2014;64(1):9-29.
15. Siegel R, Naishadham D, Jemal A. Cancer statistics, 2013. CA: A Cancer Journal for Clinicians 2013;63(1):11-30.
16. Siegel R, DeSantis C, Virgo K, Stein K, Mariotto A, Smith T, et al. Cancer treatment and survivorship statistics, 2012. CA: A Cancer Journal for Clinicians 2012;62(4):220-241.
17. Fukuoka M, Yano S, Giaccone G, Tamura T, Nakagawa K, Douillard JY, et al. Multi-institutional randomized phase II trial of gefitinib for previously treated patients with advanced non-small-cell lung cancer (The IDEAL 1 Trial) [corrected]. J Clin Oncol 2003 Jun 15;21(12):2237-2246.
18. Sadhukha T, Wiedmann TS, Panyam J. Inhalable magnetic nanoparticles for targeted hyperthermia in lung cancer therapy. Biomaterials 2013;34(21):5163-5171.
19. Tseng C-L, Su W-Y, Yen K-C, Yang K-C, Lin F-H. The use of biotinylated-EGF-modified gelatin nanoparticle carrier to enhance cisplatin accumulation in cancerous lungs via inhalation. Biomaterials 2009;30(20):3476-3485.

20. Roa WH, Azarmi S, Al-Hallak MHDK, Finlay WH, Magliocco AM, LÃ¶benberg R. Inhalable nanoparticles, a non-invasive approach to treat lung cancer in a mouse model. Journal of Controlled Release 2011;150(1):49-55.
21. Sung JC, Pulliam BL, Edwards DA. Nanoparticles for drug delivery to the lungs. Trends Biotechnol 2007;25(12):563-570.
22. Dandekar P, Venkataraman C, Mehra A. Pulmonary targeting of nanoparticle drug matrices. J Aerosol Med Pulm Drug Deliv 2010 Dec;23(6):343-353.
23. Taylor KM, Newton JM. Liposomes for controlled delivery of drugs to the lung. Thorax 1992 Apr;47(4):257-259.
24. Mansour HM, Rhee Y-S, Wu X. Nanomedicine in pulmonary delivery. Int J Nanomedicine 2009;4:299-319.
25. Chen X, Huang W, Wong BC, Yin L, Wong YF, Xu M, et al. Liposomes prolong the therapeutic effect of anti-asthmatic medication via pulmonary delivery. Int J Nanomedicine 2012;7:1139-1148.
26. Majuru S, Oyewumi M. Nanotechnology in Drug Development and Life Cycle Management. In: Villiers M, Aramwit P, Kwon G, editors. Nanotechnology in Drug Delivery. New York: Springer, 2009. p. 597-619.
27. Anderson P, Pearson M. Novel therapeutic approaches in pediatric and young adult sarcomas. Curr Oncol Rep 2006;8(4):310-315.
28. Smola M, Vandamme T, Sokolowski A. Nanocarriers as pulmonary drug delivery systems to treat and to diagnose respiratory and non respiratory diseases. Int J Nanomedicine 2008.
29. Sahib MN, Darwis Y, Peh KK, Abdulameer SA, Fung Tan YT. Incorporation of Beclomethasone Dipropionate into Polyethylene Glycol-Diacyl Lipid Micelles as a Pulmonary Delivery System. Drug Development Research 2012;73(2):90-105.
30. Gill KK, Nazzal S, Kaddoumi A. Paclitaxel loaded PEG5000-DSPE micelles as pulmonary delivery platform: Formulation characterization, tissue distribution, plasma pharmacokinetics, and toxicological evaluation. Eur J Pharm Biopharm 2011;79(2):276-284.
31. Matsumura Y. Preclinical and clinical studies of NK012, an SN-38-incorporating polymeric micelles, which is designed based on EPR effect. Advanced drug delivery reviews 2011;63(3):184-192.
32. Lu Y, Park K. Polymeric micelles and alternative nanonized delivery vehicles for poorly soluble drugs. International Journal of Pharmaceutics 2013;453(1):198-214.
33. Nanjwade BK, Bechra HM, Derkar GK, Manvi FV, Nanjwade VK. Dendrimers: Emerging polymers for drug-delivery systems. Eur J Pharm Sci 2009;38(3):185-196.
34. Bai S, Thomas C, Ahsan F. Dendrimers as a carrier for pulmonary delivery of enoxaparin, a low-molecular weight heparin. J Pharm Sci 2007;96(8):2090-2106.
35. Liu J, Chu L, Wang Y, Duan Y, Feng L, Yang C, et al. Novel peptide-dendrimer conjugates as drug carriers for targeting nonsmall cell lung cancer. Int J Nanomedicine 2011;6:59-69.
36. Kukowska-Latallo JF, Raczka E, Quintana A, Chen C, Rymaszewski M, Baker JR, Jr. Intravascular and endobronchial DNA delivery to murine lung tissue using a novel, nonviral vector. Hum Gene Ther 2000 Jul 1;11(10):1385-1395.
37. Mintzer MA, Grinstaff MW. Biomedical applications of dendrimers: a tutorial. Chemical Society Reviews 2011;40(1):173-190.

38. White SC, Lorigan P, Margison GP, Margison JM, Martin F, Thatcher N, et al. Phase II study of SPI-77 (sterically stabilised liposomal cisplatin) in advanced non-small-cell lung cancer. Br J Cancer 2006;95(7):822-828.
39. Mehrotra A, Nagarwal R, Pandit J. Lomustine loaded chitosan nanoparticles: characterization and in-vitro cytotoxicity on human lung cancer cell line L132. Chem Pharm Bull 2011;59:315-320.
40. Kim I, Byeon HJ, Kim TH, Lee ES, Oh KT, Shin BS, et al. Doxorubicin-loaded highly porous large PLGA microparticles as a sustained- release inhalation system for the treatment of metastatic lung cancer. Biomaterials 2012;33(22):5574-5583.
41. El-Sherbiny IM, McGill S, Smyth HDC. Swellable microparticles as carriers for sustained pulmonary drug delivery. J Pharm Sci 2010;99(5):2343-2356.
42. Zou W, Liu C, Chen Z, Zhang N. Studies on bioadhesive PLGA nanoparticles: A promising gene delivery system for efficient gene therapy to lung cancer. Int J Pharm 2009;370(1-2):187-195.
43. Derossi D, Calvet S, Trembleau A, Brunissen A, Chassaing G, Prochiantz A. Cell internalization of the third helix of the Antennapedia homeodomain is receptor-independent. J Biol Chem 1996 Jul 26;271(30):18188-18193.
44. Kutscher HL, Chao P, Deshmukh M, Singh Y, Hu P, Joseph LB, et al. Threshold size for optimal passive pulmonary targeting and retention of rigid microparticles in rats. J Control Release 2010 Apr 2;143(1):31-37.
45. Danhier F, Feron O, Preat V. To exploit the tumor microenvironment: Passive and active tumor targeting of nanocarriers for anti-cancer drug delivery. J Control Release 2010 Dec 1;148(2):135-146.
46. Yu MK, Jeong YY, Park J, Park S, Kim JW, Min JJ, et al. Drug-loaded superparamagnetic iron oxide nanoparticles for combined cancer imaging and therapy in vivo. Angewandte Chemie (International ed 2008;47(29):5362-5365.
47. Kurten RC. Sorting motifs in receptor trafficking. Adv Drug Deliv Rev 2003 Nov 14;55(11):1405-1419.
48. Belani CP, Goss G, Blumenschein G, Jr. Recent clinical developments and rationale for combining targeted agents in non-small cell lung cancer (NSCLC). Cancer treatment reviews 2012 May;38(3):173-184.
49. Zhou Q, Guo X, Chen T, Zhang Z, Shao S, Luo C, et al. Target-specific cellular uptake of folate-decorated biodegradable polymer micelles. The journal of physical chemistry 2011 Nov 3;115(43):12662-12670.
50. Goodwin S, Peterson C, Hoh C, Bittner C. Targeting and retention of magnetic targeted carriers (MTCs) enhancing intra-arterial chemotherapy. Journal of Magnetism and Magnetic Materials 1999;194(1-3):132-139.
51. Blanco E, Kessinger CW, Sumer BD, Gao J. Multifunctional micellar nanomedicine for cancer therapy. Experimental biology and medicine (Maywood, NJ 2009 Feb;234(2):123-131.
52. Yoo MK, Park IK, Lim HT, Lee SJ, Jiang HL, Kim YK, et al. Folate-PEG-superparamagnetic iron oxide nanoparticles for lung cancer imaging. Acta biomaterialia 2012 Apr 24.
53. Lam JK, Liang W, Chan HK. Pulmonary delivery of therapeutic siRNA. Adv Drug Deliv Rev 2012 Jan;64(1):1-15.
54. Parton RG, Richards AA. Lipid rafts and caveolae as portals for endocytosis: new insights and common mechanisms. Traffic 2003 Nov;4(11):724-738.

55. Khalil IA, Kogure K, Akita H, Harashima H. Uptake pathways and subsequent intracellular trafficking in nonviral gene delivery. Pharmacological reviews 2006 Mar;58(1):32-45.
56. Shi H, Gao X, Li D, Zhang Q, Wang Y, Zheng Y, et al. A systemic administration of liposomal curcumin inhibits radiation pneumonitis and sensitizes lung carcinoma to radiation Int J Nanomedicine 2012 24 May 2012 7(1):2601-2611.
57. Upadhyay D, Scalia S, Vogel R, Wheate N, Salama R, Young P, et al. Magnetised thermo responsive lipid vehicles for targeted and controlled lung drug delivery. Pharm Res 2012:1-12.
58. Sharma R, Saxena D, Dwivedi A, Misra A. Inhalable Microparticles Containing Drug Combinations to Target Alveolar Macrophages for Treatment of Pulmonary Tuberculosis. Pharmaceutical Research 2001;18(10):1405-1410.
59. Patlolla RR, Chougule M, Patel AR, Jackson T, Tata PNV, Singh M. Formulation, characterization and pulmonary deposition of nebulized celecoxib encapsulated nanostructured lipid carriers. J Control Release 2010;144(2):233-241.
60. Fernandez Tena A, Casan Clara P. Deposition of inhaled particles in the lungs. Arch Bronconeumol 2012;48(7):240-246.
61. Zhang J, Wu L, Chan H-K, Watanabe W. Formation, characterization, and fate of inhaled drug nanoparticles. Adv Drug Deliv Rev 2011;63(6):441-455.
62. Beck-Broichsitter M, Kleimann P, Gessler T, Seeger W, Kissel T, Schmehl T. Nebulization performance of biodegradable sildenafil-loaded nanoparticles using the Aeroneb® Pro: Formulation aspects and nanoparticle stability to nebulization. Int J Pharm 2012;422(1-2):398-408.
63. Dailey LA, Schmehl T, Gessler T, Wittmar M, Grimminger F, Seeger W, et al. Nebulization of biodegradable nanoparticles: impact of nebulizer technology and nanoparticle characteristics on aerosol features. J Control Release 2003;86(1):131-144.
64. Yang Y, Bajaj N, Xu P, Ohn K, Tsifansky MD, Yeo Y. Development of highly porous large PLGA microparticles for pulmonary drug delivery. Biomaterials 2009;30(10):1947-1953.
65. Tan Y, Yang Z, Pan X, Chen M, Feng M, Wang L, et al. Stability and aerosolization of pressurized metered dose inhalers containing thymopentin nanoparticles produced using a bottom-up process. Int J Pharm 2012;427(2):385-392.
66. Selvam P, El-Sherbiny IM, Smyth HD. Swellable hydrogel particles for controlled release pulmonary administration using propellant-driven metered dose inhalers. J Aerosol Med Pulm Drug Deliv 2011 Feb;24(1):25-34.
67. Salem H, Abdelrahim M, Eid KA, Sharaf M. Nanosized rods agglomerates as a new approach for formulation of a dry powder inhaler. Int J Nanomedicine 2011;6:311-320.
68. Sinha B, Mukherjee B, Pattnaik G. Poly-lactide-co-glycolide nanoparticles containing voriconazole for pulmonary delivery: in vitro and in vivo study. Nanomedicine 2012(0).
69. Ashurst I, Malton A, Prime D, Sumby B. Latest advances in the development of dry powder inhalers. Pharmaceutical science & technology today 2000;3(7):246-256.
70. Yang Y, Cheow WS, Hadinoto K. Dry powder inhaler formulation of lipid-polymer hybrid nanoparticles via electrostatically-driven nanoparticle assembly onto microscale carrier particles. Int J Pharm 2012;434(1-2):49-58.

71. Dong M, MÃ¼rdter TE, Philippi C, Loretz B, Schaefer UF, Lehr CM, et al. Pulmonary delivery and tissue distribution of aerosolized antisense 2'-O-Methyl RNA containing nanoplexes in the isolated perfused and ventilated rat lung. Eur J Pharm Biopharm 2012(0).
72. Ungaro F, d'Angelo I, Coletta C, d'Emmanuele di Villa Bianca R, Sorrentino R, Perfetto B, et al. Dry powders based on PLGA nanoparticles for pulmonary delivery of antibiotics: Modulation of encapsulation efficiency, release rate and lung deposition pattern by hydrophilic polymers. J Control Release 2011;157(1):149-159.
73. Guthi JS, Yang S-G, Huang G, Li S, Khemtong C, Kessinger CW, et al. MRI-Visible Micellar Nanomedicine for Targeted Drug Delivery to Lung Cancer Cells. Molecular Pharmaceutics 2009 2013/06/24;7(1):32-40.
74. Mahmoudi M, Sant S, Wang B, Laurent S, Sen T. Superparamagnetic iron oxide nanoparticles (SPIONs): Development, surface modification and applications in chemotherapy. Adv Drug Deliv Rev 2011 2011/2//;63(1-2):24-46.
75. Howell M, Mallela J, Wang C, Ravi S, Dixit S, Garapati U, et al. Manganese-loaded lipid-micellar theranostics for simultaneous drug and gene delivery to lungs. Journal of Controlled Release 2013;167(2):210-218.
76. Wang H, Zheng L, Peng C, Shen M, Shi X, Zhang G. Folic acid-modified dendrimer-entrapped gold nanoparticles as nanoprobes for targeted CT imaging of human lung adencarcinoma. Biomaterials 2013;34(2):470-480.
77. Patil JS, Sarasija S. Pulmonary drug delivery strategies: A concise, systematic review. Lung India 2012 Jan;29(1):44-49.
78. Shin CS, Kwak B, Han B, Park K. Development of an in Vitro 3D Tumor Model to Study Therapeutic Efficiency of an Anticancer Drug. Molecular Pharmaceutics 2013 2013/06/24;10(6):2167-2175.
79. Zhu M-T, Feng W-Y, Wang Y, Wang B, Wang M, Ouyang H, et al. Particokinetics and extrapulmonary translocation of intratracheally instilled Ferric oxide nanoparticles in rats and the potential health risk assessment. Toxicological Sciences 2009 February 1, 2009;107(2):342-351.
80. Choi M, Cho M, Han BS, Hong J, Jeong J, Park S, et al. Chitosan nanoparticles show rapid extrapulmonary tissue distribution and excretion with mild pulmonary inflammation to mice. Toxicol Lett 2010;199(2):144-152.
81. Sarlo K, Blackburn KL, Clark ED, Grothaus J, Chaney J, Neu S, et al. Tissue distribution of 20 nm, 100 nm and 1000 nm fluorescent polystyrene latex nanospheres following acute systemic or acute and repeat airway exposure in the rat. Toxicology 2009 Sep 19;263(2-3):117-126.
82. Hitzman CJ, Elmquist WF, Wattenberg LW, Wiedmann TS. Development of a respirable, sustained release microcarrier for 5-fluorouracil I: In vitro assessment of liposomes, microspheres, and lipid coated nanoparticles. J Pharm Sci 2006;95(5):1114-1126.
83. Hwang H-Y, Kim I-S, Kwon IC, Kim Y-H. Tumor targetability and antitumor effect of docetaxel-loaded hydrophobically modified glycol chitosan nanoparticles. J Control Release 2008;128(1):23-31.
84. Muhlfeld C, Geiser M, Kapp N, Gehr P, Rothen-Rutishauser B. Re-evaluation of pulmonary titanium dioxide nanoparticle distribution using the "relative deposition index": Evidence for clearance through microvasculature. Part Fibre Toxicol 2007;4(1):7.
85. Sung JC, Pulliam BL, Edwards DA. Nanoparticles for drug delivery to the lungs. Trends in Biotechnology 2007;25(12):563-570.

86. Sham JOH, Zhang Y, Finlay WH, Roa WH, LÃ¶benberg R. Formulation and characterization of spray-dried powders containing nanoparticles for aerosol delivery to the lung. International Journal of Pharmaceutics 2004;269(2):457-467.
87. Nesamony J, Singh PR, Nada SE, Shah ZA, Kolling WM. Calcium alginate nanoparticles synthesized through a novel interfacial cross-linking method as a potential protein drug delivery system. Journal of Pharmaceutical Sciences 2012;101(6):2177-2184.
88. Menon JU, Kona S, Wadajkar AS, Desai F, Vadla A, Nguyen KT. Effects of surfactants on the properties of PLGA nanoparticles. J Biomed Mater Res A 2012 Aug;100(8):1998-2005.
89. Tahara K, Sakai T, Yamamoto H, Takeuchi H, Hirashima N, Kawashima Y. Improved cellular uptake of chitosan-modified PLGA nanospheres by A549 cells. International Journal of Pharmaceutics 2009;382(1-2):198-204.
90. Grabowski N, Hillaireau H, Vergnaud J, Santiago LA, Kerdine-Romer S, Pallardy M, et al. Toxicity of surface-modified PLGA nanoparticles toward lung alveolar epithelial cells. International Journal of Pharmaceutics 2013;454(2):686-694.
91. Hara K, Tsujimoto H, Tsukada Y, Huang CC, Kawashima Y, Tsutsumi M. Histological examination of PLGA nanospheres for intratracheal drug administration. International Journal of Pharmaceutics 2008;356(1-2):267-273.
92. Ely L, Roa W, Finlay WH, Lobenberg R. Effervescent dry powder for respiratory drug delivery. Eur J Pharm Biopharm 2007 Mar;65(3):346-353.
93. Fernandez Tena A, Casan Clara P. Deposition of Inhaled Particles in the Lungs. Archivos de Bronconeumol 2012;48(07):240-246.
94. Patlolla RR, Chougule M, Patel AR, Jackson T, Tata PNV, Singh M. Formulation, characterization and pulmonary deposition of nebulized celecoxib encapsulated nanostructured lipid carriers. Journal of Controlled Release 2010;144(2):233-241.
95. Beck-Broichsitter M, Gauss J, Packhaeuser CB, Lahnstein K, Schmehl T, Seeger W, et al. Pulmonary drug delivery with aerosolizable nanoparticles in an ex vivo lung model. International Journal of Pharmaceutics 2009;367(1-2):169-178.
96. Manca ML, Mourtas S, Dracopoulos V, Fadda AM, Antimisiaris SG. PLGA, chitosan or chitosan-coated PLGA microparticles for alveolar delivery? A comparative study of particle stability during nebulization. Colloids Surf B Biointerfaces 2008 Apr 1;62(2):220-231.
97. Ungaro F, d'Angelo I, Coletta C, d'Emmanuele di Villa Bianca R, Sorrentino R, Perfetto B, et al. Dry powders based on PLGA nanoparticles for pulmonary delivery of antibiotics: modulation of encapsulation efficiency, release rate and lung deposition pattern by hydrophilic polymers. J Control Release 2012 Jan 10;157(1):149-159.
98. Shutava TG, Balkundi SS, Vangala P, Steffan JJ, Bigelow RL, Cardelli JA, et al. Layer-by-Layer-Coated Gelatin Nanoparticles as a Vehicle for Delivery of Natural Polyphenols. ACS Nano 2009 2012/07/05;3(7):1877-1885.
99. Gan Q, Wang T, Cochrane C, McCarron P. Modulation of surface charge, particle size and morphological properties of chitosan-TPP nanoparticles intended for gene delivery. Colloids Surf B Biointerfaces 2005 Aug;44(2-3):65-73.
100. Rajaonarivony M, Vauthier C, Couarraze G, Puisieux F, Couvreur P. Development of a new drug carrier made from alginate. Journal of Pharmaceutical Sciences 1993;82(9):912-917.
101. Cheng J, Teply BA, Sherifi I, Sung J, Luther G, Gu FX, et al. Formulation of functionalized PLGA-PEG nanoparticles for in vivo targeted drug delivery. Biomaterials 2007;28(5):869-876.

102. Marques MR, Loebenberg R, Almukainzi M. Simulated biological fluids with possible application in dissolution testing. Dissolution Technol 2011;18(3):15-28.
103. Rahimi M, Wadajkar A, Subramanian K, Yousef M, Cui W, Hsieh J-T, et al. In vitro evaluation of novel polymer-coated magnetic nanoparticles for controlled drug delivery. Nanomedicine 2010;6(5):672-680.
104. Wadajkar AS, Bhavsar Z, Ko C-Y, Koppolu B, Cui W, Tang L, et al. Multifunctional particles for melanoma-targeted drug delivery. Acta Biomater 2012;8(8):2996-3004.
105. Togao O, Tsuji R, Ohno Y, Dimitrov I, Takahashi M. Ultrashort echo time (UTE) MRI of the lung: assessment of tissue density in the lung parenchyma. Magn Reson Med 2010 Nov;64(5):1491-1498.
106. Yang SJ, Chang SM, Tsai KC, Chen WS, Lin FH, Shieh MJ. Effect of chitosan-alginate nanoparticles and ultrasound on the efficiency of gene transfection of human cancer cells. J Gene Med 2010 Feb;12(2):168-179.
107. Chan JM, Zhang L, Yuet KP, Liao G, Rhee J-W, Langer R, et al. PLGA-lecithin-PEG core-shell nanoparticles for controlled drug delivery. Biomaterials 2009;30(8):1627-1634.
108. Shutava TG, Balkundi SS, Vangala P, Steffan JJ, Bigelow RL, Cardelli JA, et al. Layer-by-Layer-Coated Gelatin Nanoparticles as a Vehicle for Delivery of Natural Polyphenols. ACS Nano 2009 2012/07/05;3(7):1877-1885.
109. Gan Q, Wang T. Chitosan nanoparticle as protein delivery carrier - Systematic examination of fabrication conditions for efficient loading and release. Colloids and Surfaces B: Biointerfaces 2007;59(1):24-34.
110. Chang C-H, Lin Y-H, Yeh C-L, Chen Y-C, Chiou S-F, Hsu Y-M, et al. Nanoparticles Incorporated in pH-Sensitive Hydrogels as Amoxicillin Delivery for Eradication of Helicobacter pylori. Biomacromolecules 2009 2012/10/15;11(1):133-142.
111. Musumeci T, Ventura CA, Giannone I, Ruozi B, Montenegro L, Pignatello R, et al. PLA/PLGA nanoparticles for sustained release of docetaxel. Int J Pharm 2006;325(1-2):172-179.
112. Li Y-P, Pei Y-Y, Zhang X-Y, Gu Z-H, Zhou Z-H, Yuan W-F, et al. PEGylated PLGA nanoparticles as protein carriers: synthesis, preparation and biodistribution in rats. Journal of Controlled Release 2001;71(2):203-211.
113. Parveen S, Sahoo SK. Long circulating chitosan/PEG blended PLGA nanoparticle for tumor drug delivery. Eur J Pharmacol 2011;670(2-3):372-383.
114. Tseng C-L, Wang T-W, Dong G-C, Yueh-Hsiu Wu S, Young T-H, Shieh M-J, et al. Development of gelatin nanoparticles with biotinylated EGF conjugation for lung cancer targeting. Biomaterials 2007;28(27):3996-4005.
115. Grenha A, Grainger CI, Dailey LA, Seijo Ba, Martin GP, RemuÃ±Ã¡n-LÃ³pez C, et al. Chitosan nanoparticles are compatible with respiratory epithelial cells in vitro. European Journal of Pharmaceutical Sciences 2007;31(2):73-84.
116. Gazori T, Haririan I, Fouladdel S, Namazi A, Nomani A, Azizi E. Inhibition of EGFR expression with chitosan/alginate nanoparticles encapsulating antisense oligonucleotides in T47D cell line using RT-PCR and immunocytochemistry. Carbohydrate Polymers 2010;80(4):1042-1047.
117. Mura S, Hillaireau H, Nicolas J, Le Droumaguet B, Gueutin C, Zanna S, et al. Influence of surface charge on the potential toxicity of PLGA nanoparticles towards Calu-3 cells. Int J Nanomedicine 2011;6:2591-2605.

118. Nam HY, Kwon SM, Chung H, Lee S-Y, Kwon S-H, Jeon H, et al. Cellular uptake mechanism and intracellular fate of hydrophobically modified glycol chitosan nanoparticles. Journal of Controlled Release 2009;135(3):259-267.
119. Chavanpatil MD, Khdair A, Gerard B, Bachmeier C, Miller DW, Shekhar MPV, et al. Surfactant-Polymer Nanoparticles Overcome P-Glycoprotein-Mediated Drug Efflux. Mol Pharm 2007 2012/10/15;4(5):730-738.
120. Chen J, Li S, Shen Q. Folic acid and cell-penetrating peptide conjugated PLGA-PEG bifunctional nanoparticles for vincristine sulfate delivery. European Journal of Pharmaceutical Sciences 2012;47(2):430-443.
121. Lin A, Sabnis A, Kona S, Nattama S, Patel H, Dong J-F, et al. Shear-regulated uptake of nanoparticles by endothelial cells and development of endothelial-targeting nanoparticles. J Biomed Mater Res Part A 2010;93A(3):833-842.
122. Lesniak A, Salvati A, Santos-Martinez MJ, Radomski MW, Dawson KA, Aberg C. Nanoparticle adhesion to the cell membrane and its effect on nanoparticle uptake efficiency. J Am Chem Soc 2013 Jan 30;135(4):1438-1444.
123. He C, Hu Y, Yin L, Tang C, Yin C. Effects of particle size and surface charge on cellular uptake and biodistribution of polymeric nanoparticles. Biomaterials 2010 May;31(13):3657-3666.
124. Paola Rosanna D, Salvatore C. Reactive oxygen species, inflammation, and lung diseases. Current pharmaceutical design 2012;18(26):3889-3900.
125. Merkel OM, Beyerle A, Librizzi D, Pfestroff A, Behr TM, Sproat B, et al. Nonviral siRNA Delivery to the Lung: Investigation of PEGâ˜PEI Polyplexes and Their In Vivo Performance. Molecular Pharmaceutics 2009 2014/02/22;6(4):1246-1260.
126. Huang YC, Vieira A, Huang KL, Yeh MK, Chiang CH. Pulmonary inflammation caused by chitosan microparticles. Journal of Biomedical Materials Research Part A 2005;75A(2):283-287.
127. Huang YC, Vieira A, Yeh MK, Chiang CH. Pulmonary Anti-inflammatory Effects of Chitosan Microparticles Containing Betamethasone. Journal of Bioactive and Compatible Polymers 2007 January 1, 2007;22(1):30-41.
128. Sahoo SK, Panyam J, Prabha S, Labhasetwar V. Residual polyvinyl alcohol associated with poly (d,l-lactide-co-glycolide) nanoparticles affects their physical properties and cellular uptake. J Control Release 2002;82(1):105-114.
129. Lee P-W, Hsu S-H, Wang J-J, Tsai J-S, Lin K-J, Wey S-P, et al. The characteristics, biodistribution, magnetic resonance imaging and biodegradability of superparamagnetic core-shell nanoparticles. Biomaterials 2010;31(6):1316-1324.
130. Xu C, Xu K, Gu H, Zhong X, Guo Z, Zheng R, et al. Nitrilotriacetic acid-modified magnetic nanoparticles as a general agent to bind histidine-tagged proteins. J Am Chem Soc 2004 2012/07/13;126(11):3392-3393.
131. Cheng F-Y, Wang SP-H, Su C-H, Tsai T-L, Wu P-C, Shieh D-B, et al. Stabilizer-free poly(lactide-co-glycolide) nanoparticles for multimodal biomedical probes. Biomaterials 2008;29(13):2104-2112.
132. Butoescu N, Jordan O, Burdet P, Stadelmann P, Petri-Fink A, Hofmann H, et al. Dexamethasone-containing biodegradable superparamagnetic microparticles for intra-articular administration: Physicochemical and magnetic properties, in vitro and in vivo drug release. Eur J Pharm Biopharm 2009;72(3):529-538.
133. Cartiera MS, Johnson KM, Rajendran V, Caplan MJ, Saltzman WM. The uptake and intracellular fate of PLGA nanoparticles in epithelial cells. Biomaterials 2009;30(14):2790-2798.

134. Davda J, Labhasetwar V. Characterization of nanoparticle uptake by endothelial cells. Int J Pharm 2002;233(1-2):51-59.
135. Wang L, Neoh K-G, Kang E-T, Shuter B, Wang S-C. Biodegradable magnetic-fluorescent magnetite/poly(dl-lactic acid-co-alpha,beta-malic acid) composite nanoparticles for stem cell labeling. Biomaterials 2010;31(13):3502-3511.
136. Wang YX. Superparamagnetic iron oxide based MRI contrast agents: Current status of clinical application. Quant Imaging Med Surg 2011;1(1):35-40.
137. Kawashima Y, Yamamoto H, Takeuchi H, Fujioka S, Hino T. Pulmonary delivery of insulin with nebulized dl-lactide/glycolide copolymer (PLGA) nanospheres to prolong hypoglycemic effect. J Control Release 1999;62(1-2):279-287.
138. Bivas-Benita M, Romeijn S, Junginger HE, Borchard G. PLGA-PEI nanoparticles for gene delivery to pulmonary epithelium. Eur J Pharm Biopharm 2004;58(1):1-6.
139. Swartz MD, Peterson CB, Lupo PJ, Wu X, Forman MR, Spitz MR, et al. Investigating Multiple Candidate Genes and Nutrients in the Folate Metabolism Pathway to Detect Genetic and Nutritional Risk Factors for Lung Cancer. PLoS One 2013;8(1):e53475.
140. Fajersztajn L, Veras M, Barrozo LV, Saldiva P. Air pollution: a potentially modifiable risk factor for lung cancer. Nature Reviews Cancer 2013;13(9):674-678.
141. Ventola CL. The Nanomedicine Revolution: Part 1: Emerging Concepts. Pharmacy and Therapeutics 2012;37(9):512.
142. Hock SC, Ying YM, Wah CL. A review of the current scientific and regulatory status of nanomedicines and the challenges ahead. PDA Journal of Pharmaceutical Science and Technology 2011;65(2):177-195.
143. Petros RA, DeSimone JM. Strategies in the design of nanoparticles for therapeutic applications. Nat Rev Drug Discov 2010 Aug;9(8):615-627.
144. Liechty WB, Peppas NA. Expert opinion: Responsive polymer nanoparticles in cancer therapy. Eur J Pharm Biopharm 2012 Feb;80(2):241-246.
145. Guan J, Hong Y, Ma Z, Wagner WR. Protein-reactive, thermoresponsive copolymers with high flexibility and biodegradability. Biomacromolecules 2008 Apr;9(4):1283-1292.
146. Yoo M-K, Park I-K, Lim H-T, Lee S-J, Jiang H-L, Kim Y-K, et al. Folate-PEG-superparamagnetic iron oxide nanoparticles for lung cancer imaging. Acta Biomaterialia 2012;8(8):3005-3013.
147. Leahy JJ, Golding BT, Griffin RJ, Hardcastle IR, Richardson C, Rigoreau L, et al. Identification of a highly potent and selective DNA-dependent protein kinase (DNA-PK) inhibitor (NU7441) by screening of chromenone libraries. Bioorg Med Chem Lett 2004 Dec 20;14(24):6083-6087.
148. O'Shannessy DJ, Yu G, Smale R, Fu Y-S, Singhal S, Thiel RP, et al. Folate receptor alpha expression in lung cancer: diagnostic and prognostic significance. Oncotarget 2012;3(4):414.
149. Yuan Z, Li W-T, Ye X-D, Liu S-Y, Xiao X-S. Folate receptor-mediated targeted polymeric gadolinium complexes for magnetic resonance imaging in pulmonary tumor xenografts. Experimental and therapeutic medicine 2012;3(5):903-907.
150. Depan D, Shah J, Misra RDK. Controlled release of drug from folate-decorated and graphene mediated drug delivery system: Synthesis, loading efficiency, and drug release response. Materials Science and Engineering: C 2011;31(7):1305-1312.

151. Wang F, Zhang D, Duan C, Jia L, Feng F, Liu Y, et al. Preparation and characterizations of a novel deoxycholic acid-O-carboxymethylated chitosan-folic acid conjugates and self-aggregates. Carbohydrate Polymers 2011;84(3):1192-1200.
152. Kim JC, Saha D, Cao Q, Choy H. Enhancement of radiation effects by combined docetaxel and flavopiridol treatment in lung cancer cells. Radiother Oncol 2004 May;71(2):213-221.
153. Kosaka T, Fukaya K-i, Tsuboi S, Pu H, Ohno T, Tsuji T, et al. Comparison of various methods of assaying the cytotoxic effects of ethanol on human hepatoblastoma cells(HUH-6 line). Acta Medica Okayama 1996;50(3):151-156.
154. Tang BC, Fu J, Watkins DN, Hanes J. Enhanced efficacy of local etoposide delivery by poly (ether-anhydride) particles against small cell lung cancer< i> in vivo</i>. Biomaterials 2010;31(2):339-344.
155. Zhao T, Chen H, Dong Y, Zhang J, Huang H, Zhu J, et al. Paclitaxel-loaded poly (glycolide-co-Îµ-caprolactone)-bD-Î±-tocopheryl polyethylene glycol 2000 succinate nanoparticles for lung cancer therapy. Int J Nanomedicine 2013;8:1947.
156. Srivatsan A, Jenkins SV, Jeon M, Wu Z, Kim C, Chen J, et al. Gold Nanocage-Photosensitizer Conjugates for Dual-Modal Image-Guided Enhanced Photodynamic Therapy. Theranostics 2014;4(2):163.
157. Steinberg G, Borch RF. Synthesis and evaluation of pteroic acid-conjugated nitroheterocyclic phosphoramidates as folate receptor-targeted alkylating agents. Journal of medicinal chemistry 2001;44(1):69-73.
158. Cheng F-Y, Su C-H, Yang Y-S, Yeh C-S, Tsai C-Y, Wu C-L, et al. Characterization of aqueous dispersions of Fe3O4 nanoparticles and their biomedical applications. Biomaterials 2005;26(7):729-738.
159. Li G, Guo L, Wen Q, Zhang T. Thermo- and pH-sensitive ionic-crosslinked hollow spheres from chitosan-based graft copolymer for 5-fluorouracil release. International Journal of Biological Macromolecules 2013;55(0):69-74.
160. Huang Y-, • Cheng, Lam U-, • Ian. Chitosan/fucoidan pH sensitive nanoparticles for oral delivery system. Journal of the Chinese Chemical Society 2011;58(6):779-785.
161. van Eeden SF, Tan WC, Suwa T, Mukae H, Terashima T, Fujii T, et al. Cytokines involved in the systemic inflammatory response induced by exposure to particulate matter air pollutants (PM10). American Journal of Respiratory and Critical Care Medicine 2001;164(5):826-830.
162. Li B, Dong C, Wang G, Zheng H, Wang X, Bai C. Pulmonary epithelial CCR3 promotes LPS-induced lung inflammation by mediating release of IL-8. Journal of Cellular Physiology 2011;226(9):2398-2405.
163. McRitchie DI, Isowa N, Edelson JD, Xavier AM, Cai L, Man H-Y, et al. Production of tumour necrosis factor Î± by primary cultured rat alveolar epithelial cells. Cytokine 2000;12(6):644-654.
164. Kosinski AM, Brugnano JL, Seal BL, Knight FC, Panitch A. Synthesis and characterization of a poly(lactic-co-glycolic acid) core + poly(N-isopropylacrylamide) shell nanoparticle system. Biomatter 2012;2(4):195-201.
165. Amin K, Dannenfelser RM. In vitro hemolysis: guidance for the pharmaceutical scientist. J Pharm Sci 2006 Jun;95(6):1173-1176.
166. Krzyzaniak JF, Alvarez Nunez FA, Raymond DM, Yalkowsky SH. Lysis of human red blood cells. 4. Comparison of in vitro and in vivo hemolysis data. J Pharm Sci 1997 Nov;86(11):1215-1217.

167. Wadajkar AS, Menon JU, Tsai Y-S, Gore C, Dobin T, Gandee L, et al. Prostate cancer-specific thermo-responsive polymer-coated iron oxide nanoparticles. Biomaterials 2013;34(14):3618-3625.
168. Panyam J, Labhasetwar V. Biodegradable nanoparticles for drug and gene delivery to cells and tissue. Advanced Drug Delivery Reviews 2003;55(3):329-347.
169. Mitra A, Mishra L, Li S. Technologies for deriving primary tumor cells for use in personalized cancer therapy. Trends in Biotechnology 2013;31(6):347-354.
170. Romijn HJ. Development and advantages of serum-free, chemically defined nutrient media for culturing of nerve tissue. Biology of the Cell 1988;63(3):263-268.
171. Kang SW, Bae YH. Cryopreservable and tumorigenic three-dimensional tumor culture in porous poly(lactic-co-glycolic acid) microsphere. Biomaterials 2009 Sep;30(25):4227-4232.
172. Fischbach C, Chen R, Matsumoto T, Schmelzle T, Brugge JS, Polverini PJ, et al. Engineering tumors with 3D scaffolds. Nat Methods 2007 Oct;4(10):855-860.
173. Xu X, Sabanayagam CR, Harrington DA, Farach-Carson MC, Jia X. A hydrogel-based tumor model for the evaluation of nanoparticle-based cancer therapeutics. Biomaterials 2014 Mar;35(10):3319-3330.
174. Hutchinson L, Kirk R. High drug attrition rates--where are we going wrong? Nat Rev Clin Oncol 2011 Apr;8(4):189-190.
175. Horning JL, Sahoo SK, Vijayaraghavalu S, Dimitrijevic S, Vasir JK, Jain TK, et al. 3-D tumor model for in vitro evaluation of anticancer drugs. Mol Pharm 2008 Sep-Oct;5(5):849-862.
176. Ricci C, Moroni L, Danti S. Cancer tissue engineering - new perspectives in understanding the biology of solid tumours - a critical review. OA Tissue Engineering 2013;1(1):4.
177. Choi SW, Zhang Y, Xia Y. Three-dimensional scaffolds for tissue engineering: the importance of uniformity in pore size and structure. Langmuir 2010 Dec 21;26(24):19001-19006.
178. Huang CC, Wei HJ, Yeh YC, Wang JJ, Lin WW, Lee TY, et al. Injectable PLGA porous beads cellularized by hAFSCs for cellular cardiomyoplasty. Biomaterials 2012 Jun;33(16):4069-4077.
179. Ke CJ, Chiang WL, Liao ZX, Chen HL, Lai PS, Sun JS, et al. Real-time visualization of pH-responsive PLGA hollow particles containing a gas-generating agent targeted for acidic organelles for overcoming multi-drug resistance. Biomaterials 2013 Jan;34(1):1-10.
180. Sahoo SK, Panda AK, Labhasetwar V. Characterization of Porous PLGA/PLA Microparticles as a Scaffold for Three Dimensional Growth of Breast Cancer Cells. Biomacromolecules 2005 2013/06/19;6(2):1132-1139.
181. Tanaka M, Inase N, Fushimi K, Ishibashi K, Ichioka M, Sasaki S, et al. Induction of aquaporin 3 by corticosteroid in a human airway epithelial cell line. American Journal of Physiology - Lung Cellular and Molecular Physiology 1997 November 1, 1997;273(5):L1090-L1095.
182. Jiang RD, Shen H, Piao YJ. The morphometrical analysis on the ultrastructure of A549 cells. Rom J Morphol Embryol 2010;51(4):663-667.
183. Edelman M, Quam H, Mullins B. Interactions of gemcitabine, carboplatin and paclitaxel in molecularly defined non-small-cell lung cancer cell lines. Cancer Chemotherapy and Pharmacology 2001;48(2):141-144.

184. Liebmann J, Cook J, Lipschultz C, Teague D, Fisher J, Mitchell J. Cytotoxic studies of paclitaxel (Taxol) in human tumour cell lines. British journal of cancer 1993;68(6):1104.
185. Zhang P, Gao WY, Turner S, Ducatman BS. Gleevec (STI-571) inhibits lung cancer cell growth (A549) and potentiates the cisplatin effect in vitro. Molecular cancer 2003;2(1):1.
186. Xin Y, Yin F, Qi S, Shen L, Xu Y, Luo L, et al. Parthenolide reverses doxorubicin resistance in human lung carcinoma A549 cells by attenuating NF-ÎºB activation and HSP70 up-regulation. Toxicology Letters 2013;221(2):73-82.
187. Li F, Awale S, Tezuka Y, Kadota S. Cytotoxicity of constituents from Mexican propolis against a panel of six different cancer cell lines. Natural product communications 2010;5(10):1601-1606.
188. Zhang J, Qi H, Wu C. [Research of anti-proliferation of curcumin on A549 human lung cancer cells and its mechanism]. Journal of Chinese medicinal materials 2004;27(12):923-927.
189. Nirmalanandhan VS, Duren A, Hendricks P, Vielhauer G, Sittampalam GS. Activity of anticancer agents in a three-dimensional cell culture model. Assay and drug development technologies 2010;8(5):581-590.
190. Gerweck LE, Nygaard TG, Burlett M. Response of cells to hyperthermia under acute and chronic hypoxic conditions. Cancer research 1979;39(3):966-972.
191. Jain S, Coulter JA, Butterworth KT, Hounsell AR, McMahon SJ, Hyland WB, et al. Gold nanoparticle cellular uptake, toxicity and radiosensitisation in hypoxic conditions. Radiotherapy and Oncology 2014(0).
192. Rimann M, Graf-Hausner U. Synthetic 3D multicellular systems for drug development. Current Opinion in Biotechnology 2012;23(5):803-809.
193. Link H, Nejadnik H. MR Imaging of Stem Cell Transplants in Arthritic Joints. J Stem Cell Res Ther 2014;4(165):2.
194. Gilad AA, Walczak P, McMahon MT, Na HB, Lee JH, An K, et al. MR tracking of transplanted cells with "positive contrast" using manganese oxide nanoparticles. Magn Reson Med 2008 Jul;60(1):1-7.

Biographical Information

Jyothi Menon was born and brought up in Doha, Qatar. After completion of her schooling, she joined the University of Texas at Arlington, Arlington, TX as a 5-year (BS in Biology/ MS in Biomedical Engineering) student. As a Masters's student in Dr. Kytai Nguyen's laboratory she worked on multiple projects including investigating the effects of different surfactants on the properties of PLGA nanoparticles, and development of thermosensitive theranostic nanoparticles for targeted prostate cancer therapy. Following completion of her Master's degree, Jyothi worked briefly as a Research Assistant in the Advanced Radiological Sciences Department at the UT Southwestern Medical Center, Dallas, TX. Here, she developed nanoemulsions as probes for dual modality and dual functional cellular and molecular imaging. Driven by her research interests in the field of nanomedicine and tissue engineering, Jyothi returned to UTA in 2011 to pursue a Doctor of Philosophy degree in Biomedical Engineering. As a Doctoral student, Jyothi has been the recipient of awards such as the Provost's Level Enhanced Graduate Teaching Assistantship and Fellowship, the I Engage Mentoring Fellowship as well as the prestigious Alfred and Janet Potvin Award for Outstanding Bioengineering student. Over the course of her research career, she has also published 8 research papers, 2 conference proceedings and 3 book chapters. Jyothi has also played an active role in representing the Bioengineering department at Annual Engineering and Computers Science summer camps at UTA. Following graduation, Jyothi plans to continue pursuing a research career in biomaterials, drug delivery and tissue engineering.